© 2019 Peishi Jiang

CAUSAL HISTORY ANALYSIS OF COMPLEX SYSTEM DYNAMICS

BY

PEISHI JIANG

DISSERTATION

Submitted in partial fulfillment of the requirements
for the degree of Doctor of Philosophy in Civil Engineering
in the Graduate College of the
University of Illinois at Urbana-Champaign, 2019

Urbana, Illinois

Doctoral Committee:

Professor Praveen Kumar, Chair and Director of Research
Professor Ximing Cai
Professor Francina Dominguez
Professor Hoshin Gupta, University of Arizona
Professor Paola Passalacqua, University of Texas at Austin

Abstract

Complex system arises as a result of inter-dependencies between multiple components. The nonlinear interactions occurring in the system usually lead to emergent behaviors. The emergence prevails in many natural systems, such as the fractal dynamics of stream chemistry, the chaotic behavior of atmospheric convection, the entropy production due to the dissipative structure of plants, and so forth. Multivariate interactions of the entire system definitely play a key role in sustaining these emergent behaviors, which will not happen solely based on the dynamics of univariate or the interactions within a specific set of variables. Therefore, improving the understanding on the whole system dynamics requires the consideration of how the entire evolutionary dynamics of a system, termed *causal history*, jointly shapes its present state.

In this dissertation, the primary goal is to establish a framework for the study of whole system evolutionary dynamics from multivariate interactions. To achieve that, an information-theoretic formulation is developed to characterize the joint influence from the entire causal history to the present state of each variable using a directed acyclic graph representation. The proposed framework builds on the quantification and characterization of information flow from one source through a causal pathway and two sources through the interaction of separable pathways, which takes advantage of the idea of momentary information transfer and partial information decomposition. Momentary information transfer captures the amount of information flow between any two variables lagged at two specific points in time. Partial information decomposition characterizes the joint effect from two sources into redundant, synergistic and unique contributions. To evaluate the joint influence from the causal history, we partition it into immediate causal history, as a function of lag τ from the recent time, to capture the influence of recent dynamics, and the complementary distant causal history. Further, each of these influences are decomposed into self and cross feedbacks. Such a partition allows the characterization of the information flow from the self- and cross-dependencies with other variables in both histories.

This causal history analysis approach is then implemented to investigate the dynamics of different types of systems. It successfully illustrates the memory dependencies of short- and long-memory processes. Further, we find the information characterization differs from system to system, illustrating their various dynamics.

A long-memory process, for instance, is sustained by self-feedback-dominated recent dynamics and cross-dependency dominated earlier dynamics. In the analysis of observed stream chemistry data, this analysis indicates the key role of the flow rate in creating cross connectivities among stream solutes and also its influence on the dynamics of each solute. Meanwhile, the information from cross-dependence is non-negligible even after correcting for the dependency of flow rate in raw data. It suggests that besides its self-feedback interaction, the resulting $1/f$ signature of each solute is also maintained by the interactions with other variables in the stream.

Last, we evaluate the structure of numerical models based on the idea of information flow between variables. Since we have the ability to intervene in numerical models, the evaluation analyzes how intervening or freezing one or multiple lagged source variables impacts the dynamics of each target variable. Such interventional-effect is different from the prior observational data based analysis anchored on statistical dependencies, and thus provides a complementary view on the component interaction. The analysis of the Lorenz model illustrates the potential contradictory conclusion drawn from the two perspectives, in terms of the extent of information transferred from source variables. It, therefore, reveals the importance of numerical modelling effort in providing insights on the dynamics of the simulated natural systems, in addition to the analysis of observational data.

A better and deeper understanding of complex system dynamics is becoming a necessity due to a higher demand on multidisciplinary research nowadays. With increasing availability of observational data and complexity of numerical models, the information-theoretic metrics proposed and utilized here open new avenues for understanding complex system dynamics.

...To my family

Acknowledgments

I would like to thank my advisor, Prof. Kumar, for his consistent guidance and support in the past five years. His open mind and wide knowledge broadened my horizon in research, enlighted and improved my thinking process. His insightful ideas always surprise me and solve tons of research dilemma. Without his tremendous help, this work would not come into such a good shape. Gratitudes are also expressed to the Hydrocomplebxity research group for our shared and precious memories. Thanks for this five-year companion, Qina Yan, Kunxuan Wang, Esther Lee, Susana Roque-Malo, and Meredith Richardson. I also enjoyed and benefited from numerous conversations with Leila Hernandez and Frank Holcomb. Furthermore, I absolutely would remember: Phong Le, Debsunda Dutta, and Dongkook Woo for all the jokes, drinks and funs we had; Allison Goodwell for our fruitful discussions on the battle field of information theory; and Mostafa Elag for all the assistance at the start of my PhD.

Many thanks to my committee members, Prof. Cai, Prof. Gupta, Prof. Dominguez, and Prof. Passalacqua for all the invaluable advices and contributions to polish this work in a better shape. I am also grateful for Luigi Marini and Rui Liu, computer scientists from National Center for Supercomputing Applications. Working with them improved my coding skill and significantly enriched my knowledge in computer science.

I am very thankful for all my friends in University of Illinois, including but not limited to Dongchen Wang, Zhi Li, Xiaowen Lin, Yu Chen and Ruijie Zeng. Old friendship from all over the world is also greatly appreciated. These direct or remote companions colored my PhD life and thus made it enjoyable.

Last, I would like to express my sincere gratitude to my parents and my wife, whom I am fully indebted to for their selfless supports. Especially, Yan, thank you for your selfless sacrifice in the beginning of our life journey and bringing us our little princess, Iris.

Financial supports from NSF EarthCube Geosemantics project (ICER 1440315), NSF IMLCZO project (EAR 1331906), NSF Browndog project (ACT 1261582) and teaching assistantship from University of Illinois are acknowledged.

Table of Contents

List of Abbreviations

CDI	Conditional Directed Information
CE	Causation Entropy
CMI	Conditional Mutual Information
DAG	Directed Acyclic Graph
DI	Directed Information
kNN	k-nearest-neighbor
KL	Kullback-Leibler
MI	Mutual Information
MII	Momentary Interaction Information
MII-SCP	Momentary Interaction Information-for Separable Causal Paths
MIT	Momentary Information Transfer
MITP	Momentary Information Transfer along causal Path
MIWTR	Momentary Information Weighted Transitive Reduction
MPID	Momentary Partial Information Decomposition
OU	Ornstein-Uhlenbeck
PID	Partial Information Decomposition
TCE	Temporal Causation Entropy
TE	Transfer Entropy
TR	Transitive Reduction
WTR	Weighted Transitive Reduction

List of Symbols

X_t	subprocess X at time t
$\vec{X}_t$	multivariate process $\vec{X}$ at time t.
$\vec{X}_t^-$	all historical states of $\vec{X}$ prior to time t, termed as causal history
$C_{X_{t-\tau}\to Z_t}$	causal path from source node $X_{t-\tau}$ to Z_t in a DAG for time-series
$C_{\vec{V}\to Z_t}$	union of multiple causal paths from source nodes $\vec{V}$ to Z_t in a DAG for time-series
P_{X_t}	parents of node X_t in a DAG for time-series
$P_{C_{\vec{V}\to Z_t}}$	parents of $C_{\vec{V}\to Z_t}$ in a DAG for time-series
$\vec{W}$	condition set for MPID
$\vec{W}_\tau$	condition set for computing $\mathcal{J}$ with immediate and distant histories separated by τ
$P_{\vec{B}}^{\vec{A}}$	union set between $P_{\vec{A}}$ and $\vec{B}$
$I(\vec{A};\vec{B})$	mutual information between $\vec{A}$ and $\vec{B}$
$I(\vec{A};\vec{B}\mid\vec{C})$	conditional mutual information between $\vec{A}$ and $\vec{B}$ given $\vec{C}$
$I_{Y\to Z}^{TE,full}(\tau)$	transfer entropy from the previous τ states of Y to Z_t
$I_{Y\to Z}^{TE}(\tau)$	transfer entropy from a specific state of Y, $Y_{t-\tau}$, to Z_t
$I_{X_{t-\tau}\to Z_t}^{MIT}$	MIT from node $X_{t-\tau}$ to Z_t through a directed edge
$I_{X_{t-\tau}\to Z_t}^{MITP}$	MITP along causal path from node $X_{t-\tau}$ to Z_t through $C_{X_{t-\tau}\to Z_t}$
$\Delta I_{X_{t-\tau_X}\to Z_t\mid Y_{t-\tau_Y}}^{M}$	MII of $Y_{t-\tau_Y}$ on $C_{X_{t-\tau_X}\to Z_t}$
$\Delta I_{\{X_{t-\tau_X},Y_{t-\tau_Y}\}\to Z_t}^{MSCP}$	MII-SCP of the sources $X_{t-\tau_X}$ and $Y_{t-\tau_Y}$ and the target Z_t
$\mathcal{T}$	information flow from the entire causal history
$\mathcal{D}$	information flow from the distant causal history
$\mathcal{J}$	information flow from the immediate causal history
R	redundant information in PID
S	synergistic information in PID
U	unique information in PID

R_c	redundant information in MPID
S_c	synergistic information in MPID
U_c	unique information in MPID
$R_{\mathcal{T}}$	redundant information from self- and cross-dependencies of the causal history
$S_{\mathcal{T}}$	synergistic information from self- and cross-dependencies of the causal history
$U_{self,\mathcal{T}}$	unique information of the self-dependence in the causal history
$U_{cross,\mathcal{T}}$	unique information of the cross-dependence in the causal history
$R_{\mathcal{J}}$	redundant information from self- and cross-dependencies of the immediate causal history
$S_{\mathcal{J}}$	synergistic information from self- and cross-dependencies of the immediate causal history
$U_{self,\mathcal{J}}$	unique information of the self-dependence in the immediate causal history
$U_{cross,\mathcal{J}}$	unique information of the cross-dependence in the immediate causal history
$R_{\mathcal{D}}$	redundant information from self- and cross-dependencies of the distant causal history
$S_{\mathcal{D}}$	synergistic information from self- and cross-dependencies of the distant causal history
$U_{self,\mathcal{D}}$	unique information of the self-dependence in the distant causal history
$U_{cross,\mathcal{D}}$	unique information of the cross-dependence in the distant causal history
$\mathcal{I}$	interaction information
$\mathcal{I}_{\mathcal{D}}$	interaction information of the distant causal history
$\mathcal{I}_{\mathcal{J}}$	interaction information of the immediate causal history

Chapter 1

Introduction

Complex systems, that are systems exhibiting emergent behaviors of forms and functions, arise as a result of nonlinear dynamics and feedback interactions among multiple components in the system. Complexity is ubiquitous in nature. For instance, plants emerge as dissipative systems regulating the incoming and outgoing fluxes, such as water, carbon dioxide, radiation, etc., as well as interacting with its surrounding environments to maximize the overall entropy production [Schneider and Kay, 1994]. Stream solutes usually show fractal signature, indicating self-organized dynamics in the watershed due to their internal transporting/mixing dynamics as well as their interactions with atmospheric forcing and subsurface processes [Kirchner et al., 2000].

One key feature associated with the complexity of a system is that **the whole is greater than sum of the parts**. That is, the emergent characteristics associated with the whole system dynamics can only be observed or quantified through the understanding of all interacting components. On the other hand, subsystem interactions that contribute to the system-level complexity, however, do not show the same properties individually. In earth science, the emergence of the self-similar river network is found to result from the spatial randomness of the surface resistance, leading to the minimization of the total energy expenditure [Paik and Kumar, 2008]. In a brain system, such complexity can be seen as the emergence of consciousness due to the multitude of interactions in the brain network [Tononi and Edelman, 1998]. In human society, a city is not just the sum of all its physical infrastructures and the interactions among its residents, but rather it is an emergent complex system that optimizes its different functionalities such as transportation and water flow through the urban drainage system [West, 2017, Yang et al., 2017]. A thorough analysis on how the whole system dynamics enables and shapes the dynamics of each individual component would definitely lead us beyond the traditional observation of emergent behaivors, towards a more sophisticated understanding of these emerging phenomena.

Fortunately, the increasing availability of observational data, due to the rapid advance of modern observing technology, opens up more avenues for understanding complex system dynamics [Strogatz, 2000,

Neal et al., 2013]. In geoscience, different types of observational networks (e.g., AmeriFlux[1], the U.S. Climate Reference Network[2], NOAA-NCEI[3], USGS Water Data for the Nation[4], and so forth) have been deployed in the past decade. In addition to facilitating many existing data-driven approaches, such as traditional statistical approaches and different emerging machine learning techniques, these emerging vast observational data would be extremely helpful in serving as a basis for theoretical developments to achieve a more sophisticated understanding of the multivariate interactions in complex systems.

On the flip side, physical modelling, a common way for simulating a system's dynamics, serves as a white box allowing the internal interactions of a system to be viewable from the outside [Paniconi and Putti, 2015]. It allows ensemble simulations – providing multiple trajectories of dynamics, as well as intervention of the simulated system – that have the possibility to provide insights on the propagation of the interventions on system's dynamics. These two features of physical modelling are not available in nature, where intervening natural systems is hard and observational data only contain one trajectory of the dynamics. Such uniqueness enables modelling to serve as an ideal testbed to understand the complexity of the system through a characterization of its dynamics from ensemble simulations and interventions.

To capture the interactions or causal relationships among time-series data through either observations or model simulation, information theory stands out as a compelling approach [Shannon and Weaver, 1949]. This is due to its capability in capturing the nonlinear interactions among multiple components, regardless of whether the system can be intervened. Specifically, information theory provides avenues to quantitatively delineate the direction, strength, and content of influences between variables, termed **information flow**.

The goal of this dissertation is to develop an information-theoretic framework for investigating the multivariate interactions that shape the whole system dynamics, based on both observational data and physical modelling. In this chapter, we provide the background of different types of interactions in complex system dynamics as well as the corresponding quantification through information flow. Then, we state the research questions and the contributions from this work, and present the organization of the rest of the dissertation.

1.1 Background

The complexity of a system is closely related to its entire evolutionary dynamics occurring in the system. It anchors on how the past shapes the present. In other words, the inter-dependencies between the present state of each component and the historical states of all the components contain the information of how

[1] https://ameriflux.lbl.gov/
[2] https://www.ncdc.noaa.gov/crn/
[3] https://www.ncei.noaa.gov/
[4] https://waterdata.usgs.gov/nwis

the whole system behavior is sustained. For instance, the dissipative structure of an open system is first created and then maintained, due to its internal dynamics as well as its interactions with the surrounding environment through the incoming and outgoing fluxes over time [Nicolis and Prigogine, 1989]. The process of the emergence of the dynamical dynamics structure is a consequence of an enhanced interaction among the components [Rosas et al., 2018]. Meanwhile, how the complexity is sustained over time remains an open question, calling for a solution for an improved understanding of the system dynamics. Addressing this question requires illustrating different causal relationships among system components as well as developing appropriate metrics for characterizing these causal relationships.

1.1.1 Causal Relationships in a Multivariate Complex System

Understanding the causal relationships in a complex system first requires a well-defined way for identifying causality. In an elementary bivariate case, the causal relationship between a lagged source variable $Y_{t-\tau}$ and a target variable Z_t refers to how $Y_{t-\tau}$ influences Z_t. A natural way to assess the causality is to analyze how the effect of the intervention of $Y_{t-\tau}$ propagates through all the interactions in the system and eventually alters Z_t's dynamics. This is known as **Pearl causality** [Pearl, 2000]. Pearl causality can be used in understanding component interactions in modelled system, where system interventions are controllable. However, Pearl causality is infeasible in many natural systems, where only observations are available and system intervention is extremely hard if not impossible. Thus, an alternative for assessing the cause-effect relationship from statistical dependency perspective by using only observational data anchors on **Granger causality** [Granger, 1969]. In its original formulation, Granger causality [Granger, 1969] evaluates the reduction in the variance of Z_t due to the knowledge of $Y_{t-\tau}$. While Pearl causality relies on intervention of a variable in the system and the assessment of the ensuring impact on the system, Granger causality relies on the inference of such a dependence through unconstrained evolution of the system arising through all the joint interactions present therein. While the original formulation of Granger [Granger, 1969] relies only on second order measure, the approach can be extended to consider the entire probability distribution. This can be achieved using information-theoretic measures such as Shannon's entropy [Schreiber, 2000, Runge et al., 2012b]. Since the joint distribution under consideration are that of target at a specific time and that of a source at a previous time, we see this as information flow from source to target associated with the cause-effect dynamics

Directed Acyclic Graph for Time-Series

Given the causal relationship for each pair of variables, in either Pearl or Granger sense, we need an appropriate representation of the dynamical evolution for discerning the causality in a multivariate system. Consider a system with N variables, $\vec{X}_t = \{X_t, Y_t, Z_t, ...\}_N$, varying in time t. The influence from the whole system history can now be revealed as the fact that the current state of any variable $Z_t \in \vec{X}_t$ is a result of the entirety of all the earlier dynamics in the system. One common way to represents complex system dynamics is by using process network, which is a network depicting the lagged interaction between each pair of variables [Ruddell and Kumar, 2009a, Ruddell and Kumar, 2009b], illustrated through an example in a quadvariate system in Fig. 1.1(a). The number shown on the edge refers to the temporal lag associated with the causal influence between the two linked variables. Further, to visualize the temporal dependencies of the system, we illustrate the dynamics in a corresponding **Directed Acyclic Graph (DAG) representation for time-series** in Fig. 1.1(b), consisting of all the historical states $\vec{X}^-_{t+1} = \{\vec{X}_t, \vec{X}_{t-1}, \vec{X}_{t-2}, \vec{X}_{t-3}, ...\}$. Now, each node refers to a temporal variable $Z_t \in \vec{X}^-_{t+1}$. A directed edge in E linking two nodes $Y_{t-\tau}$ and Z_t, written as $Y_{t-\tau} \to Z_t$, stands for a direct causal influence from $Y_{t-\tau}$ to Z_t, where τ is a positive time lag. It can be observed from the DAG that the present state of a target variable at time t is driven by the entire dynamics prior to t in the system. We call this prior dynamics $\vec{X}^-_t = \{\vec{X}_{t-1}, \vec{X}_{t-2}, \vec{X}_{t-3}, ...\}$ as **causal history**. Then, unravelling the whole system dynamics can be translated to addressing the following question: **In what way do the states of interdependent variables from the causal history influence the present state of each target variable which leads to the emergent whole system dynamics?**

Different Causal Relationships in the DAG

Characterizing the influence from the entire causal history to a target Z_t requires the understanding of how the target is driven by different parts of the historical dynamics as captured in the DAG, including: (1) one directed edge from a source node $Y_{t-\tau}$ (Fig. 1.1(c)); (2) one causal path $C_{Y_{t-\tau} \to Z_t}$ – a set of nodes connected by a sequence of edges directing the influence from $Y_{t-\tau}$ to Z_t (Fig. 1.1(d)); (3) two causal paths – directing the influence from two sources (Fig. 1.1(e)); and (4) recent dynamics, called **immediate causal history**, and the complementary earlier dynamics, called **distant causal history**, partitioned by a time lag τ (Fig. 1.1(f)). Each individual lagged source $Y_{t-\tau}$ is the basic unit that affects the target Z_t through a directed edge or indirectly through a causal path $C_{Y_{t-\tau} \to Z_t}$. For multivariate case, such as the illustration of two lagged sources $Y_{t-\tau_Y}$ and $U_{t-\tau_U}$ in Fig. 1.1(e), each source influence the target Z_t through its own causal path individually, but would eventually have a joint effect on the target. In addition, such understanding of multivariate interactions from the entire historical dynamics further draws

upon how specific parts of the history jointly influence the target node. In this dissertation, we further explore the partitioning shown in Fig. 1.1(f): first, the interplay between immediate and distant causal histories; and second, the interplay between self-and cross-dependency dynamics. The partition in terms of immediate/distant causal histories enables the investigation of the memory dependency of the system. For instance, a long-memory process is expected to receive influences from a very early dynamics in distant causal history. Also, the partition into self-and cross-dependencies is important because of the dominance of self-feedback interactions in many natural systems. Therefore, insights from its interplay with cross-dependency would essentially help reveal the mechanism sustaining the complexity of a system. Given different causal relationships shown in Figs. 1.1(c)-(f), we now need an approach to characterize these relationships, quantified as information flow.

1.1.2 Quantifying Causal Relationships through Information Flows

Information theory is employed to delineate the causal relationships due to its capability in characterizing the nonlinear dependencies among multiple variables from time-series data. Similar to the mass and energy flows among different interactions in nature, information theory captures the flows of information provided by source variable(s) to inform the dynamics of a target variable. The resulting interactions characterized in the above causal relationships are thus termed information flow. Here, we first briefly introduce the background of information theory. Then, we review the idea of momentary information transfer developed by [Runge et al., 2012b] that captures the information flow between a pair of lagged variables either through a directed edge (Fig. 1.1(c)) or through a causal path (Fig. 1.1(d)).

Primer on Information Theory

We anchor on Shannon's entropy [Shannon and Weaver, 1949]. It quantifies the uncertainty of a variable X_t, and is given by:

$$H(Z_t) = -\sum_{z_t \in Z_t} p(z_t) \log p(z_t), \tag{1.1}$$

where $p(z_t)$ is the probability of Z_t. In a bivariate case of Z_t and $Y_{t-\tau_Y}$, the uncertainty of Z_t that remains given the knowledge of $Y_{t-\tau_Y}$ can be quantified as a corresponding conditional entropy:

$$H(Z_t|Y_{t-\tau_Y}) = -\sum_{z_t \in Z_t, y_{t-\tau_Y} \in Y_{t-\tau_Y}} p(z_t, y_{t-\tau_Y}) \log \frac{p(z_t, y_{t-\tau_Y})}{p(z_t)}, \tag{1.2}$$

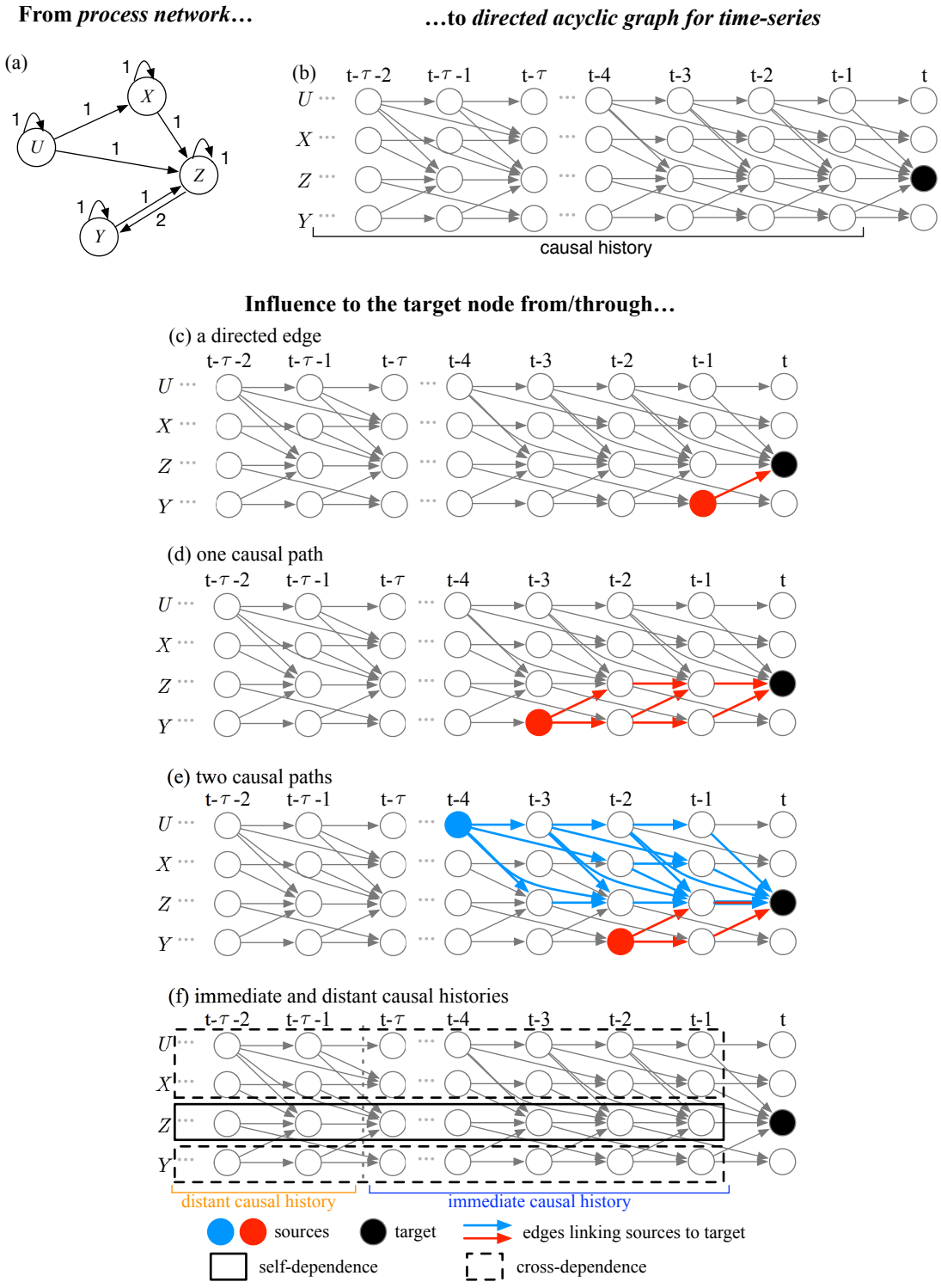

Figure 1.1: Illustration of the dynamics of a quadvariate complex system in (a) process network and (b) directed acyclic graph (DAG) representation for time-series, as well as using the DAG for showing the influence on the present state of a target from one lagged source through (c) a directed edge (d) or a causal path, (e) two lagged sources, and (f) the immediate and distant causal histories.

where $p(z_t, y_{t-\tau_Y})$ is the joint probability of Z_t and $Y_{t-\tau_Y}$. Moreover, the shared dependency between Z_t and $Y_{t-\tau_Y}$ can be measured by using Mutual Information (MI) of the two variables, which is given by:

$$\begin{aligned} I(Z_t; Y_{t-\tau_Y}) &= \sum_{z_t \in Z_t, y_{t-\tau_Y} \in Y_{t-\tau_Y}} p(z_t, y_{t-\tau_Y}) \log \frac{p(z_t, y_{t-\tau_Y})}{p(z_t)p(y_{t-\tau_Y})} \\ &= H(Z_t) - H(Z_t|Y_{t-\tau_Y}) = H(Y_{t-\tau_Y}) - H(Y_{t-\tau_Y}|Z_t). \end{aligned} \tag{1.3}$$

The last two equalities of Eq.(1.3) illustrate that $I(Z_t; Y_{t-\tau_Y})$ symmetrically measures the shared dependency between Z_t and $Y_{t-\tau_Y}$ or the reduced uncertainty of one variable given the knowledge of the other.

In addition, to have an asymmetric measure capturing the directional influence from a source to a target, Transfer Entropy (TE) [Schreiber, 2000] is proposed. TE quantifies the information transfered to a target, Z_t, from a sequence of previous states of another variable, $Y_{t-1:t-\tau} = \{Y_{t-1}, Y_{t-2}, ..., Y_{t-\tau}\}$, given the knowledge of the past states of itself, $Z_{t-1:t-\tau} = \{Z_{t-1}, Z_{t-2}, ..., Z_{t-\tau}\}$. It is computed through a conditional mutual information, and is given by:

$$I^{TE,full}_{Y \to Z}(\tau) = I(Z_t; Y_{t-1:t-\tau} \mid Z_{t-1:t-\tau}). \tag{1.4}$$

Meanwhile, to evaluate the transfer of information from a specific previous state of Y, $Y_{t-\tau}$, to Z_t given merely the immediate history of Z_t, Eq.(1.4) can be revised as:

$$I^{TE}_{Y \to Z}(\tau) = I(Z_t; Y_{t-\tau} \mid Z_{t-1}). \tag{1.5}$$

Furthermore, when a third variable $X_{t-\tau_X}$ is considered as influencing the target Z_t, in addition to $Y_{t-\tau_Y}$, the total uncertainty reduction of Z_t due to both $X_{t-\tau_X}$ and $Y_{t-\tau_Y}$ is measured as the mutual information between Z_t and the union of $X_{t-\tau_X}$ and $Y_{t-\tau_Y}$, that is, $I(Z_t; X_{t-\tau_X}, Y_{t-\tau_Y})$. To further characterize different information contents in $I(Z_t; X_{t-\tau_X}, Y_{t-\tau_Y})$, Partial Information Decomposition (PID) [Williams and Beer, 2010] has been developed to decompose the total information into (1) synergistic information – information jointly provided by $X_{t-\tau_X}$ and $Y_{t-\tau_Y}$, denoted as S; (2) redundant information – the overlapping information from the two sources, denoted as R; and (3) unique information – information provided by each source individually, denoted as U_X and U_Y, respectively. PID is then given by:

$$I(Z_t; X_{t-\tau_X}, Y_{t-\tau_Y}) = S + R + U_X + U_Y. \tag{1.6}$$

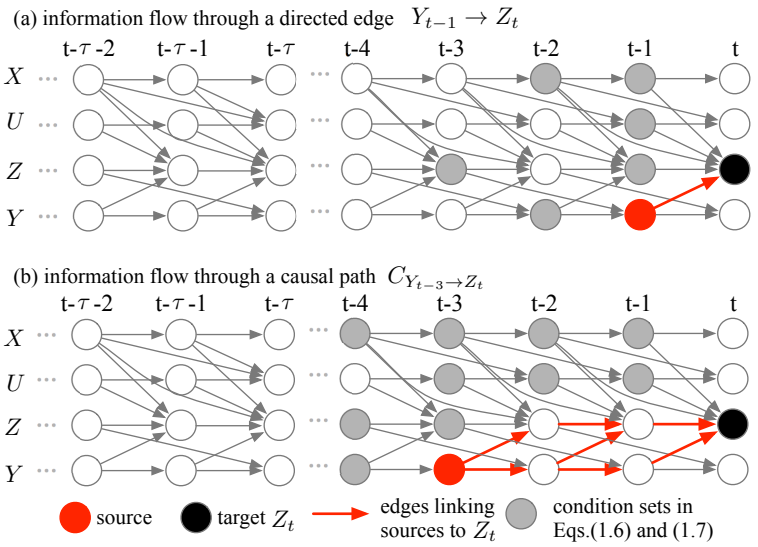

Figure 1.2: Illustration of pairwise information flow to a target node Z_t in a quadvariate complex system from (a) Y_{t-1} through a directed edge by using Momentary Information Transfer (MIT); and (b) Y_{t-3} through the corresponding causal path $C_{Y_{t-3}} \to Z_t$ by using Momentary Information Transfer along causal Path (MITP).

Information Flow in a Pairwise Interaction

When multivariate time-series observations of a complex system are available, the information flow from a lagged source $Y_{t-\tau}$ to a target Z_t has been addressed in a Granger sense. Metrics have been proposed to quantify the pairwise information flow, anchoring on the idea of momentary information [Runge et al., 2012b, Runge et al., 2012a, Runge, 2015]. It captures the information flow transferred between two lagged nodes through a directed edge or indirectly through a causal path, as shown in Figs. 1.1(c) and (d), respectively.

Consider a direct causal influence between $Y_{t-\tau}$ and Z_t through an edge, as shown in Fig. 1.1(c). That is, Z_t and $Y_{t-\tau}$ are connected with a directed edge if and only if $Y_{t-\tau}$ and Z_t are statistically dependent when conditioned on the remaining past states of the system. Mathematically, such influence can be measured as a conditional mutual information, and is given by [Runge et al., 2012b]:

$$I(Z_t; Y_{t-\tau} \mid \vec{X}_t^- \backslash Y_{t-\tau}) > 0, \tag{1.7}$$

where $\backslash$ is the exclusion symbol. The conditional mutual information (CMI) in the above inequality quantifies the information flow from $Y_{t-\tau}$ to Z_t conditioned on the knowledge of the rest of the dynamics.

The computation of CMI in Eq.(1.7) is infeasible due to the potentially infinite number of nodes in the condition set $\vec{X}_t^- \backslash Y_{t-\tau}$. To avoid this 'curse of dimensionality', the Markov property for DAG is assumed [Lauritzen et al., 1990]. Loosely speaking, this property states that a node Z_t is statistically indepen-

dent of its non-descendants if its parents P_{Z_t} are given, where $P_{Z_t} = \{X_{t-\tau} : X_{t-\tau} \in \vec{X}_{t-\tau}, \tau > 0, X_{t-\tau} \to Z_t\}$. The property implies that Z_t is independent of $\vec{X}_t^- \backslash P_{Z_t}$ given the knowledge of P_{Z_t}. Correspondingly, the CMI in Eq.(1.7) can be revised as:

$$I^{MIT}_{Y_{t-\tau} \to Z_t} = I(Z_t; Y_{t-\tau} \mid P_{Z_t}, P_{Y_{t-\tau}} \backslash P_{Z_t}), \tag{1.8}$$

which is called as Momentary Information Transfer (MIT) [Runge et al., 2012b]. Eq.(1.8) holds because under Markov property of DAG the dynamics between Z_t and $Y_{t-\tau}$ are independent of the rest of the historical states if conditioned on the parents of the two nodes. An example of the condition set is illustrated as the gray nodes in Fig. 1.2(a) for the influence from Y_{t-1} to Z_t. MIT quantifies the direct interaction between two nodes acting as source and targets, by excluding any information from other nodes that may be flowing through the source or directly to the target.

In addition to a direct influence through an edge, a lagged source node $Y_{t-\tau}$ can also indirectly affect a target node Z_t through the corresponding causal path $C_{Y_{t-\tau} \to Z_t}$. An example is illustrated as the influence from Y_{t-3} to Z_t in the quadvariate system in Fig. 1.1(d). The quantification of the information flow through $C_{Y_{t-\tau} \to Z_t}$ is the same as Eq.(1.7). However, the corresponding simplification of Eq.(1.7) based on Markov property is different from Eq.(1.8), and leads to the Momentary Information Transfer along causal Path (MITP) [Runge, 2015]:

$$I^{MITP}_{Y_{t-\tau} \to Z_t} = I(Z_t; Y_{t-\tau} \mid P_{Z_t}, P_{C_{Y_{t-\tau} \to Z_t}} \backslash P_{Z_t}), \tag{1.9}$$

where $P_{C_{Y_{t-\tau} \to Z_t}}$ are the parents of the causal path $C_{Y_{t-\tau} \to Z_t}$. Note that the condition set in Eq.(1.9) is now defined by separating the union of Z_t and $C_{Y_{t-\tau} \to Z_t}$ from the rest of earlier dynamics, as illustrated in gray nodes in Fig. 1.2(b) for the influence from Y_{t-3} to Z_t. Therefore, Eq.(1.9) gives the information flow from a single lagged source $Y_{t-\tau}$ to a target Z_t going only through the causal path $C_{Y_{t-\tau} \to Z_t}$.

1.1.3 What's Next?

PID in Eq.(1.6) characterizes the influence from two sources to a target into synergistic, redundant, and unique information content. Meanwhile, the idea of MIT and MITP captures the information flow transferred between lagged variables directly or through specific causal pathways. Together, PID and MIT/MITP, therefore, provide a way of thinking for further developments for characterizing the influence from either two causal paths or the entire causal history from observational data, as illustrated in Figs. 1.1(e) and (f), respectively. It would allow us to delineate the joint effect from the whole system dynamics, and assess how

interactions among all variables in the system leads to emergent behaviors, which is the target for this study.

Meanwhile, in addition to the causal analysis of observational time-series data in the Granger sense, numerical models provide an alternative way to characterize the interactions in a system from the perspective of Pearl causality. This is because modelled systems can be easily intervened and also offer the possibility of generating an ensemble of simulation. The interventional perspective on the interactions of a system is strategic in that it offers a complementary view allowing us to assess the components interactions in models, and correspondingly sheds light on the structure of modelled systems.

1.2 Research Question and Contribution

The primary goal of this dissertation is **to understand the emergent behaviors of complex systems by characterizing the influence from the multivariate interactions in the causal history to the present state of each target variable**. To achieve that, we investigate the joint influence to the present state of a target variable from the entire evolutionary dynamics of the system, or causal history. In particular, the following specific aims are addressed.

- Characterize the interactions of information from multiple lagged source variables to a target variable.
- Quantify the influence to a target from both its distant and immediate causal histories.
- Characterize the joint influence of the self- and cross-dependencies of a target in both distant and immediate causal histories.
- Evaluate the structure of numerical models by quantifying the change of a target's density evolution under the intervention of lagged sources.

The original contributions of this dissertation are:

- We develop a **momentary partial information decomposition** to characterize the interactions of information flows through the pathways from two lagged source variables to a target variable.
- The influence of the entire evolutionary dynamics of a system, or causal history, on the outcome of each component is systematically evaluated by using an information-theoretic framework, referred to as **causal history analysis**.
- Causal history analysis is used to illustrate the memory dependencies of different types of dynamical systems, including a short-memory system and several long-memory systems.

- Causal history analysis is shown to improve the understanding of the whole system dynamics. Specifically, it is shown that: (1) the complexity of a long-memory system is sustained by a self-dependency-dominated recent dynamics as well as a cross-dependency-dominated earlier dynamics; and (2) the information characterization in immediate and distant causal histories is able to indicate the dependence among individual components of a system.

- The analysis of the structure of the Lorenz chaotic model provides insights through complementary views of the interventional effect and the statistical dependence gives different or even constrasting interpretations on the extent of the influence from lagged source(s) to a target.

1.3 Organization

The dissertation is organized as follows.

- Chapter 2 presents the momentary partial information decomposition approach for characterizing the interactions of information resulting from two lagged sources to a target through two separable causal paths. It builds on the recent advances of momentary information transfer – quantifying the information transfer between two lagged components through a specific pathway – with partial information decomposition that allows the characterization of the interaction of causal paths initiated from two sources.

- Chapter 3 presents the causal history analysis framework. This framework partitions the entire history into immediate and distant causal histories, and provides quantitative metrics for measuring the information flows from these two components. It is applied to investigate the memory dependencies of a short-memory system as well as three long-memory systems.

- Chapter 4 further characterizes the interactions of self-and cross-dependencies in both immediate and distant causal history. We then implemented the proposed framework to analyze the dynamics of a short-memory system and three long-memory systems, based on both observed time series and model-generated synthetic data.

- Chapter 5 presents an approach for assessing the density evolution change of a target due to the intervention of one or multiple lagged sources in a numerical model using Kullback-Leibler (KL) divergence. It is then applied for analyzing the structure of the Lorenz chaotic model. Furthermore, the result based on KL divergence is compared with the corresponding MI and TE for illustrating the difference between interventional effect and the statistical dependence.

- Chapter 6 summarizes the key findings of this dissertation, and provides avenues for future work.

Chapter 2

Interactions of Information Transfer Along Separable Causal Paths

2.1 Introduction[1]

Complex natural and human systems, such as ecosystems and financial markets, emerge as a result of causal and/or self-organized feedback interactions among multiple variables. Lagged feedback of one variable on another can also be interpreted as a causal outcome at the time scale of the feedback dependence. Causality can also be characterized as the outcome of the interaction of information transfer [Pompe and Runge, 2011, Runge et al., 2012b] among the variables in the system. Therefore, the amount and quality of information transfer can be used to quantify the degree and nature of causality. Our goal in this chapter is to develop a framework for quantifying causal interaction arising from information transferred along separable paths that affect a target.

In this study, causality is interpreted as *strong Granger causality* [Eichler, 2012]. Different from the causality from an interventional perspective [Pearl, 2000], Granger causality [Granger, 1969] is anchored on the predictability of a target from one or more sources by measuring the variance of the target given the sources. Strong Granger causality takes a further step by investigating the predictability from sources based on the entire joint distribution of the variables involved [Eichler, 2012]. It is extremely useful in detecting the relationships among the variables in a complex system where only observational data is available and intervention in system is hard or impossible as in natural systems which comprise a multitude of interactions. In the rest of the chapter, we refer *causality* to indicate strong Granger causality for convenience.

When a source variable influences a target directly, or indirectly through a path comprising of nodes and links, it is called a causal path [Runge, 2015]. For example, consider a three-variable process network [Ruddell and Kumar, 2009a, Ruddell and Kumar, 2009b] shown in Fig. 2.1a, where the dynamical linkages between these components of the system are assumed to be time-invariant and constructed such that: (1) X drives both Y and Z with a lag of one time step, (2) Y drives Z at a lag of two time steps, and (3) both X and Z have a self-feedback at a lag of one time step. By representing the dynamics of

[1]This chapter is published as an article in Physical Review E, 2018 [Jiang and Kumar, 2018]

the process network in a time series graph [Runge et al., 2012a], X affects Z lagged at two time steps through a causal path (Fig. 2.1b), denoted as $C_{X_{t-2}\to Z_t}$, containing two pathways: $X_{t-2} \to X_{t-1} \to Z_t$ and $X_{t-2} \to Z_{t-1} \to Z_t$. Furthermore, considering the contribution of multiple source variables on the target, the target can be affected by different sources each having its own causal path, which can be *separable* or *non-separable*. For the non-separable case, the causal path from one source contains the causal paths of the remaining sources. For instance, the causal path $C_{X_{t-2}\to Z_t}$ includes the causal path from X_{t-1} (i.e., $C_{X_{t-1}\to Z_t}$) (Fig. 2.1c). $C_{X_{t-2}\to Z_t}$ and $C_{X_{t-1}\to Z_t}$ are non-separable because the node X_{t-1} lies in the causal path $C_{X_{t-2}\to Z_t}$. Also, the causal paths can be separable such that no source is enslaved to the causal path of another. The separability of causal paths can be either totally independent, such as the causal paths $C_{X_{t-1}\to Z_t}$ and $C_{Y_{t-3}\to Z_t}$ (Fig. 2.1d), or partially independent, such as the causal paths $C_{X_{t-2}\to Z_t}$ and $C_{Y_{t-3}\to Z_t}$ which share the pathway $Z_{t-1} \to Z_t$ (Fig. 2.1e). We call the causal paths, which transmit the information to the same target from different sources but are not enslaved to the pathways of other sources, as *separable causal paths*. Together, the causal paths from all source nodes of interest that affect a target node comprise a *causal subgraph*.

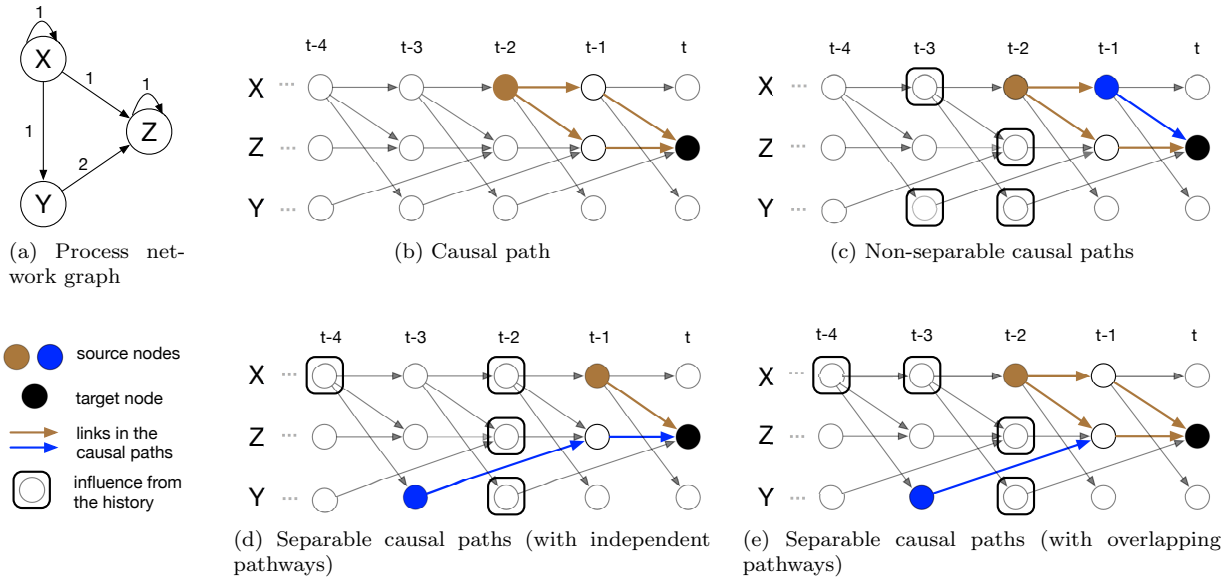

(a) Process network graph

(b) Causal path

(c) Non-separable causal paths

(d) Separable causal paths (with independent pathways)

(e) Separable causal paths (with overlapping pathways)

Figure 2.1: The illustration of a three-variable dynamical system: (a) the process network graph illustrating the lagged interaction of three variables X, Y and Z, where the numbers on the directed links represent the lagged time step; (b) the time series graph corresponding to the process graph, with the causal path $C_{X_{t-2}\to Z_t}$ whose directed links are highlighted in brown arrows; (c) the non-separable causal paths $C_{X_{t-1}\to Z_t}$ and $C_{X_{t-2}\to Z_t}$; (d) the separable causal paths with independent pathways $C_{X_{t-1}\to Z_t}$ and $C_{Y_{t-3}\to Z_t}$; and (e) the separable causal paths with overlapping pathways $C_{X_{t-2}\to Z_t}$ and $C_{Y_{t-3}\to Z_t}$ (brown and blue nodes: source nodes; black nodes: target nodes; brown and blue links: the corresponding causal paths from the sources to the target; and nodes with black circles: nodes affecting the two separable causal paths and the target node).

An emerging approach for characterizing the nature of dependency between multiple interacting variables is based on *partial information decomposition* (PID) [Williams and Beer, 2010, Barrett, 2015], also called as *information partitioning*, which is capable of providing insights from large amounts of observational or model datasets that are becoming available [Goodwell and Kumar, 2017a, Goodwell and Kumar, 2017b]. PID provides estimation of the information transfer from the sources to the target variable in terms of: (1) redundant information R, which captures overlapping information content that both sources provide to the target; (2) synergistic information S, which is only available due to the joint interaction of sources as they affect the target; and (3) unique information U that each source shares with the target. In the case of two sources (i.e., $X_{t-\tau_X}$ and $Y_{t-\tau_Y}$) driving Z_t, PID is given as [Williams and Beer, 2010, Barrett, 2015]

$$I(X_{t-\tau_X}, Y_{t-\tau_Y}; Z_t) = U_X + U_Y + S + R \tag{2.1}$$

$$I(X_{t-\tau_X}; Z_t) = U_X + R \tag{2.2}$$

$$I(Y_{t-\tau_Y}; Z_t) = U_Y + R, \tag{2.3}$$

where U_X and U_Y are unique information from $X_{t-\tau_X}$ and $Y_{t-\tau_Y}$, respectively; $I(a;b)$ is the mutual information [Cover and Thomas, 2006] between a and b; and especially, $I(X_{t-\tau_X}, Y_{t-\tau_Y}; Z_t)$ represents the mutual information between Z_t and the union of $X_{t-\tau_X}$ and $Y_{t-\tau_Y}$. Eqs.(2.1)-(2.3) further give rise to the expression of S and R in terms of interaction information $\mathcal{I}$ [Cover and Thomas, 2006] such that

$$\begin{aligned}\mathcal{I}(X_{t-\tau_X}; Y_{t-\tau_Y}; Z_t) &= I(X_{t-\tau_X}, Y_{t-\tau_Y}; Z_t) - I(X_{t-\tau_X}; Z_t) - I(Y_{t-\tau_Y}; Z_t) \\ &= S - R,\end{aligned} \tag{2.4}$$

which quantifies the amount of information bound up in $\{X_{t-\tau_X}, Y_{t-\tau_Y}, Z_t\}$ [Barrett, 2015].

PID captures the net information transfer occurring through a multitude of causal paths involved in the interaction. But due to the high level of dependencies in a complex system, it also masks our ability to discern the causal interaction within a causal subgraph consisting of specific pathways, or possible separable causal paths. For example, as illustrated in Fig. 1d, the information partitioning associated with the interaction of X_{t-1} and Y_{t-3} on Z_t will be influenced by the external factors affecting the intermediate nodes, through their own causal paths, called as *complementary causal subgraph*. Some of the nodes in the complementary causal subgraph, that are outside of the nodes of interest (e.g., $C_{X_{t-1}\to Z_t}$, $C_{Y_{t-3}\to Z_t}$, and Z_t) but have influences on them, are highlighted as nodes with black circles, including X_{t-4}, X_{t-2}, Y_{t-2} and Z_{t-2}.

Therefore, in this chapter we quantify the partial information decomposition arising from the information

transfer along separable causal paths in a manner that excludes the influence of complementary causal subgraph thereby eliminating the effects of external factors. Also, we explore (1) how the PID varies between separable and non-separable causal paths; (2) how the structure of the separable causal paths affects the information partitioning; and (3) how the noise in a complex system affects these estimates. We use the recently-proposed *momentary information transfer along causal paths* (MITP) [Runge, 2015], which allows us to isolate the information transfer between two variables along their causal path from that associated with its complementary causal subgraph. We extend this concept to characterize the causal interaction in terms of synergistic, unique and redundant information transfer through separable causal paths by using a PID framework anchored on a rescaled approach for computing the redundancy [Goodwell and Kumar, 2017a] and also provide formulations associated with other prevalent measures of redundancy. This will be termed as *momentary partial information decomposition* (MPID).

This chapter is organized as follows. First, we provide a brief review of the momentary information in Section 2.2. Then, in Section 2.3 we develop the details of the mathematical framework for MPID by adopting the rescaled approach for computing redundancy. In Section 2.4, we show that under some conditions, the proposed MPID is entirely determined by the interactions of the nodes of interest in the causal subgraph, and autonomous of how these nodes are affected by the complementary causal subgraph. This property is called the *coupling strength autonomy* (CSA) [Runge et al., 2012b]. We utilize both a linear and a nonlinear common driver model to verify the coupling strength autonomy property analytically and numerically, respectively. Moreover, in Section 2.5, we define the MPID frameworks based on three alternative redundancy measures, and discuss their properties. In Section 2.6, based on the rescaled redundancy measure, we analyze MPID and PID under both separable and non-separable causal paths by using synthetic data generated from two models of coupled logistic equations with varying noise strengths. Finally, we provide summary and conclusions in Section 2.7. Appendices A to C provide mathematical proofs of several formulations.

2.2 A Review of Momentary Information

In this section, we briefly review the concept of momentary information first proposed by Pompe and Runge [Pompe and Runge, 2011], which provides the basis for quantifying information partitioning along separable causal paths presented in the next section. This concept originates from the idea that to assess the impact of some variable X on another variable Y at time t with a specific time lag τ, the history of both $X_{t-\tau}$ and Y_t should be accounted for through conditioning so that the response of Y_t to a disturbance on $X_{t-\tau}$ accounts for the causal interaction between the two variables at the specific lag τ [Pompe and Runge, 2011].

Therefore, the momentary information quantifies the causal interaction between two lagged nodes of interest, in a time-series graph. To condition at the history of the nodes of interest, a network describing the causal relationships among the variables in the whole system is required [Eichler, 2012].

Consider a complex system with a multivariate process $\vec{X} = \{V, X, Y, Z, \dots\}_N$, where N is the number of component processes. We assume that the causal dependence between the component processes are temporally invariant. The process can be represented in a time series graph G, as illustrated in Figs. 2.1c-2.1e for a three variable system, of which the basic elements include:

- Node Z_t: a subprocess Z at a specific time t.
- All the nodes at time step t: $\vec{X}_t \equiv \{V_t, X_t, Y_t, Z_t, \dots\}_N$.
- The past or history of Z_t: $\vec{X}_t^- \equiv \{\vec{X}_{t-1}, \vec{X}_{t-2}, \dots\}$.
- Directed link (or causal link) $X_{t-\tau} \to Z_t$: implying $X_{t-\tau}$ ($\tau > 0$ is the time lag) has causal influence on Z_t.
- Parents of Z_t: $P_{Z_t} \equiv \{X_{t-\tau} : X \in \vec{X}, \tau > 0, X_{t-\tau} \to Z_t\}$. A node $X_{t-\tau}$ is a parent of Z_t if and only if there is a directed link/edge from $X_{t-\tau}$ to Z_t (i.e., $X_{t-\tau} \to Z_t$).
- Causal path from $X_{t-\tau}$ to Z_t: $C_{X_{t-\tau} \to Z_t} \equiv \{V_{t-\tau_V} : V \in \vec{X}, \tau_V > 0, X_{t-\tau} \to \cdot \to V_{t-\tau_V} \to \cdot \to Z_{t-\tau_Z}\} \cup \{X_{t-\tau}\}$.

In this study, we assume that all the causal links are identified from the criteria that only the past affects the future. The causality in this study is defined in the context of *strong Granger causality* [Granger, 1969, Eichler, 2012], that is, a pair of nodes $X_{t-\tau} \in G$ ($\tau > 0$) and $Z_t \in G$ are connected by a directed link $X_{t-\tau} \to Z_t$ if and only if:

$$X_{t-\tau} \not\perp\!\!\!\perp Z_t \mid [\vec{X}_t \backslash \{X_{t-\tau}\}], \tag{2.5}$$

where $\not\perp\!\!\!\perp$, $\mid$ and $\backslash$ are the dependent, conditioning and subtraction symbols, respectively. It is anchored on the idea that $X_{t-\tau}$ *Granger-causes* Z_t if the two are still dependent on each other when conditioned on the remaining process.

Furthermore, because the directionality of the causal relationship between two contemporaneous nodes (e.g., X_t and Y_t) is ambiguous, we do not consider the undirected contemporaneous link (a link connecting two nodes at the same time step, e.g., $X_t - Y_t$) in this study. Thus, it allows the time series graph to be a directed acyclic graph (DAG), where no directed loops exists [Spirtes et al., 2000]. To connect the DAG

with the joint probability implied by the graph, we assume *causal Markov property* [Spirtes et al., 2000] that given the parents , P_{Z_t}, of any $Z_t \in \vec{X}$, Z_t is independent of its non-descendants $\vec{X}_t^- \backslash P_{Z_t}$ in the graph, which are the earlier dynamics excluding the direct causes of Z_t.

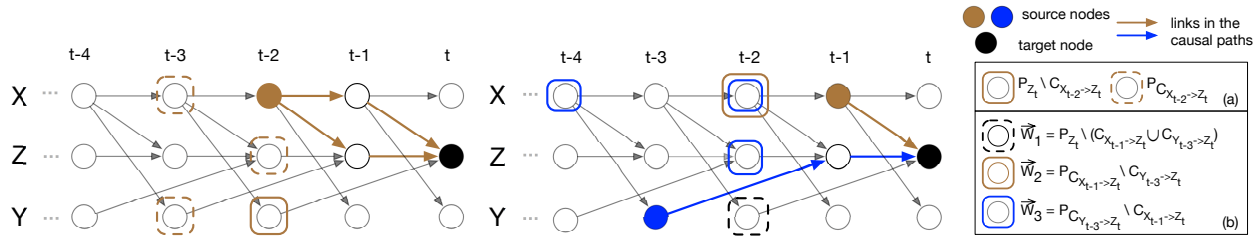

(a) The conditions for the causal path $C_{X_{t-2}\to Z_t}$ (b) The conditions for separable causal paths $C_{X_{t-1}\to Z_t}$ and $C_{Y_{t-3}\to Z_t}$

Figure 2.2: Illustration of the Markovian conditions for the causal subgraphs comprising one causal path and two separable causal paths shown in Figs. 1b and 1d, respectively. (a) The conditions for the causal path $C_{X_{t-2}\to Z_t}$ (brown solid circles: $P_{Z_t}\backslash C_{X_{t-2}\to Z_t}$ where $\backslash$ represents the subtraction operation for sets; the brown dashed circles: $P_{C_{X_{t-2}\to Z_t}}$). (b) The conditions for the separable causal paths $C_{X_{t-1}\to Z_t}$ and $C_{Y_{t-3}\to Z_t}$ (the black dashed circle: $\vec{W}_1$; the brown solid circle: $\vec{W}_2$; the blue solid circles: $\vec{W}_3$).

By drawing upon the causal Markov property, the potential infinite number of conditions in Eq.(2.5) from the past can be reduced to a finite number of conditions corresponding to the parents of the nodes of interest [Runge et al., 2012a]. Hence, the condition in Eq.(2.5) can be reduced into the parents of the two nodes such that

$$X_{t-\tau} \not\perp\!\!\!\perp Z_t \mid [P_{X_{t-\tau}} \cup (P_{Z_t}\backslash\{X_{t-\tau}\})], \tag{2.6}$$

where $P_{X_{t-\tau}}$ represents the parents of the source node $X_{t-\tau}$, and $P_{Z_t}\backslash\{X_{t-\tau}\}$ denotes the parents of Z_t excluding the node $X_{t-\tau}$ if $X_{t-\tau} \in P_{Z_t}$.

Based on Eq.(2.6), MIT $I^{MIT}_{X_{t-\tau}\to Z_t}$ in Eq.(1.8) quantifies the coupling strength between two nodes (e.g., $X_{t-\tau}$ and Z_t) linked by a directed edge. Similarly, when $X_{t-\tau}$ influences Z_t indirectly through the corresponding causal path $C_{X_{t-\tau}\to Z_t}$, MITP in Eq.(1.9) [Runge, 2015] accounts for the amount of information transferred from $X_{t-\tau}$ to Z_t via $C_{X_{t-\tau}\to Z_t}$. Consider Fig. 2.2a as an example. The conditions for $I^{MITP}_{X_{t-2}\to Z_t}$ are $\{X_{t-3}, Z_{t-2}, Y_{t-2}, Y_{t-3}\}$. By conditioning on the parents of the nodes involved (i.e., $\{Z_t\} \cup C_{X_{t-\tau}\to Z_t}$), the calculated interaction information prevents the information of the complementary causal graph from entering into the calculation.

The idea of momentary information is further extended to analyze how one node (i.e., $Y_{t-\tau_Y}$) in the causal path $C_{X_{t-\tau_X}\to Z_t}$ affects the information transfer in $C_{X_{t-\tau_X}\to Z_t}$ through momentary interaction information

(MII) [Runge, 2015]. Similar to MITP, by conditioning on the parents of the causal path, MII is given by:

$$\Delta I^{M}_{X_{t-\tau_X}\to Z_t|Y_{t-\tau_Y}} = \mathcal{I}(X_{t-\tau_X}; Y_{t-\tau_Y}; Z_t \mid [P_{C_{X_{t-\tau_X}\to Z_t}} \cup (P_{Z_t} \backslash C_{X_{t-\tau_X}\to Z_t})]), \tag{2.7}$$

which is a conditional interaction information [Cover and Thomas, 2006].

The utilization of a time series graph not only allows the visualization of the interactions among several nodes, but also facilitates the quantification of these interactions across different time points through different momentary information measures. Especially, MITP and MII [Runge, 2015] are the first attempts to quantify the information transfer between two nodes through a causal path and the casual interactions among three nodes in a causal path, which provides a starting point to develop the *momentary partial information decomposition* (MPID) described in the next section.

2.3 Momentary Partial Information Decomposition

In general, a target node Z_t is not only influenced by one lagged source node $X_{t-\tau}$ through either a direct link or a causal path, but also driven by multiple lagged source nodes $\vec{V}$ through a multitude of causal paths, which forms a causal subgraph $C_{\vec{V}\Rightarrow Z_t} \equiv \cup_{X_{t-\tau}\in\vec{V}} C_{X_{t-\tau}\to Z_t}$. Also, it is clear that the dynamics within a causal subgraph are affected by the remaining graph preceding the target, $\vec{X}_t^- \backslash C_{\vec{V}\Rightarrow Z_t}$, called as *complementary causal subgraph*. The interaction among multiple nodes in a time series graph poses a question of how to characterize the different contents of information transfer through a causal subgraph consisting of multiple causal paths, while at the same time, with the influence of its complementary causal subgraph eliminated.

In this section, we describe the mathematical framework of the *momentary partial information decomposition* (MPID) for quantifying and categorizing the information transfer to a target from a preceding causal subgraph starting with two sources with separable causal paths. First, we build on the momentary interaction information, which only considers one causal path, to formulate the *momentary interaction information for separable causal paths* (MII-SCP). Then, we review the recent advancements in PID, including the rescaled redundancy approach for estimating PID [Goodwell and Kumar, 2017a]. Lastly, based on the chosen PID framework, MPID is developed for partitioning the interaction of information transfer arising from separable causal paths into synergistic, redundant and unique components.

2.3.1 Momentary Interaction Information for Separable Causal Paths

From a time series graph perspective, the PID of a three-variable interaction at specific lagged times is induced by the information transfer from a subgraph containing two separable causal paths of the sources towards the target, such as the case shown in Fig. 2.1e. The separability of the two causal paths emphasizes the fact that neither source lies in the causal path of the other. That is, two causal paths (i.e., $C_{X_{t-\tau_X}\to Z_t}$ and $C_{Y_{t-\tau_Y}\to Z_t}$) are *separable* if $(Y_{t-\tau_Y} \notin C_{X_{t-\tau_X}\to Z_t}) \wedge (X_{t-\tau_X} \notin C_{Y_{t-\tau_Y}\to Z_t})$, where $\wedge$ is the logical AND symbol. However, it should be noted that the two causal paths can also be non-separable if one source belongs to the causal path of the other (such as the case in Fig. 2.1c), in which case, as shown below, the formulation reduces to that in Eq.(2.7).

To compute MPID, the calculated interaction information along two separable causal paths in Eq.(2.4) is required to be isolated from complementary causal subgraph containing the historical information of the dynamics. Nevertheless, MII is not an appropriate option to use as it is formulated for the situation of one causal path as shown in Eq.(2.7). Hence, the *momentary interaction information for separable causal paths* (MII-SCP) is given as

$$\Delta I^{MSCP}_{\{X_{t-\tau_X},Y_{t-\tau_Y}\}\to Z_t} = \mathcal{I}(X_{t-\tau_X}; Y_{t-\tau_Y}; Z_t \mid \vec{W}), \tag{2.8}$$

where

$$\vec{W} = \vec{W}_1 \cup \vec{W}_2 \cup \vec{W}_3 \tag{2.9a}$$

with

$$\vec{W}_1 = P_{Z_t} \backslash (C_{X_{t-\tau_X}\to Z_t} \cup C_{Y_{t-\tau_Y}\to Z_t}) \tag{2.9b}$$

$$\vec{W}_2 = P_{C_{X_{t-\tau_X}\to Z_t}} \backslash C_{Y_{t-\tau_Y}\to Z_t} \tag{2.9c}$$

$$\vec{W}_3 = P_{C_{Y_{t-\tau_Y}\to Z_t}} \backslash C_{X_{t-\tau_X}\to Z_t}. \tag{2.9d}$$

The condition set, $\vec{W}$, for the MII-SCP represents the parents of the union set of both the target Z_t and the causal paths from the two sources to the target (i.e. $C_{X_{t-\tau_X}\to Z_t}, C_{Y_{t-\tau_Y}\to Z_t}$). It consists of three parts: (1) $\vec{W}_1$, the parents of the target node P_{Z_t} excluding those in the two causal paths; (2) $\vec{W}_2$, the parents of the causal path $C_{X_{t-\tau_X}\to Z_t}$ (i.e., $P_{C_{X_{t-\tau_X}\to Z_t}}$) excluding the nodes in $C_{Y_{t-\tau_Y}\to Z_t}$, and (3) $\vec{W}_3$, the parents of $C_{Y_{t-\tau_Y}\to Z_t}$ (i.e., $P_{C_{Y_{t-\tau_Y}\to Z_t}}$) excluding those in $C_{X_{t-\tau_X}\to Z_t}$. It is noted that when the causal paths of the two sources are non-separable, MII-SCP is reduced to MII in Eq.(2.7).

In the example of the three-variable system in Fig. 2.2b, the condition $\vec{W}$ for MII-SCP between the target Z_t and two sources X_{t-1} and Y_{t-3} (i.e., $\Delta I^{MII-SCP}_{\{X_{t-\tau_1}, Y_{t-\tau_2}\} \to Z_t}$) includes (1) $\vec{W}_1 = \{Y_{t-2}\}$ (black dashed circle), (2) $\vec{W}_2 = \{X_{t-2}\}$ (brown solid circle) and (3) $\vec{W}_3 = \{X_{t-4}, X_{t-2}, Z_{t-2}\}$ (blue solid circle). Therefore, $\vec{W} = \{X_{t-2}, X_{t-4}, Y_{t-2}, Z_{t-2}\}$.

Furthermore, when two causal paths are non-separable (i.e., one source lies in the causal path of the other source), MII-SCP collapses into MII. Suppose the source $Y_{t-\tau_Y} \in C_{X_{t-\tau_X} \to Z_t}$, then $C_{Y_{t-\tau_Y} \to Z_t} \in C_{X_{t-\tau_X} \to Z_t})$). The first term in the condition $\vec{W}$, i.e., $P_{Z_t} \backslash (C_{X_{t-\tau_X} \to Z_t} \cup C_{Y_{t-\tau_Y} \to Z_t})$, is reduced to $P_{Z_t} \backslash C_{X_{t-\tau_X} \to Z_t}$. Also, the remaining terms in $\vec{W}$, i.e., $\vec{W}_2 \cup \vec{W}_3$, can be simplified to $P_{C_{X_{t-\tau_X} \to Z_t}}$, since the purpose of the two terms is to choose all the parents of the union of two causal paths which is now $C_{X_{t-\tau_X} \to Z_t}$. Therefore, the condition set $\vec{W}$ is reduced to $P_{C_{X_{t-\tau_X} \to Z_t}} \cup (P_{Z_t} \backslash C_{X_{t-\tau_X} \to Z_t})$, the same condition as in MII in (Eq.(2.7)).

2.3.2 Framework for Partial Information Decomposition

Besides MII-SCP, MPID needs to provide a further characterization of the information transfer from $X_{t-\tau_X}$ and $Y_{t-\tau_Y}$ to Z_t through the corresponding causal paths in terms of the synergistic, unique and redundant information. Nevertheless, to compute the four components U_Y, U_X, R and S in the PID from three equations Eqs.(2.1)-(2.3), one more condition is needed. To that end, various approaches for quantifying one of the components in PID, that is, redundancy, synergy and unique information, have been proposed. In addition to propose the PID framework, Williams and Beers [Williams and Beer, 2010] were also the first to propose a redundancy measure (see Section 2.5.1) based on the minimum specific information for the target at the outcome of a source value. However, this measure overestimates the redundancy [Harder et al., 2013, Ince, 2017], because it assumes that the amount of information shared between the two variables is also the same as the impact of the two variables on the target variable. In fact, it represents the upper bound of the information that can be redundantly shared with the target variable. Despite this drawback, it emphasizes the idea that the redundancy and unique information are dependent on the marginal joint distribution between each source variable and the target, which enables a series of further measures for unique [Bertschinger et al., 2014], synergistic [Griffith and Koch, 2014, Olbrich et al., 2015] and redundant [Griffith and Ho, 2015, Barrett, 2015] information. Barrett [Barrett, 2015] defined the redundancy as the minimum mutual information between each source and the target, which is equivalent to some of the early PID frameworks [Williams and Beer, 2010, Bertschinger et al., 2014, Griffith and Koch, 2014] in Gaussian systems. Furthermore, in computing the redundancy, besides anchoring the redundancy upon the marginal joint distributions between the sources and the target, there is also a trend to utilize other

aspects in the joint distribution of all the considered variables in computing the redundancy. Harder et al. [Harder et al., 2013] quantified the redundant information based on the distance between the conditional distribution of the target given each source by using Kullback-Leibler divergence. Ince [Ince, 2017] computed the redundancy as the expected pointwise change of the surprisal of the target given the sources from the local interaction information based on an entropy-maximized joint distribution, thus distinguishing the redundancy-related elements in interaction information. Goodwell and Kumar [Goodwell and Kumar, 2017a] put forward a rescaled redundancy which considers the mutual information between the sources in accounting for the minimum mutual information-based redundancy.

In this study, to formulate the momentary partial information decomposition (MPID), we adopt the PID framework based on the rescaled redundancy, R_S, [Goodwell and Kumar, 2017a], which is given by:

$$R_S = R_{min} + I_s(R_{MMI} - R_{min}), \tag{2.10a}$$

where

$$R_{MMI} = \min[I(X_{t-\tau_X}; Z_t), I(Y_{t-\tau_Y}; Z_t)] \tag{2.10b}$$

$$I_s = \frac{I(X_{t-\tau_X}; Y_{t-\tau_Y})}{\min[H(X_{t-\tau_X}), H(Y_{t-\tau_Y})]} \tag{2.10c}$$

$$R_{min} = \begin{cases} 0, & \text{if } \mathcal{I} \geq 0 \\ -\mathcal{I}, & \text{otherwise.} \end{cases} \tag{2.10d}$$

R_{MMI} represents the *minimum mutual information*, originating from the fact that the redundant information should not be larger than the smallest value of the mutual information between any source and target variables [Barrett, 2015]. We choose the rescaled approach in computing the redundancy because it is able to reduce the overestimation from R_{MMI} as well as guarantee non-negativity of PID, and it is also empirically computable from time series observational data. To ensure a non-negative PID, R_{MMI} and R_{min} are used for providing the upper and lower bounds, respectively, for the redundant information. It is noted that we assume the non-negativity of PID in this study, which is termed as "local positivity" property in [Bertschinger et al., 2013], because the non-negative partitioning is essential in illustrating physical phenomenon in a meaningful way, though there exist considerations for dropping the non-negativity condition for PID [Ince, 2017]. Furthermore, the rescaling coefficient I_s is used to scale R_{MMI} (which overestimates the redundancy) based on the mutual information between the sources. Besides, many proposed PID frameworks are computationally difficult or costly when using observational time

series data due to the requirement of an optimization procedure for computing a metric based on marginal distributions [Bertschinger et al., 2014, Griffith and Ho, 2015, Ince, 2017]. Meanwhile, the rescaled redundancy approach, which has been applied in ecohydrological time series data [Goodwell and Kumar, 2017a, Goodwell and Kumar, 2017b], is empirically computable and thus may have a broader applications associated with empirical analysis across many physical domains. Also, it is noted that the rescaled approach, as formulated in Eq.(2.10) [Goodwell and Kumar, 2017a], is applicable to the interaction between two sources similar to other redundancy measures [Harder et al., 2013, Griffith and Koch, 2014, Bertschinger et al., 2014].

Nonetheless, recognizing that there is no universal agreement on the additional condition for quantifying PID so far, we also provide the formulations for the MPIDs based on three other redundancy measures in Section 2.5.

2.3.3 Framework for Momentary Partial Information Decomposition

Based on the rescaled redundancy in Eq.(2.10), in a manner similar to MII-SCP, we propose the *momentary partial information decomposition* (MPID) by conditioning all the components in the original PID (Eqs.(2.1)-(2.3)) on $\vec{W}$ such that:

$$\Delta I^{MSCP}_{\{X_{t-\tau_X},Y_{t-\tau_Y}\}\to Z_t} = S_c - R_c \tag{2.11a}$$

$$R_c = R_{min,c} + I_{s,c}(R_{MMI,c} - R_{min,c}) \tag{2.11b}$$

$$U_{X,c} = I(Z_t; X_{t-\tau_X}|\vec{W}) - R_c \tag{2.11c}$$

$$U_{Y,c} = I(Z_t; Y_{t-\tau_Y}|\vec{W}) - R_c, \tag{2.11d}$$

where

$$R_{MMI,c} = \min[I(X_{t-\tau_X}; Z_t|\vec{W}), I(Y_{t-\tau_Y}; Z_t|\vec{W})] \tag{2.11e}$$

$$I_{s,c} = \frac{I(X_{t-\tau_X}; Y_{t-\tau_Y}|\vec{W})}{\min[H(X_{t-\tau_X}|\vec{W}), H(Y_{t-\tau_Y}|\vec{W})]} \tag{2.11f}$$

$$R_{min,c} = \begin{cases} 0, & \text{if } \Delta I^{MSCP} \geq 0 \\ -\Delta I^{MSCP}, & \text{otherwise.} \end{cases} \tag{2.11g}$$

The subscript c stands for "conditional". We note that the original suggestion of forming conditional redundancies was given by Bertschinger et al. [Bertschinger et al., 2013] [2].

[2]The conditional redundancy proposed by Bertschinger et al. [Bertschinger et al., 2013] suggests a "left chain rule", which is a generalization of the chain rule of mutual information. The "left chain rule" property is not fulfilled in most redundancy

2.4 Coupling Strength Autonomy for Momentary Partial Information Decomposition

The causal Markov property of the time series graph ensures the momentary information approaches (e.g., MII, MITP and MII-SCP) exclude the influence of the complementary causal subgraph. This allows us to approximate the causal interactions among variables of interest. However, these metrics are still dependent on the Markovian conditions, such as $\vec{W}$ in MII-SCP. Nevertheless, Runge [Runge, 2015] showed that under some conditions, MII and MITP are autonomous of how the nodes of interest interact with the nodes in the complementary causal subgraph, a property described as *coupling strength autonomy*. In this section, we generalize this property to MPID. Two conditions (i.e., *additivity* and *linearity*) used for the verification of coupling strength autonomy property in MII are also adopted here, with one more condition, *separability*, which allows the analysis of MPID when the causal paths of the two source nodes are separable. Then, the coupling strength autonomy property of MPID is shown for two common driver models. In the first model, the interaction among the variables of interest is linear, and nonlinear in the second model. For the former, the analytical solution of MPID is derived and compared with the interaction information without conditioning. For the latter, a numerical simulation is conducted to estimate both MPID and PID.

2.4.1 Coupling Strength Autonomy in MPID

Consider a multivariate stationary discrete-time process $\vec{X} = \{X, Y, Z, \dots\}_N$, where X, Y, Z, etc. are sub-processes. The process $\vec{X}$ satisfies the causal Markov property with its corresponding time series graph G as described in Section 2.2. We assume that for $\tau_X, \tau_Y \geq 0$, both the source nodes $X_{t-\tau_X}$ and $Y_{t-\tau_Y}$ are connected with the target node Z_t through two causal paths $C_{X_{t-\tau_X} \to Z_t}$ and $C_{Y_{t-\tau_Y} \to Z_t}$, respectively. Also, the union of the two causal paths and the target node is represented as $\vec{B}$, that is

$$\vec{B} = C_{X_{t-\tau_X} \to Z_t} \cup C_{Y_{t-\tau_Y} \to Z_t} \cup Z_t. \tag{2.12}$$

For the dependencies of each node $K_{t-\tau} \in \vec{B}$ ($\tau \geq 0$), the following conditions are defined:

(i) *Additivity*: Dependencies of $K_{t-\tau}$ in the following are additive:

- its parents belonging to $\vec{B}$ (denoted as $P^{\vec{B}}_{K_{t-\tau}} \equiv P_{K_{t-\tau}} \cap \vec{B}$),
- its remaining parents (denoted as $P_{K_{t-\tau}} \backslash P^{\vec{B}}_{K_{t-\tau}}$), and
- the noise term representing the modelling uncertainty.

measures but it's promising in a recent chapter about pointwise information decomposition [Finn and Lizier, 2018]

Therefore, any $K_{t-\tau} \in \vec{B}$ ($\tau \geq 0$) can be written as

$$K_{t-\tau} = f_K(P^{\vec{B}}_{K_{t-\tau}}) + g_K(P_{K_{t-\tau}} \backslash P^{\vec{B}}_{K_{t-\tau}}) + \eta^K_{t-\tau}, \tag{2.13}$$

where f_K, g_K are the arbitrary functions for $K_{t-\tau}$, and $\eta^K_{t-\tau}$ is the noise term which is assumed as independent and identically distributed (i.i.d.). It can be observed that $P^{\vec{B}}_{K_{t-\tau}}$ (i.e., the dependencies in f_K) belongs to $\vec{B}$, while $P_{K_{t-\tau}} \backslash P^{\vec{B}}_{K_{t-\tau}}$ (i.e., the dependencies in g_K) belongs to $\vec{W}$ defined in Eq.(2.8).

(ii) *Linearity in* f_K: The function f_K for each node $K_{t-\tau} \in \vec{B}$ is linear. It means the dependence of $K_{t-\tau}$ on the part of its parents belonging to $\vec{B}$ (i.e., $P^{\vec{B}}_{K_{t-\tau}}$), is linear. The linearity also implies that the nodes in $\vec{B}$ (Eq.(2.12)) linearly depend on each other.

(iii) *Separability of the causal paths* $C_{X_{t-\tau_X} \to Z_t}$ *and* $C_{Y_{t-\tau_Y} \to Z_t}$: Neither of the two sources lies in the causal path from the other source to the target. That is, two causal paths (i.e., $C_{X_{t-\tau_X} \to Z_t}$ and $C_{Y_{t-\tau_Y} \to Z_t}$) are *separable* if $(Y_{t-\tau_Y} \notin C_{X_{t-\tau_X} \to Z_t}) \wedge (X_{t-\tau_X} \notin C_{Y_{t-\tau_Y} \to Z_t})$.

Theorem: Coupling strength autonomy for momentary partial information decomposition. In a stationary discrete-time multivariate process $\vec{X}$, which meets the causal Markov property in its time series graph, the MPID for the contribution from two sources $X_{t-\tau_X}$ and $Y_{t-\tau_Y}$ ($\tau_X, \tau_Y \geq 0$) to the target Z_t have the following properties (proof is given in the Appendices A & B):

(a) If all the three conditions (i.e., *additivity*, *linearity* and *separability*) hold, MPID defined in Eqs.(2.11a)-(2.11b) can be written as:

$$\Delta I^{MSCP}_{\{X_{t-\tau_X}, Y_{t-\tau_Y}\} \to Z_t} = I(\eta^X_{t-\tau_X}; \eta^Y_{t-\tau_Y} \mid \tilde{f}_Z(\bullet) + \eta^Z_t) \tag{2.14a}$$

$$R_c = R_{min,c} \tag{2.14b}$$

$$S_c = \Delta I^{MSCP} + R_c \tag{2.14c}$$

$$U_{X,c} = I(\eta^X_{t-\tau_X}; \tilde{f}_Z(\bullet) + \eta^Z_t) - R_c \tag{2.14d}$$

$$U_{Y,c} = I(\eta^Y_{t-\tau_Y}; \tilde{f}_Z(\bullet) + \eta^Z_t) - R_c, \tag{2.14e}$$

where $R_{min,c}$ is given in Eq.(2.11b) and $\tilde{f}_Z(\bullet)$ is a linear combination of all the noise terms η_t of the nodes in $\vec{B}$, which are simplified as the symbol $\bullet$. In brief, *additivity* allows the exclusion of the dependencies not in $\vec{B}$ (i.e., $g_K(P_{K_{t-\tau}} \backslash P^{\vec{B}}_{K_{t-\tau}})$) in the calculation of the information partitioning due to the translational invariance property of both entropy and mutual information (see Appendix A for details). Furthermore, *separability* ensures both the minimum redundancy and the zeros of f_X and f_Y, because $X_{t-\tau_X}$ and $Y_{t-\tau_Y}$ now do not depend on any nodes in the two separable causal paths. Also, *linearity* converts the dependencies in the $\vec{B}$

(i.e., $f_K(P^{\vec{B}}_{K_{t-\tau}})$) to be linear functions $\tilde{f}$ of all the noise terms in $\vec{B}$ after the exclusion of the non-linear dependencies $g_K(P_{K_{t-\tau}} \backslash P^{\vec{B}}_{K_{t-\tau}})$. Therefore, the condition set $\vec{W}$ is cancelled out since the calculations are now only determined by the nodes in the causal paths and the target node (*i.e.*, $\vec{B}$) due to the *linearity* and *additivity* conditions.

(b) If only *additivity* and *linearity* hold, both f_X and f_Y can be converted into linear functions of the noise terms of the nodes in $\vec{B}$ (similar to how f_Z is converted into $\tilde{f}_Z$ in (a)). However, since *separability* does not hold, the redundancy R_c is not the minimum and f_X and f_Y can be nonzero. Hence, we can express the corresponding MPID as

$$\Delta I^{MSCP}_{\{X_{t-\tau_X}, Y_{t-\tau_Y}\} \to Z_t} = \mathcal{I}(\tilde{f}_X(\bullet) + \eta^X_{t-\tau_X}; \tilde{f}_Y(\bullet) + \eta^Y_{t-\tau_Y}; \tilde{f}_Z(\bullet) + \eta^Z_t) \tag{2.15a}$$

$$R_c = R_{min,c} + I_{s,c}(R_{MMI,c} - R_{min,c}) \tag{2.15b}$$

$$S_c = \Delta I^{MSCP} + R_c \tag{2.15c}$$

$$U_{X,c} = I(\tilde{f}_X(\bullet) + \eta^X_{t-\tau_X}; \tilde{f}_Z(\bullet) + \eta^Z_t) - R_c \tag{2.15d}$$

$$U_{Y,c} = I(\tilde{f}_Y(\bullet) + \eta^Y_{t-\tau_Y}; \tilde{f}_Z(\bullet) + \eta^Z_t) - R_c, \tag{2.15e}$$

where both $\tilde{f}_X(\bullet)$ and $\tilde{f}_Y(\bullet)$ are the linear functions of all the noise terms η_t of the nodes in $\vec{B}$ for $X_{t-\tau_X}$ and $Y_{t-\tau_Y}$, respectively, and

$$R_{MMI,c} = \min[I(\tilde{f}_X(\bullet) + \eta^X_{t-\tau_X}; \tilde{f}_Z(\bullet) + \eta^Z_t), I(\tilde{f}_Y(\bullet) + \eta^Y_{t-\tau_Y}; \tilde{f}_Z(\bullet) + \eta^Z_t)] \tag{2.16a}$$

and

$$I_{s,c} = \frac{I(\tilde{f}_X(\bullet) + \eta^X_{t-\tau_X}; \tilde{f}_Y(\bullet) + \eta^Y_{t-\tau_Y})}{\min[H(\tilde{f}_X(\bullet) + \eta^X_{t-\tau_X}), H(\tilde{f}_Y(\bullet) + \eta^Y_{t-\tau_Y})]}. \tag{2.16b}$$

(c) If only *additivity* and *separability* hold, the redundancy R_c is minimized with f_X and f_Y vanishing. However, because of the nonlinearity in f, the condition set $\vec{W}$ cannot be cancelled out. Thus, the MPID is reduced to

$$\Delta I^{MSCP}_{\{X_{t-\tau_X}, Y_{t-\tau_Y}\} \to Z_t} = I(\eta^X_{t-\tau_X}; \eta^Y_{t-\tau_Y} \mid \{f_Z(P^{\vec{B}}_{Z_t}) + \eta^Z_t\} \cup \vec{W}) \tag{2.17a}$$

$$U_{X,c} = I(\eta^X_{t-\tau_X}; f_Z(P^{\vec{B}}_{Z_t}) + \eta^Z_t \mid \vec{W}) - R_c \tag{2.17b}$$

$$U_{Y,c} = I(\eta^Y_{t-\tau_Y}; f_Z(P^{\vec{B}}_{Z_t}) + \eta^Z_t \mid \vec{W}) - R_c. \tag{2.17c}$$

It can be observed that the *additivity* and *linearity* conditions allow MPID to be dependent only on the

nodes in the union of the two causal paths and the target node (see Eqs.(2.14) and (2.15)).

Furthermore, under the *separability* condition, the redundant information R_c achieves the minimum value $R_{min,c}$ (see Eq.(2.14b)). It is intuitive that without the influence of other factors (e.g., a common driver), the two *separable* source variables are independent, and therefore, the redundant information is minimized.

2.4.2 A Common Driver Model

Now we verify the coupling strength autonomy property for MPID in both a linear and a nonlinear model solved analytically and numerically, respectively. Let's consider a common driver model involving four sub-processes (i.e., V X, Y and Z). V is the common driver of X and Y, both of which cause Z. All the causal relationships are delayed at one time step. Fig. 2.3 illustrates the process network graph and the time series graph of the model. We show that by adopting MPID, the effect of the common driver V in the PID of X, Y and Z is eliminated completely in the linear model and significantly in the nonlinear model.

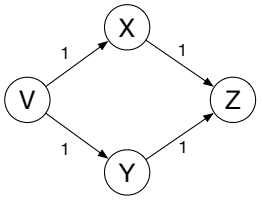

(a) The process network graph

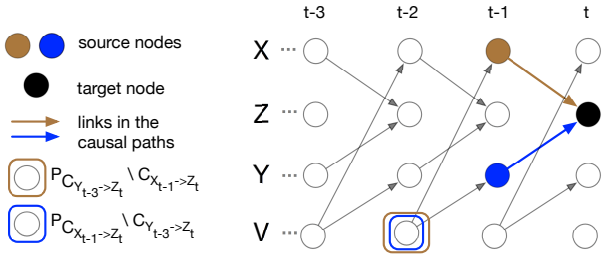

(b) The time series graph

Figure 2.3: The common driver model. (a) is the process network graph representation, where the numbers on the directed links represent the delayed time step. (b) is the time series graph representation, where brown and blue circles are the source nodes, (i.e., X_{t-1} and Y_{t-1}), black circle is the target node (i.e., Z_t), brown circle represents the nodes in $P_{C_{X_{t-1}\to Z_t}} \backslash C_{Y_{t-1}\to Z_t}$ and blue circle refers to the nodes in $P_{C_{Y_{t-1}\to Z_t}} \backslash C_{X_{t-1}\to Z_t}$. Also, $P_{Z_t} \backslash (C_{X_{t-1}\to Z_t} \cup C_{Y_{t-1}\to Z_t})$ is empty in this case. Therefore, the condition set $\vec{W}$ is only $\{V_{t-2}\}$.

A linear common driver model

The linear common driver model can be written as

$$\begin{aligned} V_t &= \eta_t^V \\ X_t &= c_{VX}\, V_{t-1} + \eta_t^X \\ Y_t &= c_{VY}\, V_{t-1} + \eta_t^Y \\ Z_t &= c_{XZ}\, X_{t-1} + c_{YZ}\, Y_{t-1} + \eta_t^Z. \end{aligned} \tag{2.18}$$

The i.i.d. noise terms for each variable are represented as η_t^V, η_t^X, η_t^Y and η_t^Z, following normal distributions $\mathcal{N}(0, \sigma_V^2)$, $\mathcal{N}(0, \sigma_X^2)$, $\mathcal{N}(0, \sigma_Y^2)$ and $\mathcal{N}(0, \sigma_Z^2)$, respectively. The coefficients, c_{VX}, c_{VY}, c_{XZ} and c_{YZ}, are the coupling strengths between variables. Especially, c_{VX} and c_{VY} quantify the effect of the common driver of V_{t-1} on X_t and Y_t, respectively. In the following, the analytical solutions of both MPID and PID for quantifying the information transfer from two sources X_{t-1} and Y_{t-1} and the target Z_t are shown sequentially.

MPID for X_{t-1}, Y_{t-1} and Z_t: According to the definition of the condition in Eq.(2.8), the condition set $\vec{W}$ for $\Delta I^{MSCP}_{\{X_{t-1}, Y_{t-1}\} \to Z_t}$ is $\{V_{t-2}\}$ as shown in Fig. 2.3b. Therefore, the analytical solutions of $\vec{W}$ for $\Delta I^{MSCP}_{\{X_{t-1}, Y_{t-1}\} \to Z_t}$, R_c and S_c are given as:

$$\Delta I^{MSCP}_{\{X_{t-1}, Y_{t-1}\} \to Z_t} = \frac{1}{2} \ln \left\{ 1 + \frac{c_{XZ}^2\, c_{YZ}^2\, \sigma_X^2\, \sigma_Y^2}{\sigma_Z^2 (\sigma_Z^2 + c_{XZ}^2\, \sigma_X^2 + c_{YZ}^2\, \sigma_Y^2)} \right\} \tag{2.19a}$$

$$R_c = 0 \tag{2.19b}$$

$$S_c = \Delta I^{MSCP}_{\{X_{t-1}, Y_{t-1}\} \to Z_t}. \tag{2.19c}$$

The derivation is available in Appendix C. It is easy to verify that the linear common driver model example fulfills all the three conditions (*linearity*, *additivity* and *separability*), thus the corresponding MPID follows the results in Eqs.(2.14a)-(2.14e). Obviously, MPID is autonomous such that it is independent of c_{VX} and c_{VY} – the impact from the common driver V_{t-2}. Moreover, in this case, because $\Delta I^{MSCP}_{\{X_{t-1}, Y_{t-1}\} \to Z_t} > 0$, the redundant information R_c achieves the minimum value $R_{min} = 0$ in MPID. It implies that there is only synergistic information in the contribution of X_{t-1} and Y_{t-1} in generating Z_t.

PID for X_{t-1}, Y_{t-1} and Z_t: The analytical solution of the interaction information $\mathcal{I}(X_{t-1}; Y_{t-1}; Z_t)$ is

given by

$$\mathcal{I}(X_{t-1};Y_{t-1};Z_t) = \frac{1}{2}\ln\Big\{\frac{(c_{XZ}^2\, b + \Gamma_X\, \sigma_Z^2)(c_{YZ}^2\, b + \Gamma_Y\, \sigma_Z^2)}{\sigma_Z^2\, \Gamma_X\, \Gamma_Y (\sigma_Z^2 + c_{XZ}^2\, \Gamma_X^2 + c_{YZ}^2\, \Gamma_Y^2 + d)}\Big\}, \tag{2.20}$$

where $b = c_{VY}^2\, \sigma_V^2\, \sigma_X^2 + c_{VX}^2\, \sigma_V^2\, \sigma_Y^2 + \sigma_Y^2\, \sigma_X^2$, $d = 2\, c_{XZ}\, c_{YZ}\, c_{VY}\, c_{VX}\, \sigma_V^2$, $\Gamma_X = c_{VX}^2\, \sigma_V^2 + \sigma_X^2$, $\Gamma_Y = c_{VY}^2\, \sigma_V^2 + \sigma_Y^2$ and $d = c_{YZ}^2\, \Gamma_Y^2 + 2\, c_{XZ}\, c_{YZ}\, c_{VY}\, c_{VX}\, \sigma_V^2$. For a full derivation, see Appendix C.

Eq.(2.20) shows that $\mathcal{I}(X_{t-1};Y_{t-1};Z_t)$ depends on c_{VX} and c_{VY} through b, d, Γ_X and Γ_Y. The dependence implies that the common driver V plays a role in determining $\mathcal{I}(X_{t-1};Y_{t-1};Z_t)$, which is in contrast to $\Delta I^{MSCP}_{\{X_{t-1},Y_{t-1}\}\to Z_t}$ which exhibits the coupling strength autonomy property. It demonstrates that in this linear system, by conditioning on the common driver V_{t-2}, the proposed momentary information measure, $\Delta I^{MSCP}_{\{X_{t-1},Y_{t-1}\}\to Z_t}$, is able to eliminate the influence from the complementary causal subgraph.

To explore this further, the coupling strength coefficients c_{VX} and c_{VY} are altered to see how V affect S and R. Suppose X and Y are strongly driven by V such that c_{VX} and c_{VY} are much larger than other coefficients in Eq.(2.18). Also, assume both the coupling coefficients c_{VX} and c_{VY} are in the same order of magnitude, that is:

$$c_{VX} \approx c_{VY} \approx h, \text{ and } h \gg c, \forall c \in \{c_{XZ}, c_{YZ}, \sigma_V, \sigma_X, \sigma_Y, \sigma_Z\}.$$

Therefore, $\mathcal{I}(X_{t-1};Y_{t-1};Z_t)$ in Eq.(2.20) can be reduced to

$$\mathcal{I}(X_{t-1};Y_{t-1};Z_t) \approx \frac{1}{2}\ln\frac{1}{h^2}. \tag{2.21}$$

Especially, when $|h| > 1$, $\mathcal{I}(X_{t-1};Y_{t-1};Z_t) < 0$, implying that $S < R$ according to the relationship among $\mathcal{I}$, S and R in Eq.(2.4). It means a strong coupling strength from the common driver V_{t-2} would result in more redundant information from X_{t-1} and Y_{t-1}, even though the dynamics among X_{t-1}, Y_{t-1} and Z_t alone do not suggest any redundancy from the two sources as shown in Eq.(2.19c). This is crucial in that the empirically estimated PID without an appropriate conditioning as in ΔI^{MSCP} would probably be influenced by other factors (e.g., the common driver in this example), thus hiding the true dynamics of the variables of interest.

A nonlinear common driver model

Next, we examine the coupling strength autonomy of MPID for a nonlinear model. The nonlinear model still follows the same causality structure of the common driver model in Fig. 2.3, but with a nonlinear

dependency between X and Y such that:

$$\begin{aligned} V_t &= \eta_t^V \\ X_t &= c_{VX}\, V_{t-1} + \eta_t^X \\ Y_t &= c_{VY}\, V_{t-1} + \eta_t^Y \\ Z_t &= c_Z\, X_{t-1}\, Y_{t-1} + \eta_t^Z. \end{aligned} \tag{2.22}$$

where c_Z is the coupling coefficient in the function of Z_t.

The MPID and the PID for X_{t-1}, Y_{t-1} and Z_t are estimated numerically for different combinations of c_{VX} and c_{VY}. c_Z and the standard deviations of all the noises (i.e., σ_V, σ_X, σ_Y and σ_Z) are set to 0.5 and 1, respectively. To compute the information-theoretic metrics (e.g., conditional entropy, conditional mutual information), the multivariate probability distribution is required and estimated based on the kernel density estimation method with the multivariate Gaussian kernel [Silverman, 1986]. For each combination of c_{VX} and c_{VY}, the sample length is 10,000.

Fig. 2.4 shows the estimated interaction information and the synergistic, redundant and unique information under both MPID and PID. It can be observed that for MPID, the redundant information, R_c, in the total information, I_{total}, is almost zero for different c_{VX} and c_{VY}, consistent with the conclusion that the redundancy is minimized when *additivity* and *separability* hold. Nevertheless, all the remaining metrics (i.e, MII-SCP, S_c, U_X, U_Y) vary with c_{VX} and c_{VY}. It suggests that the coupling strength autonomy is not entirely valid due to the nonlinearity in Z_t. Especially, both MII-SCP and S_c show higher values when both c_{VX} and c_{VY} are close to zero, illustrating more synergistic information from X_{t-1} and Y_{t-1} with the decrease of the influence from their common driver V_{t-2}.

With regards to PID (shown in the second column in Fig. 2.4), all the metrics are affected by V through c_{VX} and c_{VY}. The impacts of c_{VX} and c_{VY} on redundancy is illustrated in the increasing redundancy R with the two coefficients, consistent with the conclusion in the linear case (see Eqs.(2.20) and (2.21)). Furthermore, more interaction information $\mathcal{I}$ and synergistic information S is also observed for higher values of c_{VX} and c_{VY}.

By comparing the estimated results from MPID and PID in Fig. 2.4, we can draw the following conclusions. First, the effect from the external driver, V, on the redundancy for MPID (i.e., R_c) is negligible based on the nearly-zero values of R_c. Second, even though MII-SCP, S_c and the two unique information values ($U_{X,c}$ and $U_{Y,c}$) in MPID still depend on c_{VX} and c_{VY}, their variations in terms of the two coefficients (i.e., c_{VX} and c_{VY}) are much smaller than the corresponding metrics (i.e., $\mathcal{I}$ and S) in PID. It suggests that in

the nonlinear common driver model, the conditioning in MPID is able to significantly reduce the influences from the common driver V_{t-2} in quantifying the dynamics among X_{t-1}, Y_{t-1} and Z_t.

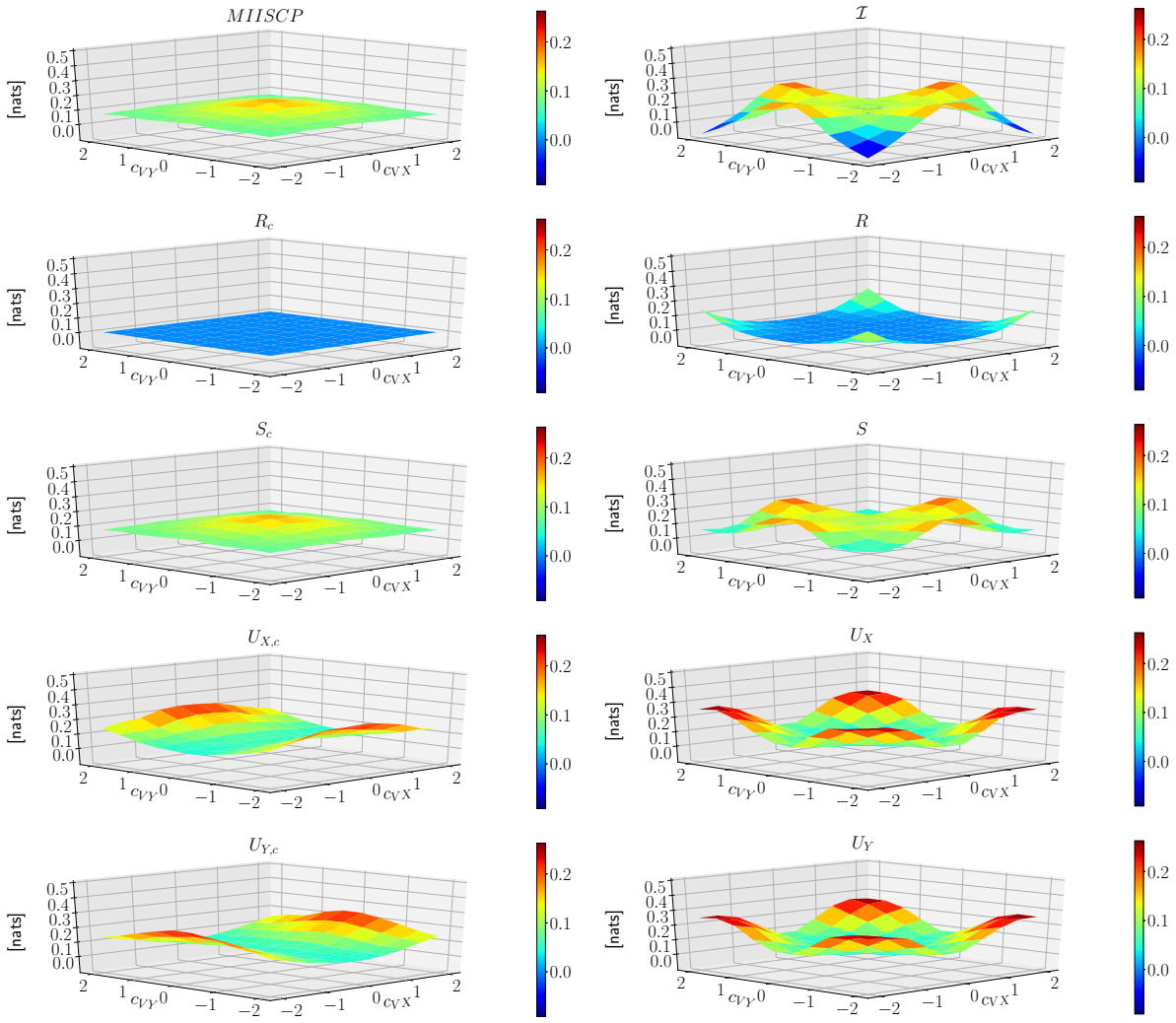

Figure 2.4: The estimated interaction information MII-SCP and $\mathcal{I}$ as well as SUR (i.e., redundant, synergistic and unique information) from both MPID (the left column) and PID (the right column) for the sources $\{X_{t-1}, Y_{t-1}\}$ and the target Z_t, based on Eq.(2.22) with a simulation time length 10000 for each combination of c_{VX} and c_{VY}.

2.5 Other Momentary Partial Information Decomposition Frameworks

In this study, we adopt the rescaled redundancy measure (Eq.(2.10)) to define the framework for the momentary partial information decomposition (MPID) in Eq.(2.11). However, because there is still no uni-

versal agreement on an appropriate condition to supplement Eqs.(2.1)-(2.3) to provide complete solution for estimating S, R, U_X and U_Y, researchers might prefer to adopt MPID based on alternate approaches, such as those in [Williams and Beer, 2010, Harder et al., 2013, Bertschinger et al., 2014, Griffith and Koch, 2014, Barrett, 2015, Ince, 2017]. Therefore, in this section, we provide the frameworks for MPID based upon three other redundancy measures based on: (1) minimum specific information R_{MSI} [Williams and Beer, 2010], (2) minimum mutual information R_{MMI} [Barrett, 2015], and (3) pointwise common change in surprisal R_{CCS} [Ince, 2017], with the corresponding conditional redundancies represented as $R_{MSI,c}$, $R_{MMI,c}$ and $R_{CCS,c}$ respectively. These conditional redundancy candidates can be used to replace the rescaled redundancy in Eq.(2.11b) for forming new MPID frameworks. However, except the $R_{MMI,c}$-based MPID, the coupling strength autonomy does not hold for the other two MPID frameworks. This is detailed at the end of this section along with other properties of these alternative MPID frameworks. Despite this, due to the causal Markov property, the proposed MPID frameworks based on various redundancy measurements are still helpful in excluding the influence of the history in quantifying the different information transfer in a causal subgraph, thus revealing the information partitioning from there alternative perspectives.

2.5.1 The Minimum Specific Information Approach

Williams and Beer [Williams and Beer, 2010] proposed the redundancy measure as the average minimum specific information over the considered input sources. The idea of defining the conditional version $R_{MSI,c}$ is to exclude the influence of the complementary causal subgraph in calculating the specific information for the two source nodes $X_{t-\tau_X}$ and $Y_{t-\tau_Y}$. Therefore, $R_{MSI,c}$ is given by:

$$R_{MSI,c} = \int \min_{A \in \{X_{t-\tau_X}, Y_{t-\tau_Y}\}} \{I(Z_t = z; A \mid \vec{W})\} p(z) dz, \tag{2.23}$$

where $I(Z_t = z; A \mid \vec{W})$ is the conditional specific information that $A \in \{X_{t-\tau_X}, Y_{t-\tau_Y}\}$ provides about the outcome $Z_t = z$ conditioned on $\vec{W}$ [Williams and Beer, 2010], and can be expressed as:

$$I(Z = z; A \mid \vec{W}) = \int_a \int_{\vec{w}} p(a, \vec{w}|z) [\ln \frac{p(z|a, \vec{w})}{p(z|\vec{w})}] da \, d\vec{w}. \tag{2.24}$$

2.5.2 The Minimum Mutual Information Approach

As part of R_c in Eq.(2.11b), the expression of $R_{MMI,c}$ is given in Eq.(2.11e).

2.5.3 The Pointwise Common Change in Surprisal Approach

Ince [Ince, 2017] characterized the redundancy, R_{CCS}, as the expected pointwise change in surprisal of the target which is common to the sources. The pointwise change in surprisal of the target Z_t is interpreted as the pointwise or local interaction information, whose joint distribution $\tilde{P}$ is estimated from the original joint distribution P based on a game-theoretic approach (see the details in [Ince, 2017]).

R_{CCS} is defined based on the interaction information $\mathcal{I}(X_{t-\tau_X}; Y_{t-\tau_Y}; Z_t)$ and its local elements. We develop the corresponding conditional version, $R_{CCS,c}$, based on the conditional interaction information $\mathcal{I}(X_{t-\tau_X}; Y_{t-\tau_Y}; Z_t \mid \vec{W})$, which is also $\Delta I^{MSCP}_{\{X_{t-\tau_X}, Y_{t-\tau_Y}\} \to Z_t}$ in Eq.(2.8), given as:

$$\mathcal{I}(X_{t-\tau_X}; Y_{t-\tau_Y}; Z_t \mid \vec{W}) = \int_{\vec{w}} \int_x \int_y \int_z p(x, y, z, \vec{w}) i(x; y; z|\vec{w}) dx\, dy\, dz\, d\vec{w}, \tag{2.25}$$

where $i(x; y; z|\vec{w})$ is the local interaction information of $\mathcal{I}(X_{t-\tau_X}; Y_{t-\tau_Y}; Z_t \mid \vec{W})$ and can be written as:

$$i(x; y; z|\vec{w}) = \log \frac{p(x, y, z \mid \vec{w}) p(x \mid \vec{w}) p(y \mid \vec{w}) p(z \mid \vec{w})}{p(x, y \mid \vec{w}) p(x, z \mid \vec{w}) p(y, z \mid \vec{w})} \tag{2.26a}$$

$$= \Delta_z h(x, y \mid \vec{w}) - \Delta_z h(x \mid \vec{w}) - \Delta_z h(y \mid \vec{w}), \tag{2.26b}$$

with the three local individual informations: $\Delta_z h(x, y|\vec{w}) = \log \frac{p(x,y,z|\vec{w})}{p(x,y|\vec{w})p(z|\vec{w})}$, $\Delta_z h(x|\vec{w}) = \log \frac{p(x,z|\vec{w})}{p(x|\vec{w})p(z|\vec{w})}$, and $\Delta_z h(y|\vec{w}) = \log \frac{p(y,z|\vec{w})}{p(y|\vec{w})p(z|\vec{w})}$. Therefore, following the idea that the redundancy is measured with pointwise common change in surprisal, $R_{CCS,c}$ can be defined as the weighted sum of the local conditional interaction information and is given by:

$$R_{CCS,c} = \int_x \int_y \int_z \int_{\vec{w}} \tilde{p}(x, y, z, \vec{w}) \Delta_z h^{com}(x, y \mid \vec{w}) dx\, dy\, dz\, d\vec{w}, \tag{2.27}$$

where

$$\Delta_z h^{com}(x, y \mid \vec{w}) = \tag{2.28}$$

$$\begin{cases} -i_{\tilde{p}}(x; y; z \mid \vec{w}), & \text{if } \operatorname{sgn} \Delta_z h(x, y \mid \vec{w}) = \operatorname{sgn} \Delta_z h(x \mid \vec{w}) \\ & \quad = \operatorname{sgn} \Delta_z h(y \mid \vec{w}) = \operatorname{sgn}[-i_{\tilde{p}}(x; y; z \mid \vec{w})] \\ 0, & \text{otherwise.} \end{cases}$$

Notice that the signs of the three local individual information and the inverse of the local interaction information have to be the same. This is because of the assumption [Ince, 2017] that the positive and

negative local information terms are fundamentally different, so that only the local (conditional) interaction information where all three local individual informations have the same signs contributes to the redundancy. Also, $\tilde{p}$ is the element of the maximum entropy distribution $\tilde{P}$ from the original joint distribution P such that:

$$\tilde{P}(X,Y,Z,\vec{W}) = \underset{Q\in\Delta_P}{\arg\max} \int_x \int_y \int_z \int_{\vec{w}} -\tilde{q}(x,y,z,\vec{w}) \log \tilde{q}(x,y,z|\vec{w}) dx\, dy\, dz\, d\vec{w}, \tag{2.29}$$

where the set of potential distributions Δ_P is selected from each candidate joint distribution Q, which has the same sources' joint distribution as well as pairwise source-target marginal joint distribution as P, and is given by:

$$\Delta_P = \left\{ Q \in \Delta : \begin{array}{r} Q(X,Z|\vec{W}) = P(X,Z|\vec{W}), \\ Q(Y,Z|\vec{W}) = P(Y,Z|\vec{W}), \\ Q(X,Y|\vec{W}) = P(X,Y|\vec{W}) \end{array} \right\}.$$

The selection of the joint distribution $\tilde{P}$ for $R_{CCS,c}$ follows a similar game-theory approach as R_{CCS} in [Ince, 2017] but is different in that the optimization in Eq.(2.29) is based on the maximization of the conditional entropy.

2.5.4 Properties of the Four Conditional Redundancies

We have provided formulations for MPID based on four different definitions for conditional redundancies as the additional condition for MPID. The four selected redundancies (i.e., R_{MSI}, R_{MMI}, R_{CCS} and R_S) originate from different perspectives. R_{MSI} and R_{MMI} render the redundancy as a function of the marginal distribution between the target and each source, which usually overestimate the redundancy. To overcome that, the rescaled redundancy, R_S, takes the source correlations into account in the redundancy computation. Furthermore, R_{CCS} is developed based on a game-theory perspective and the idea that the redundancy consists of the pointwise common change in surprisal represented as the local interaction information, which essentially utilizes the information of the whole joint distribution.

In terms of the non-negative PID or the corresponding MPID, only R_{MMI} and R_S allow a non-negative decomposition. Such local positive property [Bertschinger et al., 2013] for PID and MPID is imposed in this study because the non-negative decomposition might be essential in illustrating physical phenomenon in a meaningful way. Despite the fact the other two measures, R_{MSI} and R_{CCS}, cannot guarantee the local positivity of PID and MPID, it should also be noted that the negativity of the PID and MPID induced by

R_{CCS} and $R_{CCS,c}$, respectively, is explainable in the context of the definition for R_{CCS} [Ince, 2017].

Furthermore, coupling strength autonomy only holds for the $R_{MMI,c}$ and $R_{S,c}$-based MPID, while the other two conditional redundancy measures do not facilitate this property due to their pointwise or local information based computation. Nevertheless, the definitions for the $R_{MSI,c}$ and $R_{CCS,c}$-based MPIDs are also useful in computing MPIDs with most of the influence from the complementary causal subgraph eliminated owing to causal Markov property of the network.

In addition, when the two causal paths are separable, the conditional redundancy based on the rescaled approach is minimized as $R_{min,c}$ (see Section 2.4.1). The minimization of the redundancy vividly illustrates the separable structure of the two causal paths from the sources, making the rescaled approach (Eq.(2.10)) suitable in quantifying MPID for separable causal paths based on a causal network.

Despite their pros and cons, the three proposed MPID frameworks in this section would eventually delineate the information transfer along causal paths in a causal network from their own perspectives, and provide for potentially alternative applications.

2.6 Quantifying MPID under Different Causal Paths and Causality Structures

Given the four MPID frameworks based on different redundancy measures described above, the MPID using the rescaled redundancy is adopted for further analysis. Specifically, in this section, we aim to investigate how MPID is affected by (1) separable and non-separable causal paths and different causal network structures, and (2) the effect of noise. We use synthetic data generated from two coupled logistic equation models for both separable and non-separable causal paths.

2.6.1 Coupled Logistic Equations

The two models, each of which involves three variables, are given as:

(1) A coupled logistic equation model without self-dependency:

$$X_{i,t} = \frac{1-\epsilon}{2} \sum_{\substack{j=0 \\ j \neq i}}^{3} 4X_{j,t-1}(1 - X_{j,t-1}) + \epsilon \eta_t^{X_i}, \tag{2.30}$$

where $\eta_t^{X_i}$ is a standard uniform noise $\sim U(0,1)$, and ϵ is the noise coupling strength ranging from 0 to 1.

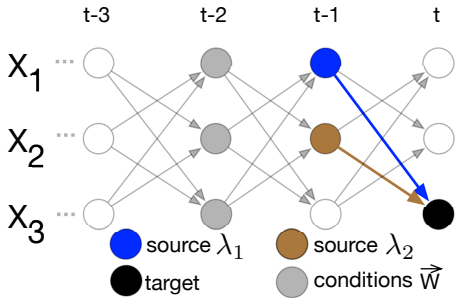

(a) Case SI – time series graph

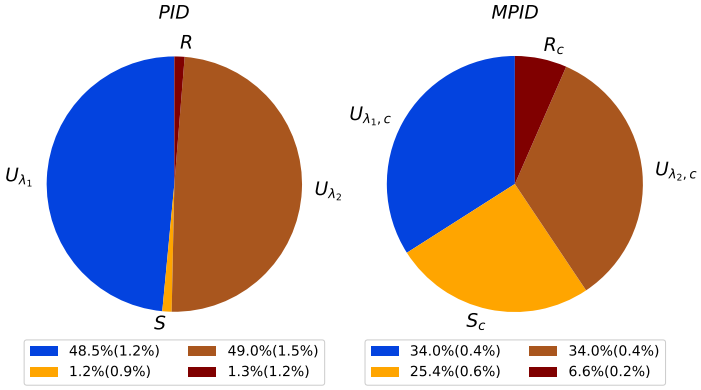

(b) Case SI – PID & MPID

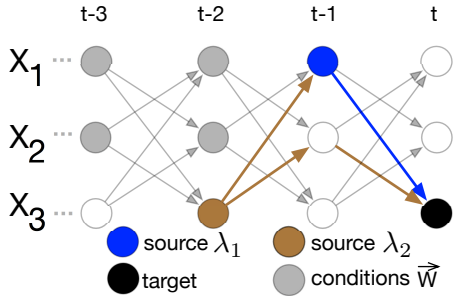

(c) Case NI – time series graph

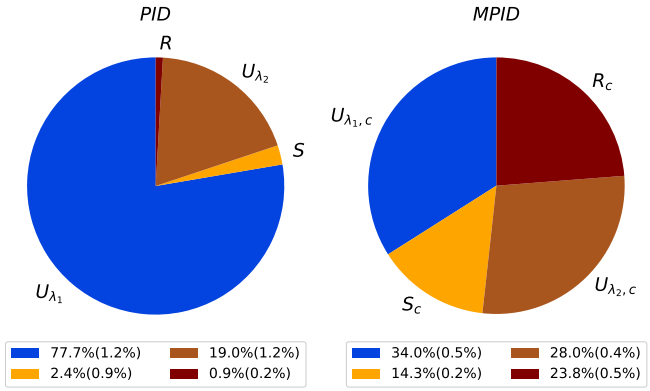

(d) Case NI – PID & MPID

Figure 2.5: Illustration of the time series graphs and the averaged information partitioning for the two cases in Eq.(2.30) (i.e., Case SI and Case NI) when the coupling strength ϵ equals to 0.5. (a) and (c) are the time series graphs of Cases SI and NI respectively (blue and brown nodes: the source nodes; black node: the target node; blue and brown directed links: the links in the causal paths of the two sources; grey solid nodes: the conditioning nodes in $\vec{W}$ for MPID in Eq.(2.8)). (b) and (d) are the pie charts of the averaged synergistic, redundant and unique information percentages from PID and MPID of Cases SI and NI respectively, with a legend showing the averaged values along with the corresponding standard deviations in the parenthesis (U_{λ_1} and $U_{\lambda_1,c}$: the unique information of $X_{1,t-1}$; and U_{λ_2} and $U_{\lambda_2,c}$: the unique information of $X_{2,t-1}$).

(2) A fully coupled logistic equation model given as

$$X_{i,t} = \frac{1-\epsilon}{3}\sum_{j=1}^{3} 4X_{j,t-1}(1-X_{j,t-1}) + \epsilon\eta_t^{X_i}. \tag{2.31}$$

For each model (Eqs.(2.30) and (2.31)), the following two situations of a causal subgraph, comprising the pathways of two sources affecting a target node, are considered for computing their MPID and PID:

- Scenario 1 (separable causal paths): the sources $\{X_{1,t-1}, X_{2,t-1}\}$ and the target $X_{3,t}$;

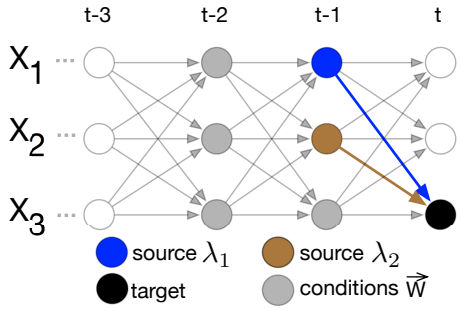

(a) Case SC – time series graph

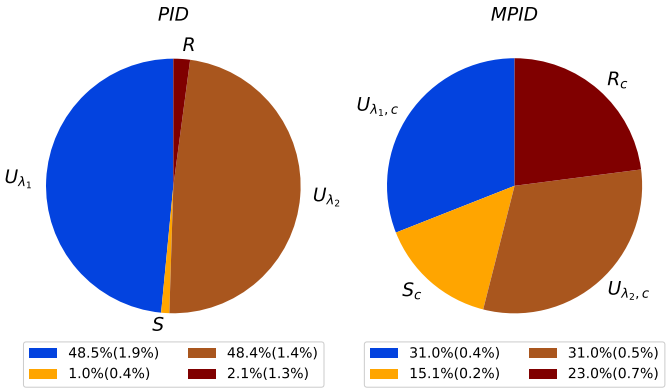

(b) Case SC – PID & MPID

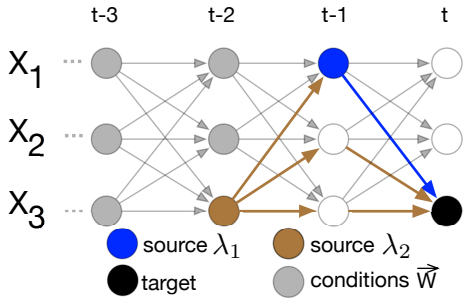

(c) Case NC – time series graph

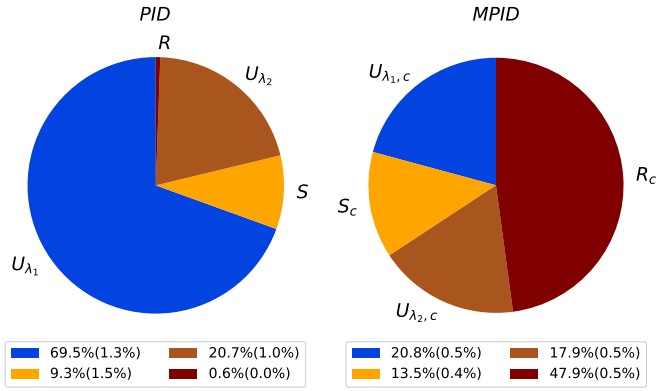

(d) Case NC – PID & MPID

Figure 2.6: Illustration of the time series graphs and the averaged information partitioning for the two cases in Eq.(2.31) (i.e., Case SC and Case NC) when the coupling strength ϵ equals to 0.5. (a) and (c) are the time series graphs of Cases SC and NC respectively (blue and brown nodes: the source nodes; black node: the target node; blue and brown directed links: the links in the causal paths of the two sources; grey solid nodes: the conditioning nodes in $\vec{W}$ for MPID in Eq.(2.8)). (b) and (d) are the pie charts of the averaged synergistic, redundant and unique information percentages from PID and MPID of Cases SC and NC respectively, with a legend showing the averaged values along with the corresponding standard deviations in the parenthesis (U_{λ_1} and $U_{\lambda_1,c}$: the unique information of $X_{1,t-1}$; and U_{λ_2} and $U_{\lambda_2,c}$: the unique information of $X_{2,t-1}$).

- Scenario 2 (non-separable causal paths): the sources $\{X_{1,t-1}, X_{3,t-2}\}$ and the target $X_{3,t}$.

For convenience, we name the four cases as follows:

- Case SI: Scenario 1 (separable) in Eq.(2.30) (without self-dependency);
- Case NI: Scenario 2 (non-separable) in Eq.(2.30) (without self-dependency);
- Case SC: Scenario 1 (separable) in Eq.(2.31) (fully coupled);
- Case NC: Scenario 2 (non-separable) in Eq.(2.31) (fully coupled).

Figs. 2.5a, 2.5c, 2.6a and 2.6c show the time series graphs of the two models and the causal subgraphs for the four cases. For both scenarios, $X_{1,t-1}$ is considered as the first source whose unique information are represented by U_{λ_1} and $U_{\lambda_1,c}$ for PID and MPID, respectively. $X_{2,t-1}$ and $X_{3,t-2}$ are taken as the second source for Scenario 1 and Scenario 2, respectively, with unique information represented as U_{λ_2} and $U_{\lambda_2,c}$ for PID and MPID, respectively.

2.6.2 Simulation Setting

We change the noise coupling strength ϵ uniformly in 19 intervals between 0 and 1 to control the influence of the noise on the two logistic models Eqs.(2.30) and (2.31) for generating synthetic data for the four cases. For each ϵ, 10,000 data points are generated for computing both MPID and PID in each case. To get an averaged behavior, ensembles of 10 trajectories are conducted for each ϵ. We first investigate the general influences of the separability of the causal paths and the network structure on MPID and PID when the coupling strength ϵ equals to 0.5. Then, we expand the analysis to explore how the noise strength shapes MPID and PID.

2.6.3 Influence of the Separability of the Causal Paths and the Network Structure on MPID/PID

The average percentages of the redundancy (i.e., R and R_c), the synergy (i.e., S and S_c) and the unique information (i.e., U_{λ_1}, $U_{\lambda_1,c}$, U_{λ_2} and $U_{\lambda_2,c}$) of both MPID and PID from an ensemble of 10 runs with $\epsilon = 0.5$ are shown in Figs. 2.5b, 2.5d, 2.6b and 2.6d. The standard deviations of MPID and PID are depicted in the parenthesis in the legends.

Comparison between PID and MPID: For all the four cases, the results of MPID and PID are different. Especially, in Case SI, Fig. 2.5b shows that there is almost no redundancy R and little synergy S from PID, while more synergy S_c (~25.4%) is observed in MPID. This is explained by the fact that $X_{3,t}$ is entirely determined by $X_{1,t-1}$ and $X_{2,t-1}$ according to Eq.(2.30), thus in MPID the exclusion of the history, that is, the complementary causal subgraph, through conditioning on $\vec{W}$ results in higher synergistic information. Furthermore, in Cases NI and NC, where the two causal paths are non-separable (Scenario 2), PID reveals near-zero redundancy of the two sources and significant unique information (69% ~78%) from $X_{1,t-1}$ (Figs. 2.5d and 2.6d). However, MPID (Cases NI and NC) indicates that unique information percentages of the sources ($U_{\lambda_1,c}$ and $U_{\lambda_2,c}$) are much closer and the proportion of the redundancy, R_c, is larger than that of PID. This is because the non-separable causal paths (Scenario 2) allows the information transfer of the source $X_{1,t-1}$ to be a part of the information transfer of the other source $X_{3,t-2}$, leading to the higher redundancy.

Also, almost identical unique information of the two sources in MPID (with $U_{\lambda_1,c}$ slightly larger) for Cases NI and NC results from the balance between the information transfer from the direct driver $X_{1,t-1}$ with one pathway and the indirect driver $X_{3,t-2}$ with multiple pathways. Even though $X_{3,t-2}$ affects the target $X_{3,t}$ indirectly, there are two and three pathways towards the target for Cases NI and NC, respectively, enhancing its unique information contribution to the target.

Different causal networks: Let's first compare the information partitioning results of Scenario 1 – the separable causal paths (i.e. Cases SI and NI shown in Figs. 2.5b and 2.6b, respectively). The synergy of the MPID in Case SI (i.e., S_c) is larger than that of Case NI. As discussed in the previous paragraph, the higher percentage of S_c in Case SI arises because the target $X_{3,t}$ is determined entirely by the two sources (i.e., $X_{1,t-1}$ and $X_{2,t-1}$) based on the causal relationship in Eq.(2.30). Nevertheless, the full coupling in Eq.(2.31) enables the target $X_{3,t}$ to be dictated by three nodes (i.e., $X_{1,t-1}$, $X_{2,t-1}$ and $X_{3,t-1}$). Therefore, for MPID in Case SC, with the knowledge of only two nodes, it is not sufficient to provide the synergistic information S_c to the target, resulting in a less synergy S_c compared with Case SI. In addition, in the comparison between Cases NI and NC, of which the two causal paths are not separable, the information partitioning patterns of both cases are consistent with each other. For example, the PIDs of both cases shows a strong unique information U_{λ_1} from X_{t-1}. However, the differences in the causal network quantitatively results in the differences in the information partitioning result. For instance, in terms of MPID, the increased redundant information R_c in Case NC is higher than that of Case SC.

Separable and non-separable causal paths: For each model, we compare the MPID results of the separable and non-separable causal paths. The comparisons (i.e., Case SI versus NI, and Case SC versus NC) reveal the same behavior in the two coupled logistic models that more redundancy in the cases of non-separable causal paths (i.e., Cases NI and NC) is estimated than that of the separable ones (i.e., Cases SI and SC). This is intuitive because in both Case NI and NC, the source $X_{1,t-1}$ lies in the causal path from the other source $X_{3,t-2}$ to the target $X_{3,t}$, thereby a part of the information transfer from $X_{3,t-2}$ to $X_{3,t}$ is overlapped or contributed by the information given by $X_{1,t-1}$, resulting in more redundancy than that of the separable causal paths in Cases SI and SC.

2.6.4 Influence of Noise

To understand how additive noise affects the estimation of MPID and PID, we plot these estimates as a function of signal-to-noise ratio (SNR) which is computed as the ratio of the variance of the logistic time series to the variance of the noise terms in Eqs.(2.30)-(2.31). Furthermore, it is well known that the coupled logistic equations are prone to synchronize depending on the lags and noise strength [Rosenblum et al., 1997,

Martí et al., 2008, Masoller and Atay, 2011, Paredes et al., 2013, Aguirre et al., 2014], which impacts the MPID and PID outcomes. To investigate whether the lagged synchronization occurs and, thus, affects MPID and PID, we also plot the similarity functions among the sources and target as well as the percentages of total information given by the two sources in the overall uncertainty for both MPID and PID over SNR in Fig. 2.7, which are defined as follows:

$$SF_{ij}(\tau) = \Big\{ \frac{E[(X_{i,t+\tau} - X_{j,t})^2]}{[E(X_{i,t+\tau}^2)E(X_{j,t}^2)]^{1/2}} \Big\}^{0.5} \tag{2.32}$$

$$I_{tot,p} = \frac{I(\lambda_1, \lambda_2; X_{tar})}{H(\lambda_1, \lambda_2, X_{tar})} \times 100\% \tag{2.33}$$

$$I_{tot,p,c} = \frac{I(\lambda_1, \lambda_2; X_{tar} \mid \vec{W})}{H(\lambda_1, \lambda_2, X_{tar} \mid \vec{W})} \times 100\% \tag{2.34}$$

where $SF_{ij}(\tau)$ is the similarity function between $X_{i,t+\tau}$ and X_j, E is the expectation function, $H(\bullet)$ and $H(\bullet \mid \bullet)$ are the Shannon's entropy and the corresponding conditional entropy [Cover and Thomas, 2006], respectively, $\{\lambda_1, \lambda_2, X_{tar}\}$ represents the two sources and the target variables in the four cases, and $I_{tot,p}$ and $I_{tot,p,c}$ are the percentages of shared information between sources and target for PID and MPID, respectively. The similarity function $SF_{ij}(\tau)$ describes the degree of synchronization between two variables X_i and X_j with a lag τ. A lower value $SF_{ij}(\tau)$ means a higher similarity between X_i and X_j with lag τ with value 0 representing a complete synchronization. The normalized total information $I_{tot,p}$ and $I_{tot,p,c}$ accounts for the amount of uncertainty reduced by the two sources λ_1 and λ_2 for the target X_{tar} against their overall uncertainty, with and without conditioning on $\vec{W}$, respectively.

Influence of SNR on $I_{tot,p}$ and $I_{tot,p,c}$: The percentages of total information behave differently for PID and MPID. For PID, $I_{tot,p}$ (the red lines in the first column of Fig. 2.7) increases with SNR. This is because with the decrease in the noise, the sources have a stronger control on the target, resulting in high $I_{tot,p}$. Meanwhile, for MPID, $I_{tot,p,c}$ (the red lines in the second column of Fig. 2.7) increases gradually until SNR is between 1 to 50. Note that higher SNR is achieved by reducing the noise coupling strength ϵ in Eqs.(2.30) and (2.31). With further increase in SNR rapidly, $I_{tot,p,c}$ initially drops down and then flattens (for Case SC) or even increases a bit (for the other cases). The decrease of $I_{tot,p,c}$ for MPID in the range $1 <$ SNR < 50 can be explained by two factors. First, the dynamics tend to be less stochastic in higher SNR and thus the condition set $\vec{W}$ is able to explain more about the target. Note that in a deterministic model, the target variable can be determined entirely by the knowledge of the condition set $\vec{W}$. Therefore, the enhanced contribution of $\vec{W}$ leads to the decline of $I_{tot,p,c}$ under high SNR. Second, the synchronization rate between each source and the target decreases when SNR becomes larger than around 1, shown as the flattened black lines with marked symbols in the second column of Fig. 2.7. Moreover, with the further growth of SNR

($\gg 1$), the target starts to be desynchronized with each source, reflected as the increase of the similarity function between the two in each case. The change of synchronization rate accounts for not only the decrease of $I_{tot,p,c}$ when SNR is slightly larger than 1, but also the increase of $I_{tot,p,c}$ for MPID when the system is much less stochastic for large SNR.

Influence of lagged synchronization on $I_{tot,p}$ and $I_{tot,p,c}$: The three similarity functions among the two sources and the target are plotted as the three types of black lines in the first and second columns of Fig. 2.7 for PID and MPID, respectively. It can be observed that when SNR is less than 1 (or the noise coupling strength ϵ is large than around 0.5), the decrease of the three similarity functions captures with the increases of both $I_{tot,p}$ and $I_{tot,p,c}$. It implies the synchronization between each source and the target with the decrease of the noise effect results in an increased proportion of uncertainty reduction in the target given the knowledge of the two sources. Moreover, $I_{tot,p,c}$ decreases significantly once SNR is in the range of 1 to 50. As explained at the end of the previous paragraph, this is due to (1) the increased information provided by the condition set $\vec{W}$ for the target in a less stochastic system, and (2) the desynchronization trend between each source and the target, which is shown as the growth of the similarity functions when SNR is larger than around 1. However, when SNR is large, that is, the system is weakly stochastic, $I_{tot,p,c}$ flattens for Case SC and goes up again for the other three cases, while at the same time, the increasing rate of the similarity functions between each source and the target declines. The decline in the increasing rate of the similarity functions reflects the slowdown of the desynchronization process between each source and the target, causing the flattening and growth of $I_{tot,p,c}$, for Case SC and the other three cases, respectively. Especially, for Cases NI and NC where the two causal paths are non-separable, the increase of $I_{tot,p,c}$ in MPID for high SNR (close to 100) is mainly due to the reduction in the rate of growth of the similarity function between the target and the first source, whose unique information, $U_{\lambda_1,c}$, (the blue dashed lines in the fourth column of Fig. 2.7) contributes to most of $I_{tot,p,c}$.

Influence of SNR on PID: For all the four cases, the synergy S (the orange lines in the third column in Fig. 2.7) is almost zero with a little increase for high SNR, while the redundancy R (the black lines in the third column in Fig. 2.7) is close to zero when SNR is less than around 1 but increases significantly for high values of SNR. The near-zero values of both S and R for SNR less than 1 are due to the dominant role of the noise in the system such that the two sources provide little information to the target, which is also manifested as the near-zero values of the corresponding $I_{tot,p}$ (the red lines in the third column of Fig. 2.7). Meanwhile, the significant increase of R for larger SNR (> 1) is due to the symmetric structure of the coupled logistic equations, whose influence is more significant in larger SNR where the system is less stochastic, resulting in a higher value of redundancy. In terms of the two unique information, for Cases SI

and SC, U_{λ_1} (the blue dashed lines) and U_{λ_2} (the sienna dashed lines) are almost identical for both sources which influence the target directly through the same logistic equation. For Cases NI and NC, the two unique information are almost zero for small SNR because of the dominant role of the noise, and start to increase with the growth of SNR with a faster increasing rate for U_{λ_1}. That U_{λ_1} is larger than U_{λ_2} when the system is less stochastic for a higher SNR illustrates the fact that the first source $X_{1,t-1}$ is a direct cause of the target $X_{3,t}$ while the second source $X_{3,t-2}$ influences the target indirectly.

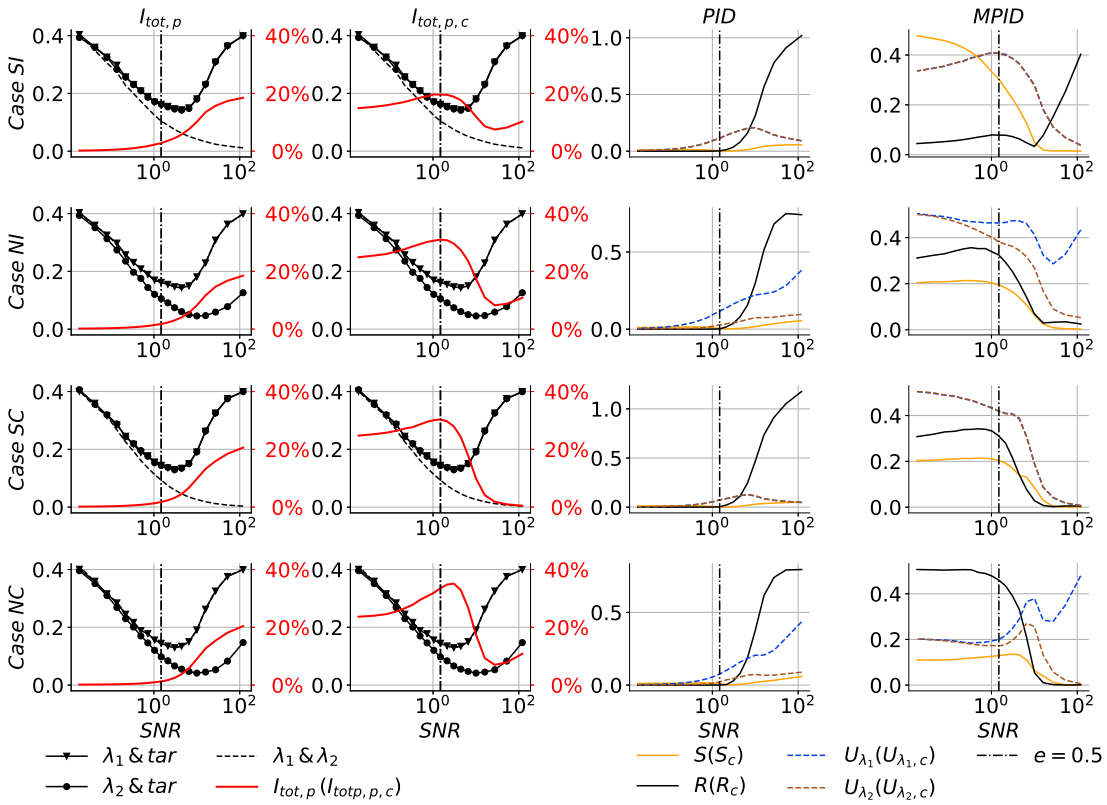

Figure 2.7: The averaged percentages of total information, PID, and MPID for the four cases based on the two coupled logistic equations in Eqs.(2.30)-(2.31) in terms of different signal-to-noise ratio (SNR). The first and second columns plot the percentages of total information in Eqs.(2.33)-(2.34) (the red line) and the similarity functions in Eq.(2.32) between the first source and the target, λ_1 & tar (the black line marked with triangles), the second source and the target, λ_2 & tar (the black line marked with solid cirles), and the two sources, λ_1 & λ_2 (the black dashed line), for PID and MPID, respectively. The first and second columns plot the synergistic (the orange line), the redundant (the black line), and the two unique information (the blue and sienna dashed lines) for PID and MPID, respectively.

Influence of SNR on MPID: For Case SI, the redundancy R_c (the orange lines in the fourth column in Fig. 2.7) and the synergy S_c (the black lines in the fourth column in Fig. 2.7) increases and decreases with SNR, respectively. Especially, S_c is much larger than R_c for SNR < 1, illustrating the fact that the target

is entirely determined by the two sources, which is not shown in the corresponding PID plot in Case SI. Meanwhile, with the increase of SNR, R_c increases rapidly while S_c decreases, as a result of the symmetric structure of the coupled logistic equations, which leads to higher redundancy. For the other three cases, both S_c and R_c are much larger than zero with $R_c > S_c$ for SNR < 1, and both start to decrease with SNR and reach around zero when SNR is close to 100. In the condition of a smaller SNR (< 1), a higher R_c results from (1) the non-separable causal paths in Cases of NI and NC, which results in an overlapped information transfer from the two sources, and (2) the fact that the target is determined by three causes in Case SC so that the synergistic information S_c given by two sources is not large enough. In the case of a larger SNR (> 1), S_c and R_c decline because of the the decreased total information $I_{tot,p,c}$. With regards to the two unique information, $U_{\lambda_1,c}$ and $U_{\lambda_2,c}$ are almost identical for the cases with separable causal paths (i.e., Cases SI and SC) since that both sources impact the target directly through the same logistic equation. For the other cases with non-separable causal path (i.e., Cases NI and NC), the two unique information are close for a noise-dominant system with a smaller SNR and start to diverge with a higher $U_{\lambda_1,c}$ when the system becomes less stochastic with a larger SNR. The increasing difference between the two unique information with SNR illustrates that in a more deterministic system, compared with the second source $X_{3,t-2}$ indirectly controlling the target $X_{3,t}$, the first source $X_{1,t-1}$ is able to provide more information to the target through its direct influence on $X_{3,t}$.

2.7 Summary and Conclusions

By employing a time series graph-based approach, where the dynamics among the components at each time step are explicitly represented, we propose the *momentary partial information decomposition* (MPID). It allows us to dissect the information transfer to a target through a preceding causal subgraph, which comprises multiple causal paths from multiple sources to the target, into synergistic, redundant and unique information. Different from the original partial information decomposition (PID), whose quantification includes the information from the entire history, MPID is able to exclude the influence from this history or the complementary causal subgraph, through conditioning, for any direct cause of the subgraph of interest in the estimation. PID and MPID together provide two ways for investigating information partitioning (with and without the influence from the complementary causal subgraph), and the comparison between them draws out different behaviors of a process network.

The adopted rescaled method for estimating redundancy (Eq.(2.10)) in information partitioning proves to be effective in MPID in excluding the influence of the complementary causal subgraph. For instance,

when the two causal paths are separable, meaning that neither of the sources belongs to the causal path of the other, the redundant information R_c in MPID is minimized. It makes sense that when two sources influence the target through different causal paths, the redundancy is reduced. Also, because there is no universal agreement on the appropriate PID method, we provide the estimations for the MPID frameworks based on the three alternative redundancy measures in Section 2.5.

Further, we investigate MPID and PID of a three-node dynamics under different causality structures and both separable and non-separable causal paths as well as the noise effect on the information partitioning. Application of PID and MPID for two coupled logistic equation models shows that compared with separable causal paths, non-separable causal paths generate more redundant information since the two sources have overlap in their causal paths towards the target. Also, the difference in causality structure gives rise to different MPID results. For instance, under two separable causal paths, more synergistic information is observed, when the target is entirely controlled by the two sources in the model without self-dependency, than the fully-coupled model where the target is also driven by an external node. Furthermore, the influence of noise on PID and especially MPID is more complex. In the two coupled logistic equations, when the system is noise dominant (low signal-to-noise ratio (SNR)), the decline of a strong noise influence is able to enhance the lag synchronization between each source and the target, which results in the growth of the total information given by the two sources towards the target for both PID and MPID (i.e., $I_{tot,p}$ and $I_{tot,p,c}$). Meanwhile, in a weak stochastic system (high signal-to-noise ratio), $I_{tot,p,c}$ might either decrease due to a higher proportion of information explained by the condition set $\vec{W}$ or increase because of the decrease of the desynchronization rate between the sources and the target. In short, the influence of noise on the estimates of PID and MPID is determined by the stochastic degree of the system as well as the causality structures of both the system and the causal subgraph of interest. Also, it is noted that the empirical results of MPID in the coupled logistic equations, which adopts the conditional rescaled redundancy measure, may differ if other conditional redundancy measures, such as those proposed in Section 2.5, were used.

Although the momentary information approach is able to exclude most of the influences from the complementary causal subgraph of interest, as pointed out by Runge [Runge et al., 2012b, Runge, 2015], the time series graph-based approach has the following limitations. First, the coupling strength autonomy property is only analytically established when both *linearity* and *additivity* hold, and not guaranteed for nonlinear cases. However, in some cases, such as the nonlinear common driver model, this *momentary* approach can still significantly reduce the impact from the history and thus better reveal the internal dynamics among the nodes of interest in terms of information partitioning. Furthermore, the Markovian conditional independence property of the graph facilitates an approximate estimation of an automonous information

partitioning. Therefore, when the functional dynamics of a complex system are unknown, MPID can provide at least a general picture of the autonomous mechanism in a causal subgraph. Second, the estimation of a high-dimensional probability distribution function, resulting from the potentially many external drivers (i.e., $\vec{W}$), requires a large amount of data, and would potentially result in biased estimation of cause-effect relationships for short datasets.

Finally, the proposed momentary partial information decomposition, which is a Granger causality-oriented framework, provides a new perspective in exploring complex systems, especially in natural systems where systems are complex, self-organized, and hard to be intervened. With the increasing availability of observational data recorded in finer resolutions [Baldocchi et al., 2001, Neal et al., 2013], a lot of investigations based on different data analysis approaches have been conducted in understanding the dynamics of different aspects in nature, such as exploring the self-organization in various ecohydrological system by using transfer entropy [Kumar and Ruddell, 2010], the quantification of the strength and delay in climatic interaction through the causal network [Runge et al., 2014], etc. The proposed framework, anchored on the information partitioning of a causal subgraph, has the potential to enable the investigation of the dynamics of multiple lagged components in terms of different types of information transfer from the sources.

Chapter 3

Information Transfer from Causal History in Complex System Dynamics

3.1 Introduction[1]

The dynamics of natural systems, such as ecosystems and climate, arise as a result of spontaneous self-organization. Their dynamical characteristics, such as existence of strange attractors or $1/f$ long-memory dependencies, arise as a result of feedback between all interacting variables. Information theory offers compelling approaches for characterizing the complex non-linear inter-dependencies present in such systems [Haken, 2006]. For example, a recent study has argued that the spontaneous formation of a self-organized structure is reflected as decrease of joint entropy of the system as well as increase of contemporaneous inter-dependencies among interacting components [Rosas et al., 2018]. However, most of the existing information-theoretic approaches are anchored on characterizing either bivariate information transfer using transfer entropy or momentary information transfer [Schreiber, 2000, Frenzel and Pompe, 2007, Runge et al., 2012b, Amblard and Michel, 2013, Sun and Bollt, 2014], or the interactions among a specific set of variables by using methods based on partial information decomposition [Williams and Beer, 2010, Goodwell and Kumar, 2017a, Goodwell and Kumar, 2017b, Goodwell et al., 2018, Jiang and Kumar, 2018], which becomes difficult when more than three variables are involved. These approaches provide important and insightful views associated with specific interactions within a system, but do not allow us to assess the entire range of information transfer among all variables. For example, we may ask how the interactions of several or all variables in a system determine the state of an individual variable at a specific time. Alternatively, we may ask how a finite time history of interactions results in an observed outcome of a specific variable at a specific time. To answer these questions, we require metrics that allow us to characterize full range of causal dependency in the system (in the Granger sense [Granger, 1969]), which structures the transfer of information that progressively influences a target variable.

Consider a system composed of N variables, $\vec{X}_t = \{X_t, Y_t, Z_t, ...\}_N$, varying in time. The current state of a variable, say $Z_t \in \vec{X}_t$, is a result of the evolutionary history of the system $\vec{X}_t^- = \{\vec{X}_{t-1}, \vec{X}_{t-2}, \vec{X}_{t-3}, ...\}$,

[1]This chapter is published as an article in Physical Review E, 2019 [Jiang and Kumar, 2019]

which we call *causal history*. We partition this history, based on a partitioning time lag τ with respect to the present, into recent or *immediate causal history* $\{\vec{X}_{t-1}, \vec{X}_{t-2}, ..., \vec{X}_{t-\tau}\}$ and the complementary *distant causal history* $\{\vec{X}_{t-\tau-1}, \vec{X}_{t-\tau-2}, ...\}$. Generally, while the information from the immediate causal history is expected to be nondecreasing with τ, the degree and convergence of information from the distant causal history informs the influence from the remaining historical dynamics beyond the lag τ. Thus, quantification of the information transfer to a target variable at time t, from both its immediate and distant causal histories, would delineate the dependency of the variable on the prior dynamics as well as the memory in the system, which are keys for understanding various complex systems [Kumar and Ruddell, 2010, Lizier et al., 2011, Jizba et al., 2012, Kirchner and Neal, 2013]. Therefore, the objective of this study is to quantify and characterize the influence of a immediate, distant, and/or entire causal history on Z_t by using an information-theoretic framework.

We use a directed acyclic time series graph approach to characterize the temporal dependencies of the system as well as for simplifying the computation of the information transfer. Specifically, we demonstrate the features of our approach in terms of: (1) Information aggregation property in the causal history, achieved through simplification from Markovian assumption in directed acyclic time series graph; (2) Discerning system memory, and its advantage over traditional methods such as lagged mutual information; (3) Characterizing the changing interaction information jointly provided by a target variable's self and cross dependencies, as a function τ, from both immediate and distant causal histories; and (4) Quantifying the change in memory dependency in a system when the influence of any particular variable is isolated from the remaining variables.

This chapter is organized as follows. First, in Section 3.2, we provide the definitions and the properties of the information transfer in both immediate and distant causal histories based on directed acyclic time series graph representation of the system. Then, in Section 3.3 we implement this approach to delineate the temporal dynamics of three different systems by quantifying the information transfer from causal history. We first identify the memory dependency of a trivariate logistic model – a short-memory system, in Section 3.3.1. Next in Section 3.3.2, we analyze the chaotic and long-memory Lorenz model for comparing the proposed approach with lagged mutual information in delineating the memory dependency of the system. Then, we investigate the information transfer in a linear trivariate Ornstein-Uhlenbeck process, whose dynamics also shows long memory property but without the existence of a stranger attractor. While the model-generated synthetic data are used for analysis in the previous three example, in the third example in Section 3.3.4, we demonstrate an application using observed stream chemistry time series data, obtained in the Upper Hafren catchment in Wales, United Kingdom [Kirchner and Neal, 2013]. Last, summary and conclusions are given

in Section 3.4.

3.2 Information Transfer from Causal History

We represent the temporal dependency in the multivariate system $\vec{X}_t$ as a time series directed acyclic graph [Runge, 2015, Eichler, 2012] as illustrated in Fig. 3.1, where each node represents a variable at a specific time step t (e.g., Z_t) and the parents of a target node or a set of nodes are denoted as $P_\bullet$ (e.g., P_{Z_t}). The directed edge linking two lagged nodes (e.g., $X_{t-\tau_X}$ and Z_t with $\tau_X > 0$) in the graph indicates the direct influence from $X_{t-\tau_X}$ to Z_t. The causal influence, assumed here in a Granger sense [Granger, 1969], from a lagged node $X_{t-\tau_X}$ to a target Z_t can be either through a directed edge or indirectly via a causal path $C_{X_{t-\tau_X}\to Z_t}$, which is a set of nodes connected by a sequence of directed edges from $X_{t-\tau_X}$ to Z_t. That is, $C_{X_{t-\tau_X}\to Z_t} \equiv \{V_{t-\tau_V} : V_t \in \vec{X}_t, \tau_V > 0, X_{t-\tau_X} \to \cdot \to V_{t-\tau_V} \to \cdot \to Z_{t-\tau_Z}\} \cup \{X_{t-\tau_X}\}$. We consider the causal influence to a target node as arising only from a node earlier in time, which results in a directed acyclic graph (DAG) of time series. In this section, based on this DAG time series graph representation, we provide the mathematical definition of causal history, its simplification for computation, the associated properties, and further analyses of causal history in terms of self and cross dependencies.

3.2.1 Definitions of Causal History

The causal history of a target node Z_t includes all the nodes that influence Z_t through causal paths in the graph, and is represented by $\vec{X}_t^- = \{\vec{X}_{t-1}, \vec{X}_{t-2}, ...\}$. Therefore, the total information, $\mathcal{T}$, to Z_t given by the causal history, can be expressed as the mutual information (MI) [Cover and Thomas, 2006] between the two, which is given by:

$$\mathcal{T} = I(Z_t; \vec{X}_t^-). \tag{3.1}$$

Further, an immediate causal history of Z_t is considered as a finite length causal history immediately preceding time t, $\vec{X}_{t-\tau} = \{X_{t-\tau}, Y_{t-\tau}, ...\}_N$ starting from all the contemporaneous source nodes at lag τ. It is represented by a multitude of causal paths, that is, $C_{\vec{X}_{t-\tau}\Rightarrow Z_t} = \cup_{X_{t-\tau}\in\vec{X}_{t-\tau}} C_{X_{t-\tau}\to Z_t}$ (the blue dashed box in Fig. 3.1a). To generalize the following theory, we define the immediate causal history as a subgraph preceding Z_t arising from a set of lagged sources $\vec{V} = \{X_{t-\tau_X}, Y_{t-\tau_Y}, ...\}$ to Z_t, $C_{\vec{V}\Rightarrow Z_t} = \cup_{V_{t-\tau_V}\in\vec{V}} C_{V_{t-\tau_V}\to Z_t}$. Then, the complementary distant causal history can be naturally expressed as the remaining part of the causal history, $\vec{X}_t^- \backslash C_{\vec{V}\Rightarrow Z_t}$, where $\backslash$ is the subtraction operator (the red dashed box in Fig. 3.1a). By using the chain rule of MI [Cover and Thomas, 2006], the total information $\mathcal{T}$ can be

decomposed into the information from (1) the immediate causal history, $\mathcal{J}$, and (2) the distant causal history, $\mathcal{D}$, such that:

$$\begin{aligned}\mathcal{T} &= I(Z_t; C_{\vec{V}\Rightarrow Z_t}, \vec{X}_t^- \backslash C_{\vec{V}\Rightarrow Z_t}) \\ &= \underbrace{I(Z_t; \vec{X}_t^- \backslash C_{\vec{V}\Rightarrow Z_t})}_{=\mathcal{D}} + \underbrace{I(Z_t; C_{\vec{V}\Rightarrow Z_t} | \vec{X}_t^- \backslash C_{\vec{V}\Rightarrow Z_t})}_{=\mathcal{J}} \\ &= \mathcal{D} + \mathcal{J}. \end{aligned} \tag{3.2}$$

Eq.(3.2) expresses that the information from the distant causal history, $\mathcal{D}$, is provided by all the lagged nodes not in the immediate history, i.e., $\vec{X}_t^- \backslash C_{\vec{V}\Rightarrow Z_t}$, through their mutual information with Z_t; while the information from the recent dynamics, $\mathcal{J}$, is accounted for by the conditional mutual information (CMI) between the target and the immediate causal history conditioned on the distant history.

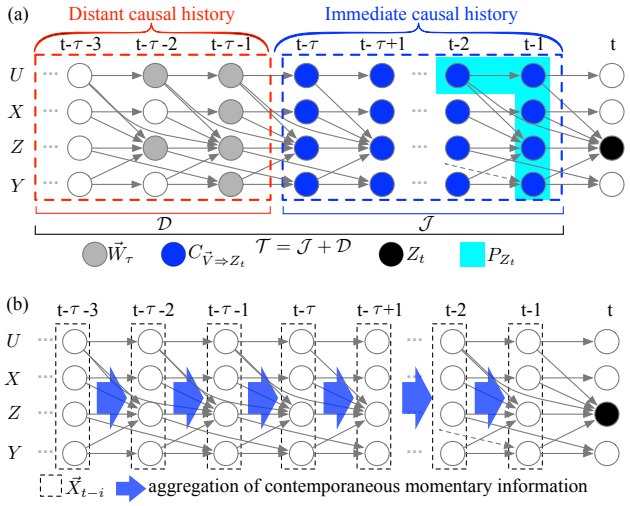

Figure 3.1: Illustration of the causal history $\vec{X}_t^-$ of a target node Z_t. (a) The partition of $\vec{X}_t^-$ into an immediate causal history, $C_{\vec{V}\Rightarrow Z_t}$ (the dashed blue box), and the complementary distant causal history, $\vec{X}_t^- \backslash C_{\vec{V}\Rightarrow Z_t}$ (the dashed red box). The parents of the target Z_t [Eq.(3.3)], P_{Z_t}, are identified by the cyan colored box. (b) The aggregation of contemporaneous momentary information from each set of contemporaneous nodes $\vec{X}_{t-i}$ (the dashed hollow box) at an early time step $t-i$ in the causal history [Eq.(3.10)].

3.2.2 Simplifications of $\mathcal{T}$, $\mathcal{J}$, and $\mathcal{D}$

It is noted that the empirical computations of $\mathcal{T}$, $\mathcal{J}$, and $\mathcal{D}$ in Eq.(3.2) are infeasible due to the potentially infinite number of nodes in $\vec{X}_t^-$ and $\vec{X}_t^- \backslash C_{\vec{V}\Rightarrow Z_t}$. Therefore, to address this challenge and connect the time series graph with the underlying joint probability, we assume the Markov property for DAG ([Lauritzen et al., 1990], theorem 1). This is consistent with prior work [Runge et al., 2012b], which states

that any node Z_t in the graph is independent of all its non-descendants given the knowledge of its parents P_{Z_t} [Spirtes et al., 2000]. For the graph in Fig. 3.1, for example, this implies that given its parents P_{Z_t} (the cyan colored box), the target node Z_t is conditionally independent of the rest of its non-descendants, $\vec{X}_t^- \backslash P_{Z_t}$.

Now, the main idea of reducing the dimensions in $\mathcal{T}$, $\mathcal{J}$ and $\mathcal{D}$ originates from the connection between conditional independence and the node separation in the graph based on the Markov property. The simplification of $\mathcal{T}$ can be immediately achieved by using chain rule as follows (note that $P_{Z_t} \subset \vec{X}_t^-$):

$$\begin{aligned}\mathcal{T} &= I(Z_t; P_{Z_t}, \vec{X}_t^- \backslash P_{Z_t}) \\ &= I(Z_t; P_{Z_t}) + \underbrace{I(Z_t; \vec{X}_t^- \backslash P_{Z_t} \mid P_{Z_t})}_{=0} \\ &= I(Z_t; P_{Z_t}),\end{aligned} \tag{3.3}$$

which is the mutual information between Z_t and its parents P_{Z_t} (see Fig. 3.1a). The zero value for $I(Z_t; \vec{X}_t^- \backslash P_{Z_t} \mid P_{Z_t})$ results from the Markov property that separates Z_t from the remaining historical nodes given its parents.

Furthermore, the distant causal history, $\vec{X}_t^- \backslash C_{\vec{V} \Rightarrow Z_t}$, which serves in Eq.(3.2) as the condition set and information contributor in $\mathcal{J}$ and $\mathcal{D}$, respectively, can be partitioned into two parts: (1) the parents of both Z_t and the immediate causal history $C_{\vec{V} \Rightarrow Z_t}$ excluding those in the immediate causal history, denoted as $\vec{W}_\tau = P_{C_{\vec{V} \Rightarrow Z_t} \cup Z_t} \backslash C_{\vec{V} \Rightarrow Z_t}$ (the grey nodes in Fig. 3.1a), and (2) the remaining nodes, $\vec{X}_t^- \backslash (C_{\vec{V} \Rightarrow Z_t} \cup \vec{W}_\tau)$. Then, in a similar manner as for $\mathcal{T}$, the Markov property and the chain rule also facilitate the simplifications for $\mathcal{D}$:

$$\begin{aligned}\mathcal{D} &= I(Z_t; \vec{W}_\tau, \vec{X}_t^- \backslash (C_{\vec{V} \Rightarrow Z_t} \cup \vec{W}_\tau)) \\ &= I(Z_t; \vec{W}_\tau) + \underbrace{I(Z_t; \vec{X}_t^- \backslash (C_{\vec{V} \Rightarrow Z_t} \cup \vec{W}_\tau) \mid \vec{W}_\tau)}_{=0} \\ &= I(Z_t; \vec{W}_\tau),\end{aligned} \tag{3.4}$$

and for $\mathcal{J}$:

$$\begin{aligned}\mathcal{J} &= I(Z_t; C_{\vec{V} \Rightarrow Z_t} | \vec{X}_t^- \backslash C_{\vec{V} \Rightarrow Z_t}) \\ &= I(Z_t; C_{\vec{V} \Rightarrow Z_t} | \vec{W}_\tau).\end{aligned} \tag{3.5}$$

Both, the zero value for $I(Z_t; \vec{X}_t^- \backslash (C_{\vec{V}\Rightarrow Z_t} \cup \vec{W}_\tau) \mid \vec{W}_\tau)$ and the reduction of the condition set of $\mathcal{J}$ into $\vec{W}_\tau$ in Eqs.(3.4) and (3.5), respectively, are due to the conditional independence between Z_t and $\vec{X}_t^- \backslash (C_{\vec{V}\Rightarrow Z_t} \cup \vec{W}_\tau)$ given the knowledge of $\vec{W}_\tau$, which separates the immediate finite history associated with Z_t and Z_t itself from the remaining history. In fact, a decomposition of $C_{\vec{V}\Rightarrow Z_t}$, into (1) $P_{Z_t}^{C_{\vec{V}\Rightarrow Z_t}} \equiv P_{Z_t} \cap C_{\vec{V}\Rightarrow Z_t}$ – the direct causes of Z_t in the immediate causal history, and (2) $C_{\vec{V}\Rightarrow Z_t} \backslash P_{Z_t}^{C_{\vec{V}\Rightarrow Z_t}}$ – the remaining intermediate nodes in $C_{\vec{V}\Rightarrow Z_t}$, enables a further simplification of $\mathcal{J}$, that is (see Appendix D for derivations):

$$\mathcal{J} = I(Z_t; P_{Z_t}^{C_{\vec{V}\Rightarrow Z_t}} \mid \vec{W}_\tau), \tag{3.6}$$

which is achieved by taking the chain rule expansion based on $C_{\vec{V}\Rightarrow Z_t}$ and dropping off the other term because of the conditional independence of Z_t with the remaining history given its parents. Also, by substituting Eqs.(3.4) and (3.5) back to Eq.(3.2) and noticing $P_{Z_t} \subset P_{Z_t}^{C_{\vec{V}\Rightarrow Z_t}} \cup \vec{W}_\tau$, we can again utilize the Markov property to get:

$$\mathcal{T} = I(Z_t; P_{Z_t}^{C_{\vec{V}\Rightarrow Z_t}}, \vec{W}_\tau) = I(Z_t; P_{Z_t}),$$

which reduces to Eq.(3.3) as we should expect and is constant in terms of the time lag τ. We also note that the quantities $\mathcal{J}$ and $\mathcal{D}$ are functions of τ, but this is not included in the notation for brevity as this does not cause any ambiguity.

3.2.3 Information Aggregation Property of $\mathcal{T}$ and $\mathcal{J}$

The simplifications in Eqs.(3.3)-(3.6) imply an important property of information aggregation from intermediate nodes to the direct causes of the node(s) of interest. For all the three information transfer measures, the information accumulate at the nodes that are either the parents of the target node Z_t [P_{Z_t} for $\mathcal{T}$ in Eq.(3.3) and $P_{Z_t}^{C_{\vec{V}\Rightarrow Z_t}}$ for $\mathcal{J}$ in Eq.(3.6)] or the parents of the union of Z_t and its immediate causal history [$\vec{W}_\tau$ for $\mathcal{D}$ in Eq.(3.4)]. This property, derived from the Markov property for DAG, illustrates that the latest observations actually contain all the information of the earlier dynamics in the system, transferred via the causal paths, and influence the states of the variables at the next stage.

Further insights associated with such information aggregation property can be obtained by a decomposition of both $\mathcal{T}$ and $\mathcal{J}$. We separate $C_{\vec{V}\Rightarrow Z_t}$ into τ set of nodes, where τ is the maximum time lag between the target Z_t and the earliest node in the source nodes $\vec{V}$, that is, $\tau = \arg\max_k \{X_{t-k} : X_{t-k} \in C_{\vec{V}\Rightarrow Z_t}\}$. Each set of nodes $\vec{V}_{t-i}$ represents all the contemporaneous nodes in $C_{\vec{V}\Rightarrow Z_t}$ at the time step $t-i$ $(1 \leq i \leq \tau)$, that is, $\vec{V}_{t-i} = \{V_{t-\tau_V} : V_{t-\tau_V} \in C_{\vec{V}\Rightarrow Z_t} \mid \tau_V = i\}$. It is clear that $C_{\vec{V}\Rightarrow Z_t} = \cup_{i=1}^{\tau} \vec{V}_{t-i}$ and $\vec{V}_{t-i_1} \cap \vec{V}_{t-i_2} = \emptyset$

for $i_1 \neq i_2$. Therefore, we can express $\mathcal{J}$ in Eq.(3.5) as:

$$\mathcal{J} = I(Z_t; \vec{V}_{t-1}, ..., \vec{V}_{t-\tau} \mid \vec{W}_\tau),$$

and by using the chain rule for conditional mutual information [Shannon and Weaver, 1949], we get:

$$\mathcal{J} = \sum_{i=1}^{\tau} I(Z_t; \vec{V}_{t-i} \mid \vec{W}_\tau, \vec{V}_{t-i-1}, ..., \vec{V}_{t-\tau}). \tag{3.7}$$

Note that $\{\vec{V}_{t-i-1}, ..., \vec{V}_{t-\tau}\}$ are actually the remaining parents of both Z_t and the subgraph $C_{\vec{V}_{t-i} \Rightarrow Z_t}$ initiated by $\vec{V}_{t-i}$, which are not in $\vec{W}_\tau$. Therefore, the condition set in Eq.(3.7), $\{\vec{W}_\tau, \vec{V}_{t-i-1}, ..., \vec{V}_{t-\tau}\}$, in fact contains the parents of the union of Z_t and $C_{\vec{V}_{t-i} \Rightarrow Z_t}$, or $P_{C_{\vec{V}_{t-i} \Rightarrow Z_t} \cup Z_t}$. Also, due to the Markov property of the time series DAG, $P_{C_{\vec{V}_{t-i} \Rightarrow Z_t} \cup Z_t}$ separates $C_{\vec{V}_{t-i} \Rightarrow Z_t} \cup Z_t$ from their non-descendants, including the remaining nodes in the conditions in Eq.(3.7), and thus gives:

$$\begin{aligned} \mathcal{G}_i &\equiv I(Z_t; \vec{V}_{t-i} \mid \vec{W}_\tau, \vec{V}_{t-i-1}, ..., \vec{V}_{t-\tau}) \\ &= I(Z_t; \vec{V}_{t-i} \mid P_{C_{\vec{V}_{t-i} \Rightarrow Z_t} \cup Z_t} \backslash C_{\vec{V}_{t-i} \Rightarrow Z_t}) \end{aligned} \tag{3.8}$$

where $\mathcal{G}_i$ is the generalized version of the momentary information transfer along causal paths [Runge, 2015, Jiang and Kumar, 2018] from multiple source nodes $\vec{V}_{t-i}$ to Z_t along the multiple causal paths $C_{\vec{V}_{t-i} \Rightarrow Z_t}$. It quantifies the uncertainty reduction in Z_t due to $\vec{V}_{t-i}$ conditioned on the parents of both Z_t and $C_{\vec{V}_{t-i} \Rightarrow Z_t} \cup Z_t$,

Correspondingly, Eq.(3.7) can thus be simplified as:

$$\mathcal{J} = \sum_{i=1}^{\tau} \mathcal{G}_i = \sum_{i=1}^{\tau} I(Z_t; \vec{V}_{t-i} \mid P_{C_{\vec{V}_{t-i} \Rightarrow Z_t} \cup Z_t} \backslash C_{\vec{V}_{t-i} \Rightarrow Z_t}). \tag{3.9}$$

This equation elucidates that the information given by a sequence of dynamics preceding Z_t, i.e., its immediate causal history, is an accumulation of the momentary information transfer from the contemporaneous dynamics at each time step involved in this finite history.

Such accumulation of momentary information can be generalized to the total information $\mathcal{T}$ if the source nodes $\vec{V}$ of the immediate causal history are taken as all the variables at an infinite past, $\vec{X}_{t-\tau} = \{V_{t-\tau}, X_{t-\tau}, Y_{t-\tau}, Z_{t-\tau}, ...\}$, with $\tau \to \infty$. In this case, the immediate causal history is naturally the whole causal history itself, and thus $\mathcal{J} = \mathcal{T}$, which based on Eq.(3.9) gives:

$$\mathcal{T} = \lim_{\tau \to \infty} \sum_{i=1}^{\tau} I(Z_t; \vec{X}_{t-i} \mid P_{C_{\vec{X}_{t-i} \Rightarrow Z_t} \cup Z_t} \backslash C_{\vec{V}_{t-i} \Rightarrow Z_t}). \tag{3.10}$$

By relating the above equation with Eq.(3.2), again we see that the momentary information from all the previous intermediate nodes in the causal history are accumulated at the nodes that directly influence the target Z_t, as shown in Fig. 3.1b. Note that, a measure similar to Eqs.(3.7)-(3.10) is proposed in [Runge et al., 2012b], called the decomposed transfer entropy. It approximates the information coming from all the historical states of a source variable $\vec{X}_t^-$ as the summation of individual conditional mutual information from each lagged $X_{t-\tau}$ in a finite set of $\vec{X}_t^-$. This is different from the information aggregation of $\mathcal{J}$ and $\mathcal{T}$ proposed here in that Eqs.(3.9) and (3.10) approximate the information from the historical states of multiple source variables to the target.

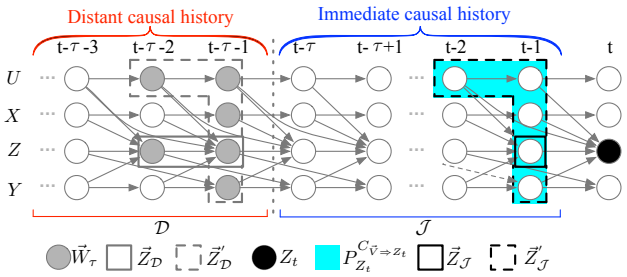

Figure 3.2: Illustration of the self and cross dependencies in both simplified immediate and distant causal histories for a target Z_t (the black node). The self-dependencies, $\vec{Z}_\mathcal{J}$, and the complementary part, $\vec{Z}'_\mathcal{J}$, in the simplified immediate causal history, $P_{Z_t}^{C_{\vec{V}\Rightarrow Z_t}}$, are identified in solid and dashed black boxes, respectively. The self-dependencies, $\vec{Z}_\mathcal{D}$, and the complementary part, $\vec{Z}'_\mathcal{D}$, in the simplified distant causal history, $\vec{W}_\tau$, are identified in solid and dashed grey boxes, respectively.

3.2.4 Interactions from Self-Feedbacks in $\mathcal{J}$ and $\mathcal{D}$

To further dissect the information transfer we characterize the interaction information arising from self and cross dependencies of a target variable Z_t in both immediate and distant causal histories. Note that interaction information between two sets of source nodes $\vec{A}$ and $\vec{B}$ contributing information to Z_t is given as:

$$\begin{aligned}\mathcal{I} &= I(Z_t; \vec{A}|\vec{B}) - I(Z_t; \vec{A}) \\ &= I(Z_t; \vec{A}, \vec{B}) - [I(Z_t; \vec{A}) + I(Z_t; \vec{B})].\end{aligned} \tag{3.11}$$

For distant causal history, represented by $\vec{W}_\tau$, the two decomposed parts include: (1) a self-feedback component of Z_t, $\vec{Z}_\mathcal{D} \equiv \{V_{t-\tau} \in \vec{W}_\tau \mid V = Z\}$ (the grey box in Fig. 3.2); and (2) the complementary component, $\vec{Z}'_\mathcal{D} \equiv \vec{W}_\tau \backslash \vec{Z}_\mathcal{D}$ (the dashed grey box in Fig. 3.2). The difference between $\mathcal{D}$ and the summation of the mutual information between Z_t and each of the two components in $\vec{W}_\tau$ then accounts for an interaction information,

$\mathcal{I}_{\mathcal{D}}$, which is given by:

$$\mathcal{I}_{\mathcal{D}} = \mathcal{D} - [I(Z_t; \vec{Z}_{\mathcal{D}}) + I(Z_t; \vec{Z}'_{\mathcal{D}})]. \tag{3.12}$$

$\mathcal{I}_{\mathcal{D}}$ quantifies the interaction information in Eq.(3.11) transferred to the target Z_t from its self-dependency, $\vec{Z}_{\mathcal{D}}$, as well as the complementary component, $\vec{Z}'_{\mathcal{D}}$,in distant history. A negative $\mathcal{I}_{\mathcal{D}}$ [i.e., $\mathcal{D} < I(Z_t; \vec{Z}_{\mathcal{D}}) + I(Z_t; \vec{Z}'_{\mathcal{D}})$] shows a net redundancy in the interaction between the two components, while a positive $\mathcal{I}_{\mathcal{D}}$ [i.e., $\mathcal{D} > I(Z_t; \vec{Z}_{\mathcal{D}}) + I(Z_t; \vec{Z}'_{\mathcal{D}})$] illustrates a net synergistic influence on the target.

Similarly, the simplified immediate causal history of Z_t, represented by $P_{Z_t}^{C_{\vec{V} \Rightarrow Z_t}}$, can be partitioned into (1) a component containing the self-dependence of the target, $\vec{Z}_{\mathcal{J}} \equiv \{V_{t-\tau} \in P_{Z_t}^{C_{\vec{V} \Rightarrow Z_t}} \mid V = Z\}$ (the black box in Fig. 3.2); and (2) the complementary part, $\vec{Z}'_{\mathcal{J}} \equiv P_{Z_t}^{C_{\vec{V} \Rightarrow Z_t}} \backslash \vec{Z}_{\mathcal{J}}$ (the dashed black box in Fig. 3.2). The corresponding interaction information from the two parts of immediate causal history, $\mathcal{I}_{\mathcal{J}}$, can be computed as:

$$\mathcal{I}_{\mathcal{J}} = \mathcal{J} - [I(Z_t; \vec{Z}_{\mathcal{J}} \mid \vec{W}_\tau) + I(Z_t; \vec{Z}'_{\mathcal{J}} \mid \vec{W}_\tau)], \tag{3.13}$$

quantifying the conditional interaction information to Z_t from its self and cross dependencies in the immediate causal history.

We also note that in [Runge, 2015], the interaction information is used for investigating how the influence from a source node $X_{t-\tau}$ to Z_t is intervened by the immediate nodes in the causal path $C_{X_{t-\tau} \to Z_t}$. In this study, we evaluate the interaction effects on Z_t from immediate and distant causal histories in terms of: first, Z_t's own history, and second, historical states of the other variables.

3.3 Applications

To illustrate the capability of the approach described above for delineating the temporal dependency of a system, we quantify the information transfer from the causal history in three different systems. We first characterize the temporal dependency of a short-memory system through a trivariate logistic model. Then, we illustrate how the proposed approach is different from lagged mutual information in addressing system's memory dependency using an example of a chaotic system – the Lorenz model. Further, we compare the Lorenz model with a trivariate Ornstein-Uhlenbeck process to investigate how the information transfer differs in processes with and without strange attractor. Finally, we quantify the memory dependency from time series observations, representing catchment chemistry, which is known to have long-term dependency.

Especially, by decomposing the distant history into the self-feedback of the target and the complementary component characterizing information transfer from other interacting variables, we observe the redundancy-dominated $\mathcal{J}$, as well as consistent nonzero and synergy-dominated $\mathcal{D}$ in both the Lorenz model and the stream chemistry system, which we conjecture as sustaining chaotic and fractal features of the two systems.

3.3.1 Trivariate Logistic System: a Short-Memory System

In the following, we empirically analyze the information transfer in the causal history of a nonlinear model-generated synthetic data. Consider a trivariate coupled logistic system in Eq.(2.31). To investigate the total information and its two components to the target node $X_{3,t}$, we consider the immediate causal history as the causal subgraph $C_{\{X_{1,t-\tau},X_{2,t-\tau},X_{3,t-\tau}\}\Rightarrow X_{3,t}}$ starting at an earlier time step $t-\tau$ ($\tau \geq 1$) (see Fig. 3.3a). $\mathcal{J}$, $\mathcal{D}$ and $\mathcal{T}$ are calculated for τ ranging from 1 to 50 and $\epsilon \in [0.1, 0.2, 0.3, 0.5, 0.8]$. For each pair of τ and ϵ, 10,000 data points are generated to conduct the empirical estimations, with an ensemble of 10 runs for each to get an average behavior. To avoid the infinite dimensions in Eq.(3.2) in the computation, we compute $\mathcal{T}$, $\mathcal{D}$ and $\mathcal{J}$ based on Eqs.(3.3), (3.4), and (3.6), respectively. The k-nearest-neighbor (kNN) estimator [Kraskov et al., 2004, Frenzel and Pompe, 2007] is adopted for the estimation of $\mathcal{J}$, $\mathcal{T}$ and $\mathcal{D}$ with $k = 5$ (low k facilitates a low bias of the estimated MI and CMI [Frenzel and Pompe, 2007]). In the next two applications, the computation of $\mathcal{T}$, $\mathcal{D}$, and $\mathcal{J}$ are also conducted in the same manner.

The contribution of immediate causal history $\mathcal{J}$, and the proportion of distant causal history, $\mathcal{D}$, in the total information transfer $\mathcal{T}$, $\mathcal{D}/\mathcal{T}$, are shown in Fig. 3.3b. We observe that for the range of noise coupling strengths ϵ, $\mathcal{J}$ and $\mathcal{D}/\mathcal{T}$ increases and decreases, respectively, with lag τ, and $\mathcal{D}/\mathcal{T}$ achieves asymptotic convergence to zero when the lag is sufficiently large. In particular, the convergence to zero of $\mathcal{D}/\mathcal{T}$ illustrates that this trivariate coupled logistic model has a short memory for influencing the target. Further, the decrease of $\mathcal{J}$ with increasing coupling strength ϵ implies that a strong noise can reduce the information transfer from the preceding finite length period and, thus, also reduce the total information in this short-memory system.

Also, it is noted that the curves in $\mathcal{D}/\mathcal{T}$ decrease with increasing τ but intersect for different values of ϵ. This is because of different interactions and synchronization of coupled logistic maps as a function of ϵ [Rosenblum et al., 1997, Atay et al., 2004, Paredes et al., 2013]. Therefore, we compute the lag synchronization for each pair of lagged variables $X_{i,t-\tau}$ and $X_{j,t}$ ($i, j \in \{1, 2, 3\}$) with τ ranging from 1 to 50, which is given by:

$$\mathcal{S}_{ij}(\tau) = \left\{ \frac{E[(X_{i,t-\tau} - X_{j,t})^2]}{[E(X_{i,t-\tau}^2)E(X_{j,t}^2)]^{1/2}} \right\}^{0.5}, \tag{3.14}$$

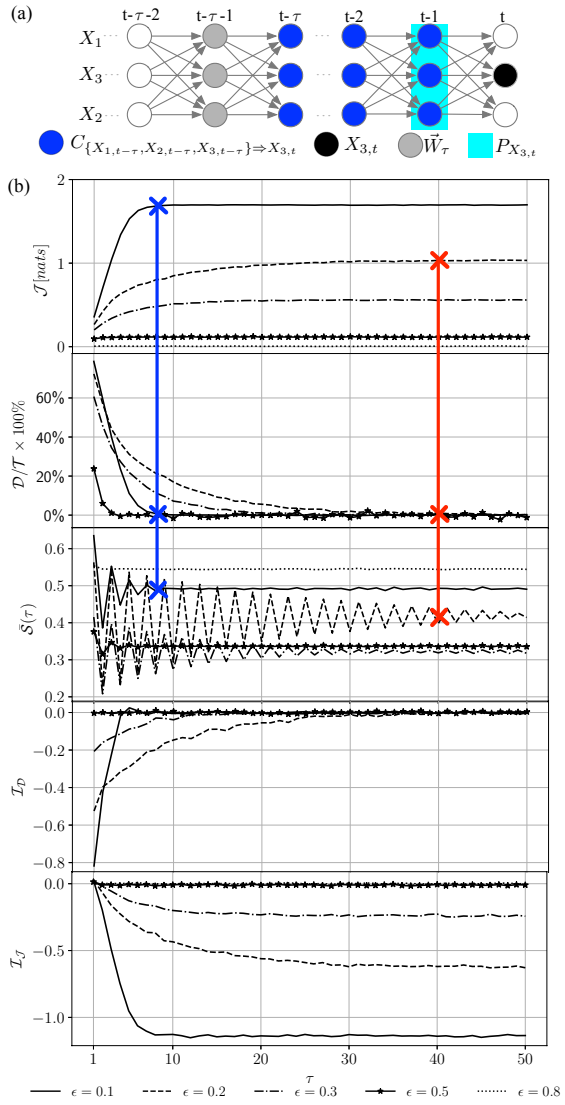

Figure 3.3: Illustration of the trivariate coupled logistic model. (a) The time-series graph of the system with the causal subgraph $C_{\{X_{1,t-\tau},X_{2,t-\tau},X_{3,t-\tau}\}\Rightarrow X_{3,t}}$ as the immediate causal history (the representations of the nodes are the same as in Fig. 3.1a). (b) Plots of $\mathcal{J}$, $\mathcal{D}/\mathcal{T}$, $\bar{\mathcal{S}}$, $\mathcal{I}_\mathcal{D}$ and $\mathcal{I}_\mathcal{J}$ for τ ranging from 1 to 50 with $\epsilon \in [0.1, 0.2, 0.3, 0.5, 0.8]$ (blue and red crosses, connected through a vertical line, represent the convergence points of $\mathcal{J}$, $\mathcal{D}/\mathcal{T}$, and $\bar{\mathcal{S}}$ for $\epsilon = 0.1$ and $\epsilon = 0.2$, respectively; note that results for $\epsilon = 0.8$ are not plotted (except $\mathcal{J}$) due to its high variability resulting from a near-zero total information $\mathcal{T}$).

where E is the expectation function. Since the dynamics is highly symmetric in terms of $\{X_1, X_2, X_3\}$ for this trivariate model, we compute the averaged lag synchronization $\bar{\mathcal{S}}(\tau)$ as:

$$\bar{\mathcal{S}}(\tau) = \frac{\sum_{i,j} \mathcal{S}_{ij}(\tau)}{9}, \tag{3.15}$$

which is sketched in the middle plot of Fig. 3.3b. It shows that for each noise coupling strength ϵ, $\bar{\mathcal{S}}$

oscillates for small τ, and then the amplitude decreases and $\bar{\mathcal{S}}$ eventually converges with increasing τ, implying a consistent similarity structure between each pair of lagged variables given an ϵ. The convergence of the averaged lag synchronization, $\bar{\mathcal{S}}$, implies that the similarity between a target $X_{j,t}$ and a lagged history node $X_{i,t-\tau}$ gradually becomes invariant with increasing τ. It is consistent with the convergences of both $\mathcal{J}$ and $\mathcal{D}/\mathcal{T}$ for each ϵ, which are illustrated for $\epsilon = 0.1$ and $\epsilon = 0.2$ in blue and red crosses, respectively.

Further, the interaction information $\mathcal{I}_{\mathcal{D}}$ and $\mathcal{I}_{\mathcal{J}}$ increases and decreases with time lag τ, and then converges to zero and a negative value, respectively. The rapid convergence to the asymptotic values suggests no synergy or redundancy for this short-memory model. Meanwhile, the drop of $\mathcal{I}_{\mathcal{J}}$ with increasing τ means the contributions from self and cross dependencies in the immediate causal history share a higher redundancy.

3.3.2 The Lorenz Model: a Comparison with Lagged Mutual Information

Now, we perform the analysis of the Lorenz model to investigate the difference between the proposed measures of causal history and traditional methods such as lagged mutual information in capturing the temporal dependency of a system, as well as to understand the potential interdependencies embedded in its chaotic behavior. The Lorenz model is prototypical of its chaotic behavior [Lorenz, 1963], that is, its dynamics are contained in a strange attractor with a fractal dimension between 2 and 3, and its governing equation is given by a system of three variables X_t, Y_t and Z_t as:

$$\frac{dX_t}{dt} = \sigma(Y_t - X_t) \tag{3.16a}$$

$$\frac{dY_t}{dt} = X_t(\rho - Z_t) - Y_t \tag{3.16b}$$

$$\frac{dZ_t}{dt} = X_t Y_t - \beta Z_t, \tag{3.16c}$$

where the parameters σ, ρ and β in this study are set as 10, 28, and 8/3, respectively.

To analyze the information dynamics in the system as well as the resulting long-term dependence, we empirically quantify the influence on a target $U_t \in \{X_t, Y_t, Z_t\}$ based on (1) the lagged mutual information between each pair of variables $I(U_t; V_{t-\tau dt})$, where $V_t \in \{X_t, Y_t, Z_t\}$, and τ and dt are the lag step and the time interval, respectively; (2) the information transfer from the immediate and distant causal histories for each variable, $\mathcal{J}$ and $\mathcal{D}$, respectively; and (3) the interaction information contributed by a self-feedback and the corresponding complementary components in both distant and immediate causal history, $\mathcal{I}_{\mathcal{D}}$ and $\mathcal{I}_{\mathcal{J}}$, as indicated in Eqs.(3.12) and (3.13), respectively. The immediate causal history is now the subgraph $C_{\{X_{t-\tau dt}, Y_{t-\tau dt}, Z_{t-\tau dt}\} \Rightarrow U_t}$ (see Fig. 3.4a), from which we can observe that given a time lag τdt the representative distant causal history $\vec{W}_\tau = \{X_{t-(\tau+1)dt}, Y_{t-(\tau+1)dt}, Z_{t-(\tau+1)dt}\}$. The measures are calculated for

τ ranging from 1 to 1000 with the time interval $dt = 0.01$. 10,000 data points are generated to conduct the empirical estimations, with an ensemble of 10 runs to get an average behavior.

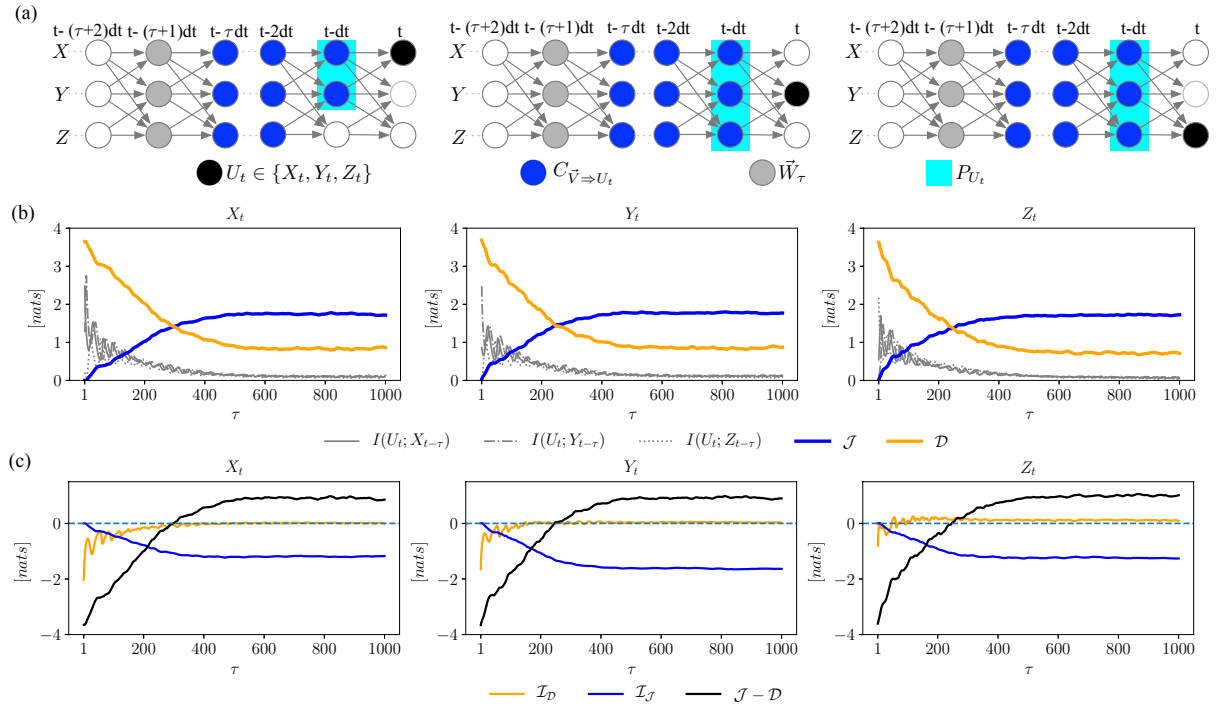

Figure 3.4: Illustration of the Lorenz model with parameters $\sigma = 10$, $\rho = 28$ and $\beta = 8/3$. (a) The times series graph of the system with the causal subgraph $C_{\{X_{t-\tau}, Y_{t-\tau}, Z_{t-\tau}\} \Rightarrow U_t}$ ($U \in \{X, Y, Z\}$) as the immediate causal history. (b) The corresponding plots of the lagged mutual information, $\mathcal{J}$, and $\mathcal{D}$ for the time lag τ ranging from 1 to 1000. (c) The corresponding plots of $\mathcal{I}_\mathcal{D}$, $\mathcal{I}_\mathcal{J}$, and $\mathcal{J} - \mathcal{D}$ for the time lag τ ranging from 1 to 1000.

The results of the lagged mutual information, $\mathcal{D}$, and $\mathcal{J}$ are shown in Fig. 3.4b. The quantities $\mathcal{J}$ and $\mathcal{D}$ increases and decreases, respectively, with increasing τ, converging to some nonzero values when τ is around 500. The consistent nonzero $\mathcal{D}$ for large τ arises from the fact that the Lorenz system is a long-memory process such that information provided from the distant history informs the present dynamics. Meanwhile, the lagged mutual information, $I(U_t; V_{t-\tau dt})$, for all the three variables shows strong oscillations and gradually decays to zero. The oscillations are due to the chaotic behavior where the 'butterfly' trajectory of the strange attractor in this phase space determines the frequency of these oscillations, and the slow decay to zero reflects the long term dependency. However, the lagged mutual information does not show the consistent information contributed from the past as $\mathcal{D}$ does. Therefore, the proposed information transfer from the causal history provides a view for analyzing the memory dependency of the system that is complementary to traditional methods such as lagged mutual information.

Furthermore, the difference between $\mathcal{J}$ and $\mathcal{D}$ as well as their interaction information $\mathcal{I}_\mathcal{J}$ and $\mathcal{I}_\mathcal{D}$, shown

in Fig. 3.4(c), illustrate different roles of the immediate and distant causal histories in shaping the target. First, the recent dynamics of the Lorenz model has a stronger influence on the target than the remaining earlier dynamics as time lag τ becomes larger than around 200. This is evidenced by the convergence of $\mathcal{J} - \mathcal{D}$ to a positive value (the black thick line). Also, the convergence of $\mathcal{I}_{\mathcal{J}}$ to a negative value (the blue thick line) implies a higher redundancy effect from the interaction information of cross and self dependencies in the immediate causal history, as observed in the trivariate chaotic map. Meanwhile, the convergence of $\mathcal{I}_{\mathcal{D}}$ to zero (the orange thick line) suggests a balanced contribution from synergistic and redundant effects, each of which are not necessarily zero in the Lorenz model due to the nonzero convergence of $\mathcal{D}$ plotted in Fig.3.4(b). In short, the Lorenz model with a strange attractor shows each variable is affected by (1) a strong influence given by immediate causal history with dominant redundant effects from the self and cross dependencies, and (2) less influence from distant causal history with balanced redundancy and synergistic effects.

3.3.3 The Ornstein-Uhlenbeck Process: a Long-Memory Process Without Strange Attractor

To investigate the difference between processes with and without strange attractors in terms of the information transfer from causal history, we now conduct the analysis on a trivariate linear Ornstein-Uhlenbeck (OU) process with long-term dependency. The OU process is chosen such that the model has the same structure of the directed acyclic time series graph as the Lorenz model shown in Fig. 3.4(a) and it is stationary, which is given by:

$$\frac{dX_t}{dt} = -0.5X_t + 0.3Y_t + \zeta_X \tag{3.17a}$$

$$\frac{dY_t}{dt} = 0.4X_t - 0.4Y_t - 0.3Z_t + \zeta_Y \tag{3.17b}$$

$$\frac{dZ_t}{dt} = 0.4X_t + 0.6Y_t - 0.7Z_t + \zeta_Z, \tag{3.17c}$$

where ζ_X, ζ_Y and ζ_Z are independently and identically distributed noise terms following standard normal distribution. As in the analysis of the Lorenz model, we quantify the influence on each variable in the OU process in terms of lagged mutual information, the information from immediate and distant causal history $\mathcal{J}$ and $\mathcal{D}$, and their interaction information $\mathcal{I}_{\mathcal{J}}$ and $\mathcal{I}_{\mathcal{D}}$. The computation settings of the above information-theoretic measures are the same as the Lorenz model. The trajectory and the time series of each variable of the OU process are plotted in Fig. 3.5(a) with time interval $dt = 0.01$ and 10,000 simulated data points, visually showing that the dynamics are confined in a three-dimensional confined domain which is not a

strange attractor.

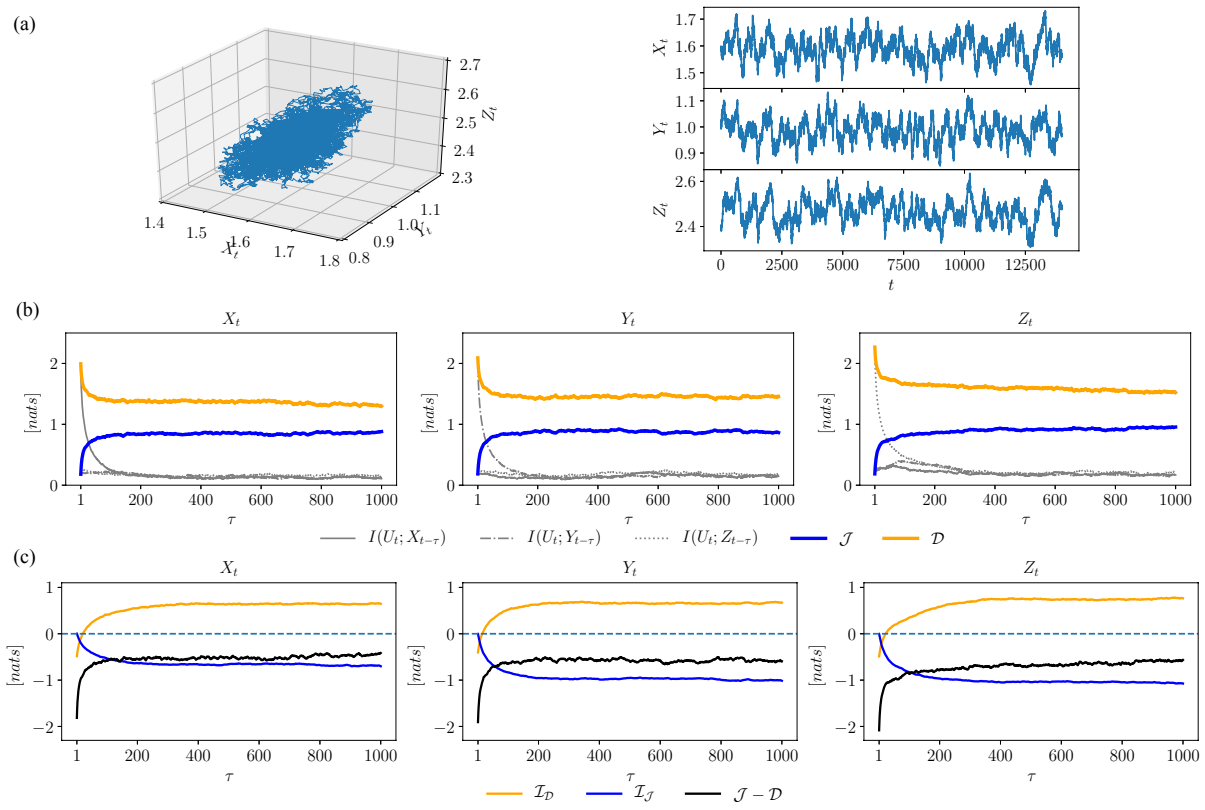

Figure 3.5: Illustration of the Ornstein-Uhlenbeck (OU) process in Eq.(3.17). (a) The trajectories of the process (left) and the time series of each variable (right). (b) The corresponding plots of the lagged mutual information, $\mathcal{J}$, and $\mathcal{D}$ for the time lag τ ranging from 1 to 1000. (c) The corresponding plots of $\mathcal{I}_\mathcal{D}$, $\mathcal{I}_\mathcal{J}$, and $\mathcal{J} - \mathcal{D}$ for the time lag τ ranging from 1 to 1000.

The long-memory property of the OU process in Eq.(3.17) is evidenced in the non-zero convergence of $\mathcal{D}$ and a slow-decay of the auto mutual information of each variable in Fig. 3.5(b), as also observed in the Lorenz model (Fig. 3.4(b)). Nevertheless, different from the Lorenz model which shows a higher convergence value in $\mathcal{J}$, the convergence value of $\mathcal{D}$ in the OU process is larger. It indicates that, for the OU process, the distant causal history always provides more information to the target than the immediate causal history no matter how much of the finite recent dynamics are considered. Further, while the interaction information $\mathcal{I}_\mathcal{J}$ and $\mathcal{I}_\mathcal{D}$ still decreases and increases with the time lag τ, respectively, similar to the Lorenz model, $\mathcal{I}_\mathcal{D}$ in the OU process converges a value larger than zero. The convergence of $\mathcal{I}_\mathcal{D}$ to a positive value implies a net synergistic effect from the interaction contribution to the target. In summary, compared with the Lorenz model, the evolutionary dynamics of the OU process, which shows a similar long-term dependency but without a strange attractor, contains a more dominant influence from distant causal history with a net synergistic effect on each variable in the process.

3.3.4 Catchment Chemistry Data: an Observed Long-Memory System

We now employ our approach to analyze the water solutes in the Upper Hafren in Wales, where the stream chemistry records are found to have $1/f$ fractal signatures reflecting long-term dependencies due to the complex interactions occurring in the catchment [Kirchner et al., 2000, Kirchner and Neal, 2013]. In this application, the logarithm of flow rate, $\ln Q$, and six water chemistry variables, Na^+, Cl^-, Al^{3+}, Ca^{2+}, $SO4^{2-}$ and pH, are chosen for analysis, which are sampled every 7-h from March 2007 to Jan 2009. The 1/f fractal signatures are found in the corrected chemistry data, where the trend of the logarithm of stream flow is excluded [Kirchner and Neal, 2013]. Both the raw and the flow rate-corrected data are available from [Kirchner and Neal, 2013], which are used here. Here, we construct the time series graph for both the raw data and the flow rate-corrected data by using the Tigramite algorithm [Runge et al., 2012b, Runge, 2015, Runge et al., 2015, Runge et al., 2017] – a modified PC algorithm [Spirtes et al., 2000] anchored on the conditional independence test to remove any spurious relationship between each pair of nodes.

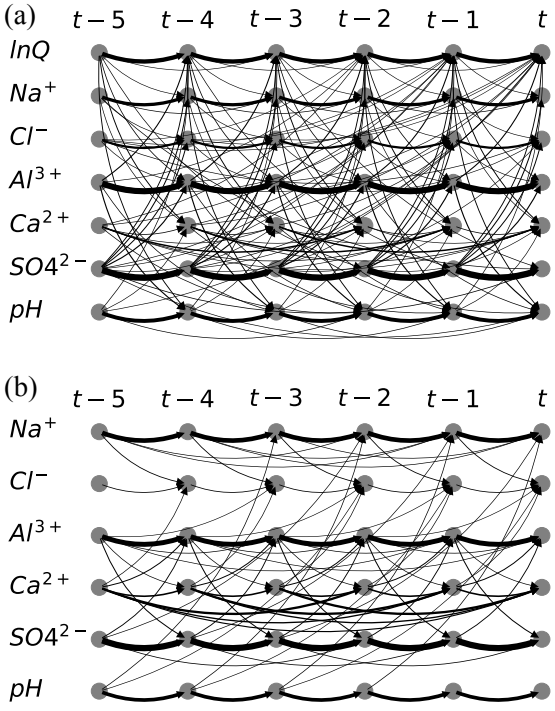

Figure 3.6: Time-series graph constructed by using the Tigramite algorithm from (a) observed logarithm of flow rate and six catchment chemistry time series data; and (b) the six catchment chemistry data with the variation of logarithmic flow rate corrected. The thickness of edges represents the coupling strength between two nodes computed by momentary information transfer shown in Fig. E.1 (see the details of the graph construction in Appendix E).

The two resulting time series graphs are shown in Fig. 3.6 (see the details of the graph construction

in Appendix E), where coupling strengths in each directed edge, represented as the thickness of the edge, is computed as the momentary information transfer (MIT) [Runge et al., 2012a] between the two nodes. We can observe strong self-feedback dependencies (shown as thick edges) for most variables in both graphs. Meanwhile, the remaining "hairy" causal influences, in a Granger sense, illustrate the relatively weaker lagged interdependencies (shown as thin edges) among the variables, which, along with the self-feedback dependency, contribute to the current state of each variable. Furthermore, the comparison between the two graphs shows that with the influence of flow rate excluded, the graph constructed from the flow rate-corrected data (Fig. 3.6b) contains fewer cross-dependencies (Fig. 3.6a). It reflects the fact that flow rate (based mixing) plays a key role in establishing the connectivities among the stream chemistry variables.

Based on the graphs, we now compute the information transfer measures, $\mathcal{T}$ and $\mathcal{D}$, and the interaction information $\mathcal{I}_{\mathcal{J}}$ and $\mathcal{I}_{\mathcal{D}}$ in Eqs.(3.12) and (3.13), respectively. The immediate causal history is initiated by all the five variables with a same time lag τ ranging from 1 to 400 (117 days for 7hr dataset). Again, $\mathcal{T}$ and $\mathcal{D}$ are first calculated based on Eqs.(3.3)-(3.4) with the number of nearest neighbors $k = 5$ (in kNN method).

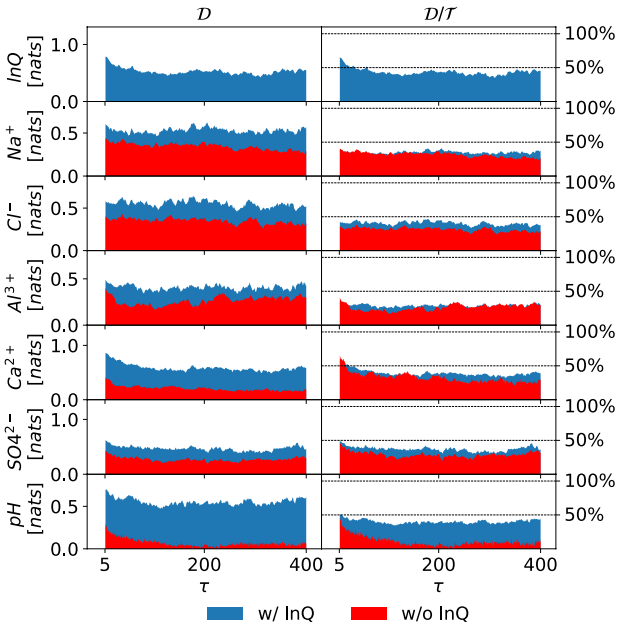

Figure 3.7: Plots of the information transfers $\mathcal{D}$ (left) and the proportion $\mathcal{D}/\mathcal{T}$ (right) over the time lag τ for the raw data and the flow rate-corrected data taking the immediate causal history initiated from all the variables with a same lag τ based on the estimated time series graph in Fig. 3.6.

The plots of $\mathcal{D}$ and the proportion $\mathcal{D}/\mathcal{T}$ as a function of τ shown in Fig. 3.7 are insightful. First, for all the variables in both graphs, the information from the distant causal history, $\mathcal{D}$ (the left column of Fig. 3.7), drops rapidly at small lags τ but starts to converge to a value far from zero for larger time lags (except for

pH). Such persistent non-zero $\mathcal{D}$ reflects the long-term dependence present in the water chemistry data, and illustrates that the dynamics from a distant causal history in the stream plays an important role in shaping the current states of the solutes [Kirchner et al., 2000]. Further, the right column of Fig. 3.7 shows that, for each variable in both networks, the percentage of the convergence value of $\mathcal{D}$ in the total information $\mathcal{T}$ is less than 50%, illustrating a more dominant influence from the immediate causal history. Also, by comparing the dynamics with and without flow rate, both $\mathcal{D}$ and its percentage in the total information, $\mathcal{D}/\mathcal{T}$, decrease when the influence of flow rate is excluded. It illustrates that flow rate is an important driving variable that connects various water stream variables, and contributes to maintaining the long-memory dependence. However, this dependence varies for different variables. Specifically, for variables that are highly dependent on flow rate, such as Ca^{2+} and pH, $\mathcal{D}$ declines significantly when the influence of flow rate is excluded. For other variables, especially Na^{+} and Cl^{-} the majority of which originates from the oceanic sources through atmospheric pathways in this close-to-coast location [Feng et al., 2004], $\mathcal{D}$ drops to a lesser degree and thus still holds a relatively strong memory persistence due to their lower dependencies on flow rate.

Further, the interaction information $\mathcal{I}_{\mathcal{J}}$ and $\mathcal{I}_{\mathcal{D}}$ of the immediate and distant causal histories, respectively, as a function of lag τ are plotted in Fig. 3.8. First, we see that when the influence of the flow rate is included (the left column of Fig. 3.8), $\mathcal{I}_{\mathcal{J}}$ decreases with increasing τ and converges to a negative value, suggesting the prevalence of strong redundant influence in the immediate causal history. Meanwhile, $\mathcal{I}_{\mathcal{D}}$ flattens out to zero as τ becomes larger than around 20. The convergence of $\mathcal{I}_{\mathcal{D}}$ to zero implies a balanced synergistic and redundant effects from the self and cross dependencies in the distant causal history. Moreover, in the network without the influence of flow rate (the right column of Fig. 3.8), $\mathcal{I}_{\mathcal{J}}$ also converges to zero, indicating a balance of synergistic and redundant contribution.

Also, notice that there exist oscillations in different information-theoretic measures shown in both Figs. 3.7 and 3.8 even when the values converge for large τ. This is possibly due to the bias induced by the estimation of the proposed high-dimensional information-theoretic measures [Runge et al., 2012a, Runge, 2015, Jiang and Kumar, 2018] with a limited amount of data points, which are around 1000$\sim$2000 for the estimation of $\mathcal{D}$ for different time lags. A shuffle test is also conducted for the computation of $\mathcal{D}$, to ensure that most of the values are statistically significant at $\alpha = 0.05$ significance level (see Appendix E for details).

3.4 Conclusion

We have developed information-theoretic measures to partition the influence of total causal history ($\mathcal{T}$) into two components, immediate ($\mathcal{J}$) and distant ($\mathcal{D}$) causal history. While the information from the

immediate causal history quantifies the impact on the state of a specific variable from trajectories of recent dynamics, its complement, the distant causal history, illustrates such impact stemming from the remaining older history.

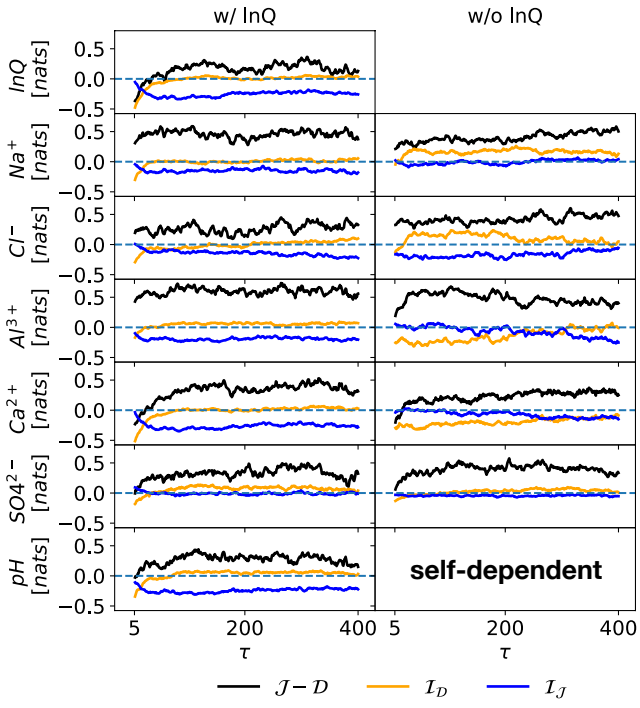

Figure 3.8: Plots of the interaction information from distant causal history, $\mathcal{I}_{\mathcal{D}}$ in Eq.(3.12) (black line), and immediate causal history, $\mathcal{I}_{\mathcal{J}}$ in Eq.(3.13) (blue line), over the time lag τ for the raw data and the flow rate-corrected data taking the immediate causal history initiated from all the variables with a same lag τ based on the estimated time series graph in Fig. 3.6.

By employing the Markov property for directed acyclic graph, we reduce the dimensions of $\mathcal{T}$, $\mathcal{D}$ and $\mathcal{J}$ to make the computations of the three measures feasible. The Markov property based simplification further results in the information aggregation property of the time series directed acyclic graph, that is, the information transferred from earlier dynamics in the causal history accumulate at the nodes directly influencing the target node(s). Moreover, the dimension reduction also enables further partitions of both the immediate and distant causal histories into self and cross dependencies, and allows us to quantify their interaction information contribution to a target.

It is noted that while the dimension of $\mathcal{T}$ is now reduced to only the parents of the target, the cardinalities of $\mathcal{D}$ and $\mathcal{J}$ can still be high due to the inclusion of the parents of the immediate causal history. For instance, in the stream chemistry example, the dimensions of $\mathcal{D}$ and $\mathcal{J}$ are around 30 and 40, respectively, as shown in Fig. E.3. Such high dimensions might result in biased information-theoretic estimation based on limited datasets. Future research is required to further reduce the dimensionality.

We take the opportunity to distinguish the causal history formulation presented here with some relevant prior work. These include transfer entropy [Schreiber, 2000], causation entropy [Sun and Bollt, 2014], momentary information transfer [Runge et al., 2012b], and directed information [Kramer, 1998]. These existing information-theoretic measures quantify the coupling strength between two (lagged) variables with or without the knowledge of other variable(s), while the proposed causal history analysis investigates how the entire evolutionary dynamics involving all variables in a system influences a target variable. This uniqueness of considering contribution from multiple variables enables analyses that are not possible otherwise. The followings is a brief summary of the differences with these different information-theoretic approaches.

Transfer entropy (TE) [Schreiber, 2000] quantifies the information transfered to a target, Z_t, from a sequence of previous states of another variable, $X_{t-1:t-\tau} = \{X_{t-1}, X_{t-2}, ..., X_{t-\tau}\}$, given the knowledge of the past states of itself, $Z_{t-1:t-\tau} = \{Z_{t-1}, Z_{t-2}, ..., Z_{t-\tau}\}$. It is computed through a conditional mutual information, and is given by in Eq.(1.4). Momentary information transfer (MIT) in Eq.(1.8) [Runge et al., 2012b], on the other hand, considers the information transfer to Z_t from a specific lagged variable $X_{t-\tau}$ given the knowledge of the entire historical states.

The idea of conditioning, which prevents the influence from the nodes in the condition set in influencing the quantification of coupling strength, is also used in causation entropy (CE) [Sun and Bollt, 2014]. CE from a source variable with lag 1, X_{t-1}, to the a target, Z_t, conditioned on a third variable, Y_t, with lag 1, and is given by:

$$I^{CE}_{X\to Z|Y} = I(Z_t; X_{t-1} \mid Y_{t-1}). \tag{3.18}$$

Notice that causation entropy is a generalization of transfer entropy in Eq.(1.4) with $\tau = 1$, that is $I^{CE}_{X\to Z|Z} = I^{TE}_{X\to Z}(1)$.

Further, another measure called Directed Information (DI) [Amblard and Michel, 2013] quantifies how a limited historical dynamics of a source variable, $X_{t-\tau:t}$, affects the dynamical trajectory of the target variables, $Z_{t-\tau:t}$. This is given as:

$$I^{DI}_{X\to Z}(\tau) = \sum_{i=1}^{\tau} I(Z_{t-i}; X_{t-1:t-i} \mid Z_{t-1:t-i+1}). \tag{3.19}$$

When the knowledge of the dynamical trajectory of the third variables, $Y_{t-\tau:t}$ is given, it is converted into

a conditional directed information (CDI) [Amblard and Michel, 2013], given by:

$$I^{CDI}_{X\to Z|Y}(\tau) = \sum_{i=1}^{\tau} I(Z_{t-i}; X_{t-1:t-i} \mid Z_{t-1:t-i+1}, Y_{t-1:t-i}). \tag{3.20}$$

Different from I^{TE}, I^{MIT} and I^{CE}, which quantify the influence to a target from a lagged source variable, I^{DI} and I^{CDI} consider the influence from the past dynamics preceding time t as well as the instantaneous dynamics at time t.

In addition to pairwise interactions, a variation of Eq.(3.18), temporal causation entropy (TCE) is used for inferring the Markov order of a process [Cafaro et al., 2015], which is given by:

$$I^{TCE}(\tau) = I(Z_t; \vec{Z}_t^{-} \backslash Z_{t-1:t-\tau} \mid Z_{t-1:t-\tau}). \tag{3.21}$$

which is the conditional mutual information between Z_t and its earlier dynamics, $\vec{Z}_t^{-} \backslash Z_{t-1:t-\tau}$, given the immediate dynamics $Z_{t-1:t-\tau}$. The calculation of I^{TCE} in Eq.(3.21) involves the division of the entire history of a process into two parts based on a time lag τ, which looks similar to the partition of immediate and distant causal histories at a first glance. However, they differ in both the purposes and the technical details. While I^{TCE} is used to infer the Markov order of a process based on the smallest τ when I^{TCE} equals to zero in Eq.(3.21), the causal history analysis investigates the contribution from both immediate and distant causal histories. The different orientation in the causal history analysis, along with its multivariate nature of the analysis, indicate that this work adds significantly to the discourse associated with such studies.

All these existing information-theoretic measures (i.e., I^{TE}, I^{MIT}, I^{CE}, I^{DI} and I^{CDI}), except I^{TCE}, quantify the coupling strengths between two (lagged) variables from different perspectives. On the other hand, the proposed approach for causal history analysis presented in our work is initiated from a different perspective. It aims at analyzing how the target is driven by the entire evolutionary dynamics, which involves multivariate interactions in a complex system. By analyzing the whole history of the system, it allows the partition of the causal history into an immediate and distant components as well as quantification of these quantities. Furthermore, the instantaneous influence, which is explored in I^{DI} and I^{CDI}, is not considered as cause-effect relationship in this study. This is because the directionality of such causal influence between two contemporaneous nodes is unclear and the contemporaneous dynamics is not considered as causal 'history'.

The quantification of the information from the immediate and distant causal histories sketches the memory dependency of the system, which are illustrated with four examples with varying memories. Further, in addition to characterizing the memory dependency of a complex system, the proposed approach also delineates some key features of the complexity associated with its dynamics, which are not captured by other

traditional method such as lagged mutual information. First, for the Lorenz model and the OU process, while lagged mutual information slowly goes to zero with increasing time lag τ, the information from distant causal history $\mathcal{D}$ converges to a nonzero value with large lags. It implies a persistent information influence over long time scale in the system's evolutionary dynamics. Second, we observe that the analyzed models have different characteristics of information transfer. For instance, while the interaction information of distant causal history, $\mathcal{I}_{\mathcal{D}}$, flattens out in both the Lorenz model and the logistic map, the convergence of $\mathcal{I}_{\mathcal{D}}$ to zero in the Lorenz model suggests that there is a balanced synergy and redundancy jointly contributed by the self and cross dependencies. However, in the OU process, which also has long memory but no strange attractor, there turns out to be a net synergy effect in the distant causal history as $\mathcal{I}_{\mathcal{D}}$ converges to a positive value. Further, the differences in the interaction information of the immediate causal history, $\mathcal{I}_{\mathcal{J}}$, also illustrate the various dynamics in different systems. The comparison between the stream chemistry system with and without the influence of flow rate shows that the existence of the flow rate is able to enhance the redundant effect from self and cross dependencies in immediate causal history.

By involving multiple components as well as the causal influences among them, the proposed measures address an unresolved problem, that of quantifying the causal influence on the current state of a variable from the evolutionary dynamics of the entire system. It is different from what has been addressed so far by existing information-theoretic measures, which is usually anchored on pairwise interactions or multivariate analysis associated with specific parts of the system [Schreiber, 2000, Runge et al., 2012b, Sun and Bollt, 2014, Jiang and Kumar, 2018]. This uniqueness, therefore, facilitates addressing the questions of how the complexity of a system is sustained over time, which is reflected in varying memory dependency. With the increasing availability of observations in various domains, this work can open up avenues for new data-driven approaches for the study of complex system dynamics.

Chapter 4

Using Information Flow for Whole System Understanding from Component Dynamics

4.1 Introduction

Present day advances in sensor and communication technologies and declining costs are allowing us to observe the dynamics of our environment at ever increasing temporal frequency and spatial density. Simultaneous multivariate observations at high frequencies are opening up an unprecedented opportunity to understand and characterize deeply embedded inter-dependencies that govern process dynamics in our environment. How can we best use such high dimensional data, arising from a number of simultaneously measured variables, to ask questions that take us beyond component level relationships to expose whole system behavior, and enable us to identify system level attributes from component dynamics? On the flip side, can we also understand how system level constraints govern component level dynamics? In this paper we aim to present a framework to address such questions by quantifying information flow among variables to characterize causal dependencies in complex systems [Balasis et al., 2013, Bollt et al., 2018, Goodwell et al., view].

Complex systems arise from nonlinear interactions among its multiple components or variables. The complexity of an open system results as self-organized dynamics and associated patterns for form and function [Nicolis and Prigogine, 1989], which is a collective behavior resulting from the interactions among each component of the system. This draws upon the well-known idea that the whole is greater than the union of the parts. Coherent understanding of whole system dynamics from time-series observations of several components in such systems can only provide an approximate picture as all variables may not be observed. Further, the variables observed may not be at a sufficiently high resolution that reveals all dependencies. In addition, there is the possibility that a variable that is not observed may be an important driver of several components resulting in strong apparent dependencies that may otherwise be weak or nonexistent. Even if such a driver is in the mix of observed variables, it is not immediately apparent how its influence on the other linked variables should be isolated so as to allow the analysis of the driven components. Our goal, therefore, is to maximize the understanding that is possible using the entirety of the available data

recognizing that the sampling structure of the data imposes limitations. Towards this goal, we aim to quantify the cross-dependencies among variables through the dynamical evolution of the system, so as to characterize the inter-dependencies that lead to a better understanding of the whole system behavior. We develop the framework under minimal but necessary set of assumptions that are required to make the problem tractable and provide statistically robust inference.

To achieve this goal we use information flow as the currency of exchange between interacting variables. Information is encoded in patterns of variation of a signal. In a dynamical system, information flow captures the propagation of fluctuations among variables [Goodwell et al., 2018]. These fluctuations may be externally instigated, such as variability in solar radiation or rainfall in the context of a hydrologic response of a watershed, or internally generated through non-linearities in the system. Analysis of such information flow has the potential to characterize interactions across multivariate causal dependencies linked to whole system dynamics. The objective of this paper is to present specific approach and formulations to achieve this goal. We synthesize prior results and then present new formulations to develop the framework. The proposed approach also provides a pathway that unifies the apparently dichotomous reductionist and holistic approaches for studying system behavior by demonstrating that an understanding of detailed component dynamics can lead to better whole system understanding.

Consider a multivariate complex system with N variables, $\vec{X}_t = \{X_t, Y_t, Z_t, ...\}_N$, varying in time t. The current state of any variable $Z_t \in \vec{X}_t$ is in fact a result of the entirety of all the earlier dynamics in the system. We call this prior dynamics $\vec{X}_t^- = \{\vec{X}_{t-1}, \vec{X}_{t-2}, \vec{X}_{t-3}, ...\}$ as causal history in Chapter 3. The interactions from the causal history can be parsed in a number of ways. For example, it can be divided into immediate and complementary distant causal history, partitioned at some time lag $\tau > 0$. The quantification of the influences from immediate and distant causal histories, as a function of τ, would provide insights on the interplay between the influence of recent and prior dynamics on Z_t. The dynamics of Z_t is also sustained by the dependencies on its own past as well as the interactions with other variables. Our approach describes how such interactions can be computed from observed multivariate time-series data. Based on the quantification of information flow immediate and distant causal history on the outcome of a variable in Chapter 3, in section 4.2 we then present ways for capturing the interaction between self- and cross-feedback between the target and other variables in the system. We show that this results in a challenge that is often referred to as the curse of dimensionality [Bellman, 1957], requiring us to evaluate high dimensional probability distribution functions. In section 4.3 we develop an approximation to reduce the dimensionality using weighted transitive reduction [Bosnacki et al., 2010] using momentary information transfer [Runge et al., 2012a]. In Section 4.4 we illustrate the approach through two applications. The first

considers solute dynamics using published stream chemistry data as was used in [Jiang and Kumar, 2019]. The other three analyze the dynamics of three synthetic models: (1) a short-memory logistic model; and (2) two long-memory models – the Lorenz model and the OrnsteinUhlenbeck process. Based on the these applications, we find that (1) the dynamics of a short-memory process is dicated by its recent dynamics containing both self-and cross-dependency interactions; (2) the dynamics of a long-memory process are sustained by a self-feedback-dominated recent dynamics as well as a cross-dependency-dominated prior dynamics; and (3) the unique dynamics of each component in different long-memory processes can be indicated by characterizing the corresponding information flow in causal history. Section 4.5 provides a discussion and conclusion.

4.2 Quantifying Multivariate Interactions

In addition to the temporal separation of the causal history, the analysis of multivariate time-series using DAG representation also allows for the partition of the immediate and distant causal histories into self- and cross-dependencies, as shown in Fig. 4.1(a). A study of how self-feedback and historical states of other related variables, from both recent and distant dynamics, jointly affect the current state of a target variable would potentially help reveal how multivariate interactions lead to evolutionary behavior of a system. Our goal now is to make this notation more precise.

Specifically, for each variable $Z_t \in \vec{X}_t$ of a system, we partition the distant causal history into two components: self-dependence and cross-dependence. The first considers how a variable's own history influences its present state, while the latter captures the influence of all other variables. Practically, instead of the original distant causal history, $\vec{X}_t^- \backslash C_{\vec{X}_{t-\tau} \Rightarrow Z_t}$, we dissect $\vec{W}_\tau$ containing the information from earlier dynamics and directly affects the immediate causal history and Z_t, into: (1) self-dependence, $\vec{Z}_\mathcal{D} \equiv \{V_{t-\tau} : V = Z, V_{t-\tau} \in \vec{W}_\tau\}$ (the orange box in Fig. 4.1(b)); and (2) cross-dependence, $\vec{Z}'_\mathcal{D} \equiv \vec{W}_\tau \backslash \vec{Z}_\mathcal{D}$ (the dashed orange box in Fig. 4.1(b)). The total information from the distant causal history, represented now by $\vec{W}_\tau$, is quantified as $\mathcal{D}$ in Eq.(3.4). The partitioning of $\vec{W}_\tau$ into $\vec{Z}_\mathcal{D}$ and $\vec{Z}'_\mathcal{D}$ further allows the decomposition of $\mathcal{D}$ into synergistic, redundant, and unique information by using the PID framework, which is given by:

$$\mathcal{D} = I(Z_t; \vec{W}_\tau) = I(Z_t; \vec{Z}_\mathcal{D}, \vec{Z}'_\mathcal{D}) \tag{4.1a}$$

$$= S_\mathcal{D} + R_\mathcal{D} + U_{self,\mathcal{D}} + U_{cross,\mathcal{D}}, \tag{4.1b}$$

where $S_\mathcal{D}$ and $R_\mathcal{D}$ are the synergistic and redundant information from distant causal history, respectively,

and $U_{self,\mathcal{D}}$ and $U_{cross,\mathcal{D}}$ are the unique information from the self- and cross-dependencies, respectively.

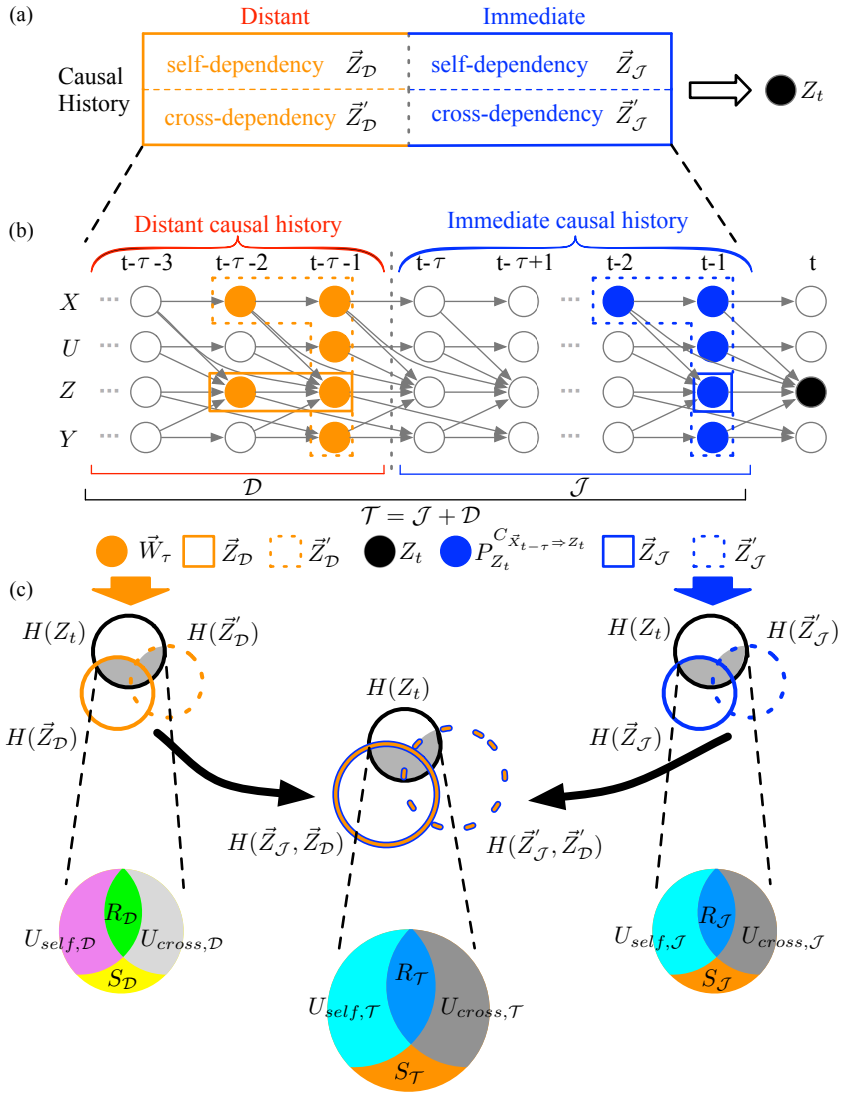

Figure 4.1: Illustration of causal history $\vec{X}_t^-$ of a target Z_t. (Top) The partition of $\vec{X}_t^-$ into four parts: the self- and cross-dependencies in the immediate causal history, represented by $\vec{Z}_{\mathcal{J}}$ and $\vec{Z}'_{\mathcal{J}}$, respectively, as well as the self- and cross-dependencies in the distant causal history, represented by $\vec{Z}_{\mathcal{D}}$ and $\vec{Z}'_{\mathcal{D}}$, respectively. (Middle) The representation of the temporal dynamics of a complex system in the directed acyclic graph for time-series. (Bottom) The (momentary) Partial Information Decomposition (PID) of the causal history as well as its immediate and distant parts in terms of the interplay between the corresponding self- and cross-dependencies.

Likewise, for immediate causal history, we divide $P_{Z_t}^{C_{\vec{X}_{t-\tau} \Rightarrow Z_t}}$, which contains information from the immediate past and directly influences Z_t, into the self- and cross-dependencies, represented by $\vec{Z}_{\mathcal{J}} \equiv \{V_{t-\tau} : V = Z, V_{t-\tau} \in P_{Z_t}^{C_{\vec{X}_{t-\tau} \Rightarrow Z_t}}\}$ (the blue box in Fig. 4.1(b)) and $\vec{Z}'_{\mathcal{J}} \equiv P_{Z_t}^{C_{\vec{X}_{t-\tau} \Rightarrow Z_t}} \backslash \vec{Z}_{\mathcal{J}}$ (the dashed blue box in Fig. 4.1(b)), respectively. The corresponding PID from the two parts of the immediate causal history is

given by:

$$\mathcal{J} = I(Z_t; P_{Z_t}^{C_{\vec{X}_{t-\tau} \Rightarrow Z_t}} \mid \vec{W}_\tau) = I(Z_t; \vec{Z}_\mathcal{J}, \vec{Z}'_\mathcal{J} \mid \vec{W}_\tau) \tag{4.2a}$$

$$= S_\mathcal{J} + R_\mathcal{J} + U_{self,\mathcal{J}} + U_{cross,\mathcal{J}}, \tag{4.2b}$$

where the subscript $\mathcal{J}$ refers to the information partitioning under the immediate causal history. Note that different from the PID for $\mathcal{D}$ in Eq.(4.1b), the partitioning of $\mathcal{J}$ requires the conditioning on $\vec{W}$ to prevent the influence of distant history in computing $\mathcal{J}$, following the similar idea of MPID for characterizing information flow to a target from two causal paths in Eq.(2.11).

A closer look at Eqs.(3.2), (4.1) and (4.2) reveals that the sums of $\mathcal{J}$ and $\mathcal{D}$ as well as their PID elements in fact give rise to the PID of the information from the entire causal history, $\mathcal{T}$, in terms of self- and cross-dependencies. The PID for $\mathcal{T}$ is therefore given by:

$$\mathcal{T} = I(Z_t; P_{Z_t}) = \mathcal{J} + \mathcal{D} \tag{4.3a}$$

$$= S_\mathcal{J} + R_\mathcal{J} + U_{self,\mathcal{J}} + U_{cross,\mathcal{J}} + S_\mathcal{D} + R_\mathcal{D} + U_{self,\mathcal{D}} + U_{cross,\mathcal{D}} \tag{4.3b}$$

$$= \underbrace{S_\mathcal{J} + S_\mathcal{D}}_{=S_\mathcal{T}} + \underbrace{R_\mathcal{J} + R_\mathcal{D}}_{=R_\mathcal{T}} + \underbrace{U_{self,\mathcal{J}} + U_{self,\mathcal{D}}}_{=U_{self,\mathcal{T}}} + \underbrace{U_{cross,\mathcal{J}} + U_{cross,\mathcal{D}}}_{=U_{cross,\mathcal{T}}} \tag{4.3c}$$

$$= S_\mathcal{T} + R_\mathcal{T} + U_{self,\mathcal{T}} + U_{cross,\mathcal{T}}, \tag{4.3d}$$

where the subscript $\mathcal{T}$ refers to the PID in the context of the entire causal history. Eq.(4.3) illustrates that each information content from the entire causal history (i.e., synergy, redundancy and unique information) due to the interplay between self- and cross- dependencies is additively contributed by the corresponding information content from its both distant and immediate histories.

In this study, we employ the rescaled approach of [Goodwell and Kumar, 2017a] for computing the PID of $\mathcal{D}$ and $\mathcal{T}$ in Eqs.(4.1) and (4.3) as well as the momentary PID for $\mathcal{J}$ in Eq.(4.2). The rescaled approach estimates the redundant information by considering the mutual dependency between two sources and ensures a non-negative information partitioning. Further, the empirical estimation of all the information-theoretic measures is conducted based on the k-nearest neighbor (kNN) method [Kraskov et al., 2004, Frenzel and Pompe, 2007]. The number of nearest neighbors, k, is set to 5 for facilitating a low bias of (conditional) mutual information [Kraskov et al., 2004, Frenzel and Pompe, 2007]. In the analysis presented later in Section 4.4, we first compute $\mathcal{D}$ and $\mathcal{J}$, along with their (momentary) PIDs, in Eqs.(4.1) and (4.2),

respectively. Then, the PID of $\mathcal{T}$ is obtained based on the sum of that of $\mathcal{D}$ and $\mathcal{J}$ according to Eq.(4.3).

4.3 Dimensionality Reduction Using Momentary Information Weighted Transitive Reduction

In addition to the availability of time-series data, the validity of empirically estimating the information-theoretic metrics in Eqs.(4.1)-(4.3) also depends on the number of the nodes involved. The dimensionality required in the computation can still be high even after the dimension reduction achieved through the Markov property for DAG. For example, consider the node Z_t in Fig. 4.1. Its immediate and distant causal histories are now reduced into $P_{Z_t}^{C_{\vec{X}_{t-\tau} \Rightarrow Z_t}}$ (blue nodes) and $\vec{W}_\tau$ (orange nodes), respectively. However, the dimensions of $\mathcal{J}$ and $\mathcal{D}$ as well as their associated PID can still be high for reliable estimations of these information-theoretic metrics in Eqs.(3.2), (4.1) and (4.2). Especially, the condition set, $\vec{W}_\tau$, involved in computing both $\mathcal{J}$ and $\mathcal{D}$, contains the parents of the entire immediate causal history, and accounts for most of the dimensionality in the computation of $\mathcal{J}$ and $\mathcal{D}$, as shown by the orange nodes in Fig. 4.1(b). This dimensionality can grow large quickly as the number of variables increase and/or number of lags that influence a target increases. Therefore, to address this problem, we introduce a new momentary information weighted transitive reduction (MIWTR) approach to further reduce the dimensionality involved in computing the information-theoretic measures. It builds on the weighted transitive reduction (WTR) [Bosnacki et al., 2010] for reducing complexity of graphs, which we extend for computing the information-theoretic measures.

WTR builds on the transitive reduction (TR) [Aho et al., 1972]. For an acyclic graph, TR is aimed at removing 'redundant' edges while keeping the connectivity structure of the graph. It is anchored on the idea that a transitive reduced graph can be obtained by removing any directed edge $i \to j$ in the original graph if there exists an indirect path connecting nodes i and j. However, in a weighted graph, TR potentially removes some 'important' edges that have large weights. To avoid that, WTR takes a step further by considering the weights of the edges in the reduction. That it, an edge linking i and j is removed from the original graph if and only if there exists a stronger indirect path from i to j. Otherwise, the edge is kept in the graph.

Technically, WTR is defined as follows. Consider a directed acyclic graph $\mathcal{G}_1 = (\vec{V}, E_1)$ with a set of nodes $\vec{V}$ and a set of edges E_1. We define a path from node i to node j as $p_{ij} = \{k_0 \to k_2 \to ... \to k_m\}$, where $k_0 = i$, $k_m = j$ and $k_{l-1} \to k_l \in E_1$. Note that the corresponding causal path $C_{i \to j}$ is the union of all the paths, p_{ij}, from i to j. The representative weight of the causal path $C_{i \to j}$ is defined as the maximal

transitive influence [Bosnacki et al., 2010], and is given by:

$$h_{ij} = \max_{p_{ij} \in C_{i \to j}} \Big(\min_{k \to l \in Edges(p_{ij})} \{w_{kl}\} \Big), \tag{4.4}$$

where $Edges(p_{ij})$ denotes all the edges in the path p_{ij}, and w_{kl} is the weight of the edge $k \to l$. h_{ij} is the maximum weight of all the minimum weights in each path p_{ij}. It can also be considered as the maximum allowable flow rate in all the pipes linking two nodes in a drainage system, where flow rate and pipe represents the weight w_{kl} and the path p_{ij}, respectively. In WTR, if and only if $h_{ij} > w_{ij}$, then the directed edge $i \to j$ is removed. Consider an example graph in Fig. 4.2. It consists of three nodes (i.e., A, B, and C) and three corresponding weighted edges (i.e., $A \to C$, $A \to B$ and $B \to C$). TR removes the edge $A \to C$ due to the existence of the path $A \to B \to C$ indirectly connecting A and C. Meanwhile, WTR keeps $A \to C$ because the corresponding maximal transitive influence $h_{AC} = w_{AC} = 2$. However, if the weight w_{AC} is changed to 1, $A \to C$ will be removed in WTR since now $h_{AC} = 1.5 > w_{AC} = 1$.

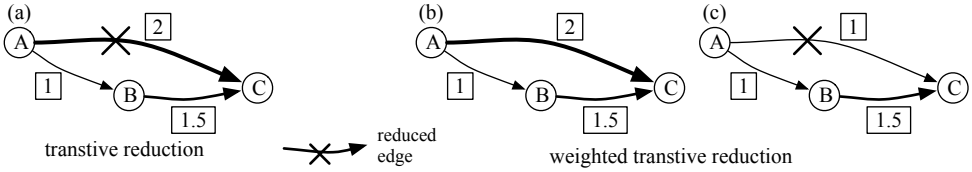

Figure 4.2: Comparison of transitive reduction (TR) and weighted transitive reduction (WTR) in a graph consisting of three nodes. (a) TR reduces the edge $A \to C$ due to the existing path $A \to B \to C$. (b) WTR keeps the edge $A \to C$ because the corresponding maximal transitive influence h_{AC} in Eq.(4.4) equals to the weight $w_{AC} = 2$. (c) when w_{AC} is reduced to 1, WTR excludes the edge $A \to C$ because now $h_{AC} = w_{BC} = 1.5 > w_{AC} = 1$.

In this study, MIWTR is developed to reduce the nodes in $\vec{W}_\tau$ for each computation of Eqs.(4.1)-(4.2), based on the WTR. The momentary information transfer for each edge defined in Eq.(1.8) is taken as the edge weight. Since MIT reflects the strength of direct coupling between a source and target, it serves as a good choice. The key idea of MIWTR is to first remove the edges linking $\vec{W}_\tau$ and the immediate history $C_{\vec{X}_{t-\tau} \to Z_t}$ by using WTR and then reduce the nodes in $\vec{W}_\tau$ which now are not connected to $C_{\vec{X}_{t-\tau} \to Z_t}$. Consider Z_t in the DAG for time-series $\mathcal{G}$ as the target and τ as the time lag for separating $\mathcal{G}$ into an immediate and a distant causal history. We now define a subgraph of $\mathcal{G}$, $\mathcal{G}_s = (\vec{V}_s, E_s)$. The node set $\vec{V}_s$ includes the union of the immediate causal history and $\vec{W}_\tau$, that is, $\vec{V}_s = C_{\vec{X}_{t-\tau} \to Z_t} \cup \vec{W}_\tau$. The edge set E_s contains all the edges in $\vec{V}_s$. The procedures for reducing $\vec{W}$ by using MIWTR is as follows.

- Implement WTR to exclude edges in $\mathcal{G}_s$, generating a new graph $\mathcal{G}_s' = (\vec{V}_s, E_s')$ where E_s' is the edges remaining after the implementation of WTR on $\mathcal{G}_s$.

- For each node $X_{t-\tau_X} \in \vec{W}_\tau$, check whether there is an edge linking $X_{t-\tau_X}$ to any node in the immediate causal history $Y_{t-\tau_Y} \in C_{\vec{X}_{t-\tau} \to Z_t}$ based on the new graph $\mathcal{G}_s^{'}$. If there is no edge $X_{t-\tau_X} \to Y_{t-\tau_Y}$, remove $X_{t-\tau_X}$ from $\vec{W}_\tau$.
- Repeat removing nodes in the previous step for every node in $\vec{W}_\tau$.
- Return the reduced $\vec{W}_\tau$.

Consider the DAG for time-series in Fig. 4.1 as an example. $\vec{W}_\tau$ in the orange nodes can be further reduced by excluding $U_{t-\tau-2}$ and $Z_{t-\tau-2}$ if the edges $U_{t-\tau-2} \to Z_{t-\tau}$ and $Z_{t-\tau-2} \to Y_{t-\tau}$ are removed by using MIWTR. A validity test for verifying the MIWTR-based reduction of $\vec{W}_\tau$ in computing Eqs.(4.1)-(4.3) is illustrated through a quadvariate logistic model in the Appendix F. We note that MIWTR algorithm needs to be implemented for each distant/immediate histories segmentation of each target variable .

4.4 Characterizing Multivariate Interaction in Causal History

The framework presented in Section 4.2 provides a number of ways by which may ask how different variables interact to determine the outcome of a specific variable at a specific time. As indicated earlier, a variable may affect another variable's outcome directly computed through momentary information transfer (Fig. 1.1(c) and Eq.(1.8)) or indirectly through a causal path (Fig. 1.1(d) and Eq.(1.9)). Two variables may interact through their corresponding causal paths (Fig. 1.1(e)) and their interaction can be partitioned using PID into synergistic, unique, or redundant contributions (Eq.(2.11)). At the next level of complexity, we can consider the interaction of all variables together influencing the outcome of any variable at time t through the framework of causal history (Fig. 1.1(f) and Eqs.(4.1)-(4.3)). Causal history can be decomposed into complementary components of immediate and distant causal histories as a function of separating time lag τ. We have shown that, both immediate and distant causal histories can be further partitioned into self- and cross-dependencies (Fig. 4.1). Each of these interaction can then be explored through PID (Eqs.(4.1)-(4.3)). We can, therefore, ask:

- How does information flow, jointly provided by the entire causal history, sustain the whole system dynamics?
- How does the characterization of such information at the system level reveal the unique contribution of each individual component in the system?

To address the above two questions, we implement the proposed causal history analysis approach to analyze the information flow in four different systems by using either time-series observations or synthetic

data: an observed stream chemistry system, a short-memory logistic model, and two long-memory systems. Then, we summarize the insights obtained from these applications.

4.4.1 Stream Chemistry Dynamics

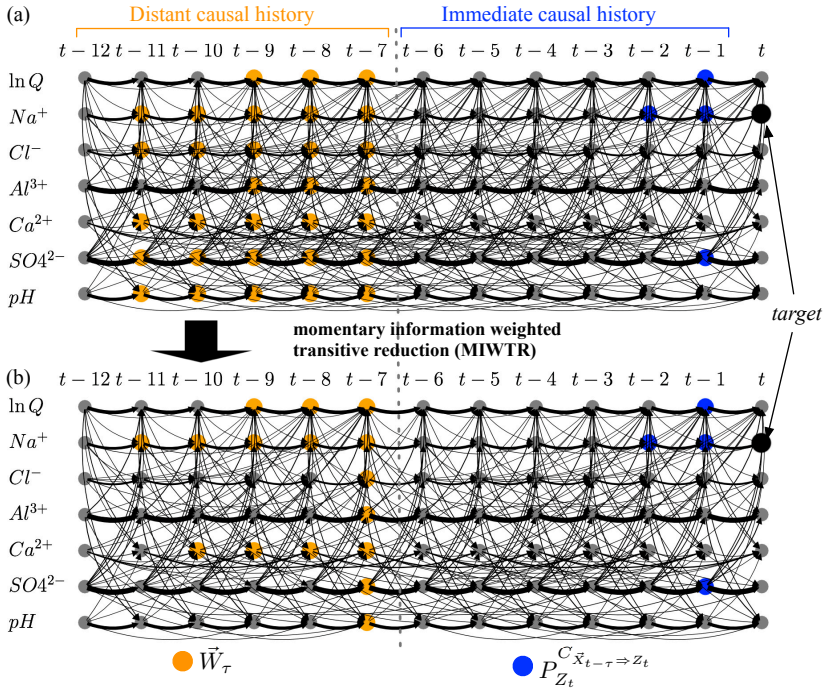

Figure 4.3: Illustration of implementing Momentary Information Weighted Transitive Reduction (MIWTR) to reduce $\vec{W}_\tau$ for the present state of Na^+ with time lag $\tau = 6$ in separating distant and immediate causal histories based on the raw data. (Top) the original identified $\vec{W}_\tau$ (orange nodes) and $P_{Z_t}^{C_{\vec{X}_{t-\tau} \Rightarrow Z_t}}$ (blue nodes) based on Eq.(3.6). (Bottom) the reduced $\vec{W}_\tau$ by using MIWTR (orange nodes) (Note that the edges linking $\vec{W}_\tau$ and immediate causal history are much less than the original DAG due to MIWTR).

We first analyze the fractal water solute data in Section 3.3.4. The causal history analysis is conducted on both raw data and the data without the influence of the flow rate. Based on the two estimated DAGs in Fig. 3.6, we compute the total, immediate and distant information flows ($\mathcal{T}$, $\mathcal{J}$, $\mathcal{D}$) from the causal history over time lag τ ranging from 5 to 400 using Eqs(3.3) (3.4) and (3.6). We also compute the corresponding PIDs using Eqs.(4.1)-(4.3). Note that $\mathcal{T}$ is obtained by the sum of the estimated $\mathcal{D}$ and $\mathcal{J}$, which are computed by using kNN estimator. The computations of $\mathcal{D}$ and $\mathcal{J}$ are based on the implementation of MIWTR. For instance, to compute the information transferred to Na^+ from immediate and distant causal history separated with time lag $\tau = 6$ by using the raw data, we first identify $\vec{W}_\tau$ in Eq.(3.4) based on the DAG generated in Fig. 3.6(a), shown as the orange nodes in the top of Fig. 4.3. Then, MIWTR is conducted to remove the nodes in $\vec{W}_\tau$ whose edges connected to the corresponding immediate causal history

are excluded by using WTR. The resulting simplified $\vec{W}_\tau$ is illustrated in the bottom of Fig. 4.3, showing the reduction of the cardinality of $\vec{W}_\tau$ from 31 to 17. MIWTR is implemented for each variable at each time lag τ in both DAGs in Figs. 3.6(a) and (b). The corresponding cardinalities with and without MIWTR are shown in Fig. F.4(a). It can be observed that for each variable a significant dimension reduction is achieved at around 5˜15 due to the simplification of $\vec{W}_\tau$. The resulting information partitioning for $\mathcal{T}$, $\mathcal{D}$ and $\mathcal{J}$ for the systems with and without the influence of flow rate over time lag τ are plotted in Fig. 4.4.

Trends of $\mathcal{T}$, $\mathcal{D}$ and $\mathcal{J}$. Figs. 4.4(a) and (b) show that for each variable in both graphs, the information from the causal history, $\mathcal{T}$, is almost constant with regards to the time lag τ. It is consistent with the fact that the influence from the entire evolutionary dynamics of the system is independent of the time lag τ for the partition of distant and immediate histories. Further, Figs. 4.4(c) and (d) provides the information from the distant and immediate causal histories, $\mathcal{D}$ and $\mathcal{J}$, respectively. For each variable, $\mathcal{D}$ and $\mathcal{J}$ are separated by the dotted black line, where the above and below the dotted line refer to $\mathcal{D}$ and $\mathcal{J}$, respectively. It can be observed that $\mathcal{D}$ and $\mathcal{J}$ decreases and increases with growing τ, respectively. It illustrates that when more states move from distant history to immediate history as τ increases, the information from recent dynamics increases while the information from earlier dynamics decreases accordingly. Moreover, the non-vanishing area above the black dotted line illustrates the non-zero convergence of $\mathcal{D}$ for each variable, reflecting the long-memory property of the system.

Characteristics of $\mathcal{T}$, $\mathcal{D}$ and $\mathcal{J}$ explaining the whole system dynamics. Further, based on the information characterization of the total information $\mathcal{T}$ in Figs. 4.4(a) and (b), we can observe that the self- and cross-dependencies contribute to different information contents in $\mathcal{T}$ of both graphs. While the unique information, $U_{cross,\mathcal{T}}$, contributes most of the information from cross-dependencies for all variables, the main contributor for the influence from self-feedback interactions differs. When the flow rate is included, the redundant information, $R_\mathcal{T}$ in Fig. 4.4(a), is stronger in the self-feedback influence. Meanwhile, when the flow rate influence is excluded, the unique information of self-dependency, $U_{self,\mathcal{T}}$ in Fig. 4.4(b), dominates. The strong redundant effect due to the flow rate, again, implies that it serves a crucial role in enhancing the connectivities among different solutes.

Moreover, a detailed characterization of information from immediate ($\mathcal{J}$) and distant ($\mathcal{D}$) causal histories of the two graphs are plotted in Figs. 4.4(c) and (d). It can be observed that the dominance of self-dependence in immediate history is independent of τ through either unique $U_{self,\mathcal{J}}$ and redundant $R_\mathcal{J}$ information. However, the influence from distant history is attributed by both self- and cross-dependencies for small τ, but is dominated only by cross-dependency through its unique information $U_{cross,\mathcal{D}}$ as τ increases. This is because the influence from self-dependency is limited in recent dynamics such that when the separation

time lag τ is too small, some of the self-dependency influence will be reflected in the distant history and squeezed back to the immediate history as τ grows. It also implies that the influence from self-feedback interaction dictates the recent dynamics of each target variable, while the the interaction with other variables dominates the dynamics of the target in a long term. This is especially insightful in understanding the $1/f$ fractal dynamics of these stream solutes. The important role of self-feedback interactoin in determining a self-similar process is well-accpeted, however, the role of interaction with the remaining dynamics of a system is usually neglected, which is now resolved through the proposed causal history analysis. It shows that the influence due to the cross interactions is significantly crucial in sustaining the long-memory behavior and thus also contributes to the self-similarity of the stream chemistry. In a more general sense, we postulate that to sustain the complex dynamics as the stream chemistry system, it requires (1) the influences from the self-feedback interactions in recent dynamics for determining the short-term trend of the system and (2) the cross-dependency in earlier dynamics for controlling the long-term trend, so that the system behaves 'complex'.

Characteristics of $\mathcal{D}$ and $\mathcal{J}$ distinguishing the component dynamics. In addition, the PID results of information from the immediate and distant causal histories reveal different dynamics of the solutes studied. In the flow-rate-dominated system, most solutes show similar PID patterns as plotted in Fig. 4.4(c). That is, for each solute, the information from distant causal history, $\mathcal{D}$, mainly consists of $U_{cross,\mathcal{D}}$ and $R_{\mathcal{D}}$, and the information from immediate causal history, $\mathcal{J}$, mainly consists of $R_{\mathcal{J}}$ and $U_{self,\mathcal{J}}$. Again, the significant redundant information in both distant and immediate causal histories - $R_{\mathcal{D}}$ and $R_{\mathcal{J}}$ - is due to the influence of flow rate. Also, different from the other solutes, SO_4^{2-} shows a stronger unique information due to its self-feedback interactions in recent dynamics, $U_{self,\mathcal{J}}$. It implies that SO_4^{2-} is less subjective to the influence of flow rate than other solutes, which is evidenced by the negligible changes between SO_4^{2-}'s PID results with and without flow rate in Fig. 4.4(d). However, when the influence of flow rate is removed, the PID patterns differs for each variable shown in the bottom rows of Fig. 4.4(d). For instance, Na^+ and Cl^- show stronger unique information due to their self-feedback dynamics in both distant and immediate causal histories, represented by $U_{self,\mathcal{D}}$ and $U_{self,\mathcal{J}}$, respectively. It is consistent with the fact that the majority of the sodium and chloride in the studied catchment, which is close to the coast, originates from the ocean through the atmospheric deposition [Neal et al., 1997]. Therefore, compared with other solutes, the states of Na^+ and Cl^- are more subjective to their own dynamics that are not overlapped with other variables. Meanwhile, for solutes with evenly mixed origins from both ocean and catchment, such as Ca^{2+} and SO_4^{2-} [Neal et al., 1997], there are higher redundant information in their distant causal histories, $R_{\mathcal{D}}$. It illustrates the shared influences from the catchment dynamics and their own dynamics on both Ca^{2+} and

SO_4^{2-}, represented by $R_{\mathcal{D}}$. Lastly, Al^{3+} shows significant and dominant redundant information from both distant and immediate histories, $R_{\mathcal{D}}$ and $R_{\mathcal{J}}$, respectively. It coincides with its solely terrestrial origin (see Table S3 in [Kirchner and Neal, 2013]), such that the catchment dynamics dictates the state of Al^{3+}.

The PID approach in conjunction with causal history framework for the solute dynamics has enabled us to characterize the whole system behavior as well the dynamics of each solute. We find that maintaining the whole system dynamics mainly results from a self-dependency-dominated immediate causal history and a cross-dependency-dominated distant causal history. Also, the characterization of information from immediate and distant causal histories indicates different origins of the studied solutes.

4.4.2 A Short-Memory Dynamics: a Trivariate Chaotic Model

To investigate the dynamics in other system, we implement the causal history analysis in a short-memory synthetic model. Consider a trivariate coupled logistic system in Eq.(2.31) with noise coupling strength $\epsilon = 0.3$. Taking $X_{3,t}$ as the target node and partitioing its immediate and distant history based on an earlier time step $t - \tau$ ($\tau \geq 1$) shown in Fig. 4.5(a), we identify $P_{X_{3,t}}$ in blue nodes, $\vec{W}_\tau$ in orange nodes, and the self-and cross-dependencies of the two histories in solid and dashed boxes, respectively. $\mathcal{J}$, $\mathcal{D}$ and their corresponding information characterization are calculated for τ ranging from 1 to 50 based on Eqs.(4.1) and (4.2), with 10,000 synthetic data points generated to conduct the empirical estimations for each τ.

The characterization of information flow from distant and immediate histories are plotted in Fig. 4.5(b), with the same colors and labels of different information characterization as Fig. 4.4. Different from the long-memory process as the stream chemistry dynamics, $\mathcal{D}$ of the chaotic model (the area above the black dotted line) converges to zero with increasing τ, indicating the short-term dependence of the process. Furthermore, we observe an overall very strong redundant information contributed by both an increasing $R_{\mathcal{J}}$ from immediate history and an decreasing $R_{\mathcal{D}}$ distant history as τ grows. The opposite changes of $R_{\mathcal{J}}$ and $R_{\mathcal{D}}$ illustrates the exchange of redundant information from earlier dynamics to recent dynamics when more historical states are considered as immediate history. And the strong overall redundancy is due to the symmetrical structure of the model in Eq.(2.31), such that the dynamics of the three variables are similar to each other and therefore provide significant overlapped information to the others. In addition, the influence from cross-dependence is now dominated by immediate history through $U_{cross,\mathcal{J}}$ rather than distant history as observed in stream chemistry dynamics. This, again, is because of the short-term dependence of the chaotic system leading to the contributions of both self- and cross-dependence interactions originating from recent dynamics.

4.4.3 Two Long-Memory Dynamics: the Lorenz Model and the Ornstein-Uhlenbeck Process

Now, let's further analyze the dynamics in two long-memory processes with and without chaotic behaviors: the Lorenz model and the Ornstein-Uhlenbeck (OU) process, respectively. The two synthetic models are given in Eqs.(3.16) and (3.17). The trajectories of the two models are sketched in Fig. 4.6(a). To characterize the information flow to each variable in Eqs.(3.16) and (3.17), we identify the parents of each target varaible, $\vec{W}_\tau$ based on the immediate and distant causal histories partitioned by a time lag τ, and the self-and cross-dependencies in the two histories in Fig. 4.6(b), as the analysis of stream chemistry dynamics and the logistic model. The information characterization in Eqs.(4.1) and (4.2) of the two histories are then computed based on 10,000 data points generated from the two models discretized with $dt = 0.01$

The PID results of the distant and immediate histories from the two models are illustrated in Fig. 4.6(c). It can be observed that most of the information characterizations of the two models are similar to that of stream chemistry dynamics with raw data in Fig. 4.4. First of all, the Lorenz model is a long memory process, indicated by the non-zero convergence of the information from distant history $\mathcal{D}$. Second, the redundant information dominates the influence from immediate history and is also non-negligible in distant history before $\mathcal{D}$ converges. It illustrates that the dynamics of each variable resemble that of the others. Further, when $\mathcal{D}$ and $\mathcal{J}$ converge, the contributions from the total information $\mathcal{T}$ are dominated by the redundant information in immediate history and unique information of cross-dependence dynamics in distant history. In a physical sense, it illustrates the roles of self-and cross-dependency dynamics in determining the short-and long-term dynamics of each variable, respectively.

Nevertheless, we can still observe the slight differences in the two models due to their unique dynamics. For the Lorenz model, before the convergence of $\mathcal{D}$, there are oscillations in the redundant information of the distant history, $R_\mathcal{D}$. This is due to the approximately periodic drawing butterfly trajectories to fill the strange attractor of the model. Specifically, the periodic spikes of $R_\mathcal{D}$ is because the dynamical trajectory goes back to the location close to the starting point after finishing one butterfly trajectory (see Fig. 4.6(a)) as τ increases, while $R_\mathcal{D}$ eventually dampens out when the dynamics are away from the beginning for filling the other part of the fractal domain. In addition, the OU process shows stronger unique information of self-feedback interaction and synergistic information in the distant history, $U_{self,\mathcal{D}}$ and $S_\mathcal{D}$, respectively. The strong $U_{self,\mathcal{D}}$ illustrates that different from the repetive butterfly trajectories in the Lorenz model, the trajectory of the OU process is more "random" when filling out its attractor shown in Fig. 4.6(a) so that the self-feedback interaction plays a more important role. The strong $S_\mathcal{D}$ in distant history, on the other hand, suggests that the joint influence from the self-and cross-dependency interactions in a long term is crucial in

confining the dynamics in its attractor.

4.4.4 Insights from the Applications

Characterizing the information flow from the causal history in the four systems reveals the whole system behavior as well as the dynamics of its each component. Therefore, it helps address the two questions raised at the beginning of this section.

First of all, dynamics sustaining the whole system behavior vary from system to system. For a short-memory system, such as the trivariate logistic model, the present state of each variable is maintained by the recent dynamics including both self-feedback interactions and the influence of the other variables. Meanwhile, for a long-memory system, the influences for sustaining the whole system behavior are mainly contributed by: a self-dependency-dominated immediate causal history and a cross-dependency-dominated distant causal history, evidenced from both observed stream chemistry system and two synthetic models. It implies that while the self-feedback interaction from recent dynamics is critical for the short-term dynamics of each variable, the cross-dependency interaction from earlier dynamics is responsible for its long-term behavior, thus enforcing the dynamics as "complex". In fact, the role of self-and cross-dependency in immediate and distant history, respectively, is common in long-memory ecohydrologic dynamics, such as the soil moisture. The trend of underground soil moisture is subjective to both its own dynamics and the influence of atmospheric signals in a long term. This is evidenced by the dominant modes in the frequencies corresponding to different ENSO signals through the spectral analysis on the observed soil moisture, illustrating the encoded long memory of atmospheric impact on soil moisture [Amenu et al., 2005]. Furthermore, the detailed information characterization of different long-memory systems can still differ from each other due to their unique dynamics. For instance, redundant information is pretty dominant in both raw data-based stream chemistry system and the Lorenz chaotic model due to the influence of flow rate and the repetitive butterfly trajectories in filling the strange attractor, respectively. However, unique information of self-feedback interaction is more important in the flow rate-influence-corrected chemistry data and the OU process, consistent with the self-similarity property and more "random" trajectories in the two systems, respectively.

Second, the dynamics of each component in a complex system can be indicated by characterizing the information from the interactions between self- and cross-dependencies in immediate and distant causal histories. This is complementary to the previous findings associated with the dynamics sustaining the whole system behavior. While the previous conclusion depicts the dynamics maintaining the complexity in a system level, this conclusion details the unique dynamics of each variable through the information characterization

on the system's dynamics. In the analysis of stream solute dynamics, while stream solutes have been widely and consistently found to have fractal and long-term dependency behaviors [Kirchner and Neal, 2013], the origin of each solute and how each solute interacts with each other differs. The different origins of solutes are indicated by the proportions of mixed redundant information and unique information from self-dependency when the dependency of the flow rate is excluded. Furthermore, in the comparison between the two synthetic models, we find that the redundant information is dominant in the Lorenz model, however, unique information of self-feedback interaction is more important in the OU process. The difference illustrates the repetitive butterfly trajectories for filling the strange attractor in the Lorenz model and relatively more "random" trajectories in the OU process.

4.5 Discussion and Conclusion

This paper presents an information-theoretic framework to understand the whole system behavior due to the multivariate interactions occurring in the whole system. A fundamental insight driving the development of the framework is that the whole is greater than the sum of the parts. In other words, the complexity results from the multivariate interactions in the entire evolutionary dynamics of the system, or causal history.

Such multivariate interaction thinking results in an improved causal history analysis for complex system dynamics. It incorporates the PID techniques with the causal history analysis for characterizing the information flow, to a target variable, from its self-feedback interactions and the cross-dependencies in both immediate and distant causal histories (see the top of Fig. 4.1). While there are many ways to partition the causal history, we argue that the proposed partitioning – in terms of the self- and cross-dependencies in a recent and prior earlier dynamics – is a reasonable way to reveal the key aspects of interactive dependencies. First, the difference between the influences from immediate and distant causal histories illustrates the memory dependency of the system [Jiang and Kumar, 2019]. Second, the strong self-feedback interaction observed in many systems, especially ecosystems, suggests its interplay with the dynamics of other variables might be one of the keys for determining the current state of each target variable. However, further research can focus on how other partitions for the causal history, such as interactions from different groups of variables, reveals different perspectives of the dynamics in complex systems.

Based on the analyses of the observed stream chemistry dynamics and the three synthetic models, we find that information characterization differs from system to system thus illustrating their different dynamics. While the furture trajectory of a short-memory system is dicated by its recent dynamics such as the logistic model, the dynamics of a long-memory system is mainly sustained by the influences from the self-dependency-

dominated immediate causal history as well as the cross-dependency-dominated distant causal history. In other words, in a long-memory system, the self-feedback interaction in recent dynamics determines the recent trend of a target variable, and the influence from the remaining system in earlier dynamics, on the other hand, adjusts the movement of the target in a long term. In the analyses of both stream chemistry system and the two long-memory synthetic models, the consistent influence on long-term dynamics is evidenced by the strong unique information of the cross-dependency, $U_{cross,\mathcal{D}}$, in distant causal history. Furthermore, the detailed characterization of information flow in different long-memory systems can still be different, indicating the unique dynamics of each individual variables. For instance, in the stream chemistry dynamics (Section 4.4.1), we observe that due to the dominant influence of flow rate, the PID contents of each solutes, analyzed based on raw data, are similar. Nevertheless, when the influence of flow rate is excluded, the resulting different PID illustrate the different origins of the stream solutes. In addition, the information of the Lorenz model encompasses dominant redundancy in both immediate ($R_{\mathcal{J}}$) and distant history ($R_{\mathcal{D}}$) due to its repetive butterfly trajectory, whereas the more "random" trajectory in the OU process results in stronger unique information from the self-feedback interaction of each variable.

Further, momentary information weighted transitive reduction (MIWTR) is employed to achieve an efficient estimation of different information theoretic measures in Eqs.(4.1)-(4.2) by reducing the cardinalities. Weighted transitive reduction is more well accepted for simplifying a directed acyclic graph than the traditional transitive reduction in that the weights or the strengths of edges are taken into account [Bosnacki et al., 2010]. That is, higher strength the edge has, less likely it will be excluded. An example of computing the information flow in a quadvariate logistic model in the Appendix with and without MIWTR verifies the feasibility of the usage of MIWTR. MIWTR would be more efficient in dimension reduction in a more complicated DAG, especially when more variables are observed and included in the graph construction.

A systematic multivariate interaction analysis enables the proposed information-theoretic framework in this study. It is fundamentally different from most existing information theoretic measures, which either only focus on pairwise interaction or interactions in a specific part of the system. This uniqueness sheds light on how the complex system dynamics are sustained over time, thus improving our understanding towards the whole system dynamics. This is especially helpful at the current age of Big data. With the increasing availability of observations, these data-driven tools will provide more insights in different scientific domains. Furthermore, they will also instigate more opportunity for assessing the modeling performance and structure of numerical models [Liang and Kleeman, 2005, Majda and Gershgorin, 2011]. With all these potentials, such data-driven approach will open up new avenues for investigating complex system dynamics.

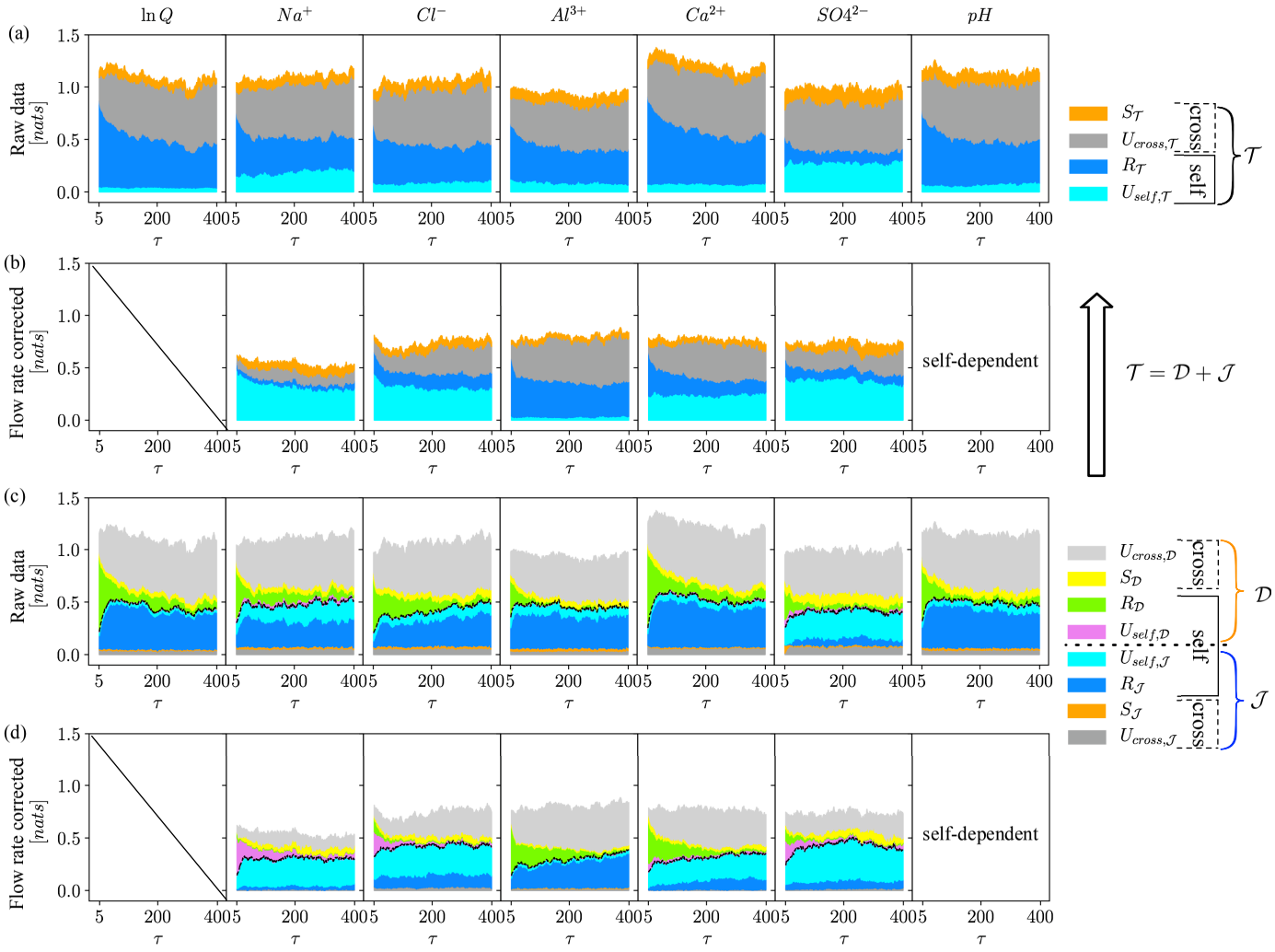

Figure 4.4: Plots of the information flows computed by using MIWTR based on the two sets of stream solute time-series data and the estimated directed acyclic time-series graphs in Fig. 3.6. (a) The partial information decomposition (PID) for the information from the causal history, $\mathcal{T}$ in Eq.(4.3). (b) The (momentary) PIDs of the immediate and distant causal histories, $\mathcal{J}$ and $\mathcal{D}$ in Eqs.(4.2) and (4.1), respectively.

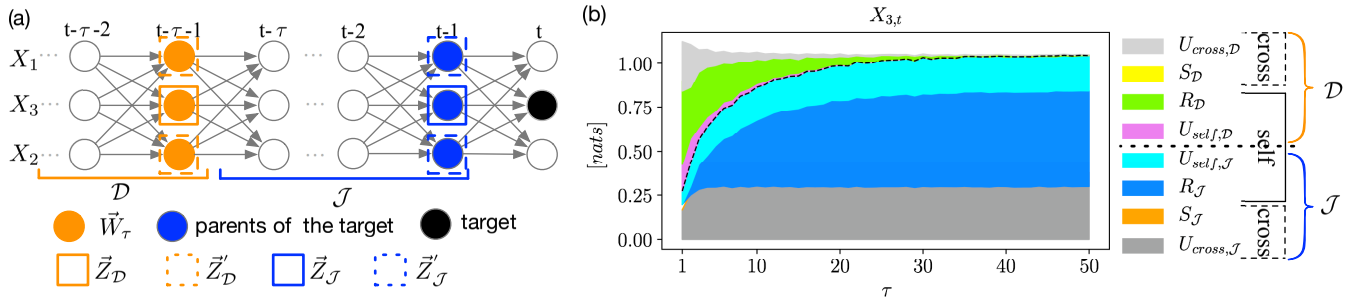

Figure 4.5: Illustration of the trivariate logistic model in Eq.(2.31). (a) The directed acyclic graph representation for time-series of the system taking $X_{3,t}$ as the target, with immediate and distant histories partitioned partitioned based on time lag τ and the self-and cross dependencies in the two histories in the two histories in solid and dashed boxes for computing information-theoretic measures, respectively. (b) The corresponding plots of the information characterizations of the two histories in Eqs.(4.1) and (4.2) ranging from 1 to 50.

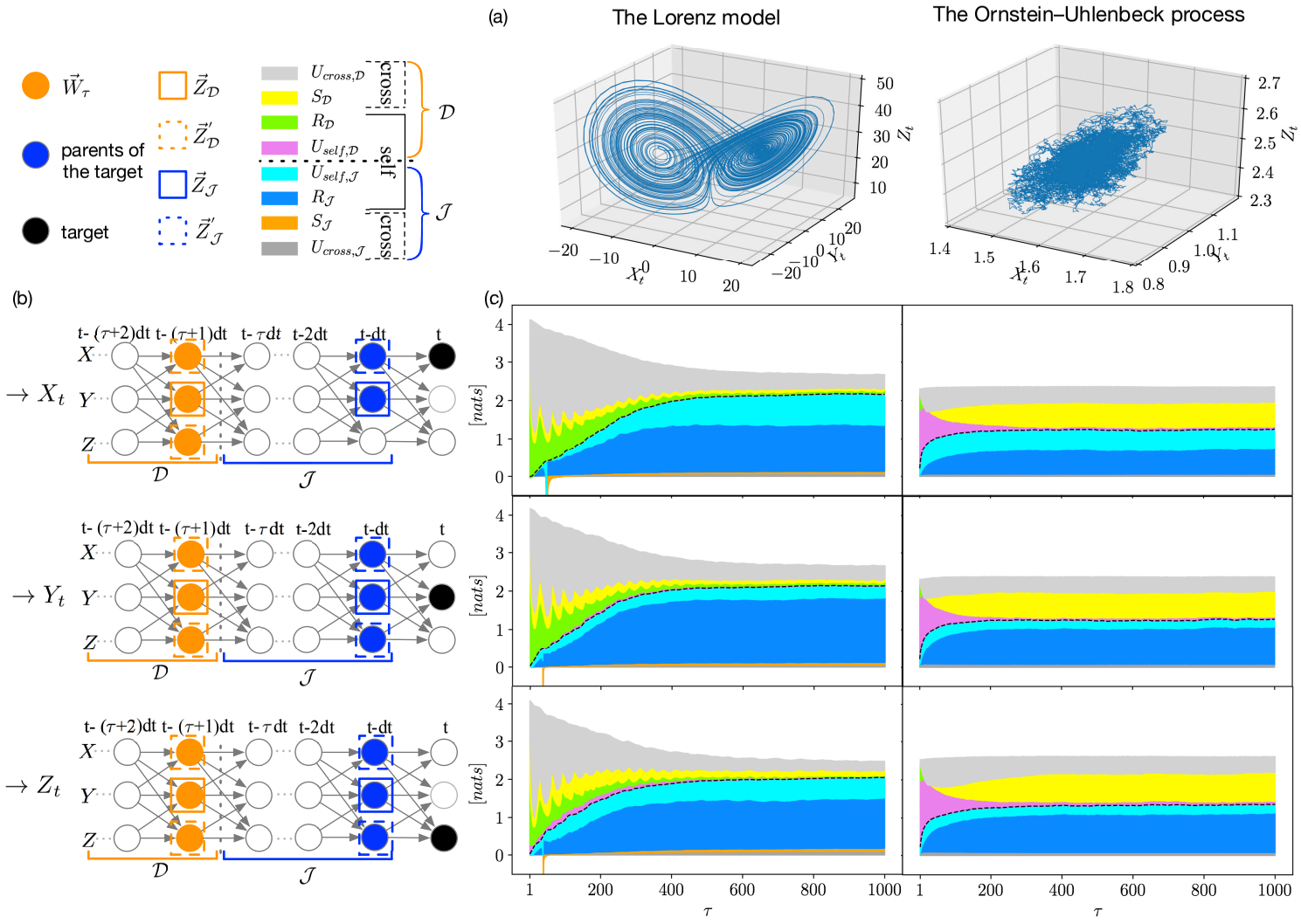

Figure 4.6: Illustration of the Lorenz model and the Ornstein-Uhlenbeck (OU) process in Eqs.(3.16) and (3.17), respectively. (a) The trajectories of the two models. (b) The directed acyclic graph representation for time-series of the system for each target variable in each model, with immediate and distant histories partitioned partitioned based on time lag τ and the self-and cross dependencies in the two histories in the two histories in solid and dashed boxes for computing information-theoretic measures, respectively. (c) The corresponding plots of the information characterizations of the two histories in Eqs.(4.1) and (4.2) ranging from 1 to 1000 in the Lorenz model (left) and the OU process (right).

Chapter 5

Evaluating the Structure of a Modelled System from an Information-Theoretic Perspective

5.1 Introduction

A complex system can be considered as an information processing system. It takes in input, processes it, and generates output with information of the system's dynamics encoded. In the previous analyses, the dynamics of complex systems are assessed with the assumption that the internal interactions are unknown. This assumption is consistent with many natural systems, where only observation data are available and the intervention of the system to achieve a different trajectory of dynamics is usually not feasible. Therefore, the causality relation between source variable(s) and a target variable, analyzed in Chapters 1-4, focuses on how the source(s) influences the target given the knowledge of (or conditioning, in a mathematical sense) all the prior dynamics in the system, called Granger causality [Granger, 1969]. For instance, Chapter 2 characterizes the influence from two lagged sources to a target by conditioning the parents of the corresponding two causal paths, as shown in Fig. 5.1(a).

Meanwhile, numerical models, aiming at simulating the dynamics of natural systems and thus also an information processing system, provide an alternative way for unravelling the interactions in a complex system. Different from natural systems, the specific nature of numerical models for simulation allows system intervention. This is extremely useful in analyzing the interventional effect, that is, how the dynamics of target(s) would change when specific source(s) are fixed to specific values. Fig. 5.1(b) sketches an example of the interventional effect by freezing two sources. Such an effect is termed Pearl causality [Pearl, 2000]. As the evaluation is conducted based on the causality relations through interventions in specific parts of the system, the dynamics unravelled in this case refer to the structure of a modelling system.

Evaluating the structures of numerical models from a system-interventional perspective is crucial, in that it enriches the analysis of complex system dynamics in addition to the analysis based solely on observational data. For instance, it can be the case that while variable $Y_{t-\tau_Y}$ has a stronger influence on a target Z_t in a Granger sense, Z_t changes more significantly when a third variable $X_{t-\tau_X}$ is intervened. Such contradictory conclusion drawn from Granger and Pearl causalities would highlight the importance of reconciling the

divergent outcomes from observational data and numerical modelling in issues such as ecosystem planning and management, where a plenty of studies focus on how a system changes in response to adjustments of anthropogenically altered initial/boundary conditions.

Therefore, the objective of this chapter is to investigate the influence on the present state of a component from one or multiple lagged source components in a dynamical system from the system-intervention perspective. In addition to the intervention, the analysis also utilizes ensemble simulation, another uniqueness of numerical models, to evaluate the change of a target due to the intervention of source variables. Ensemble simulation of a numerical model allows assessing the temporal evolution of the density of the components in the system. The cause-effect influence is then evaluated based on the change of the density evolution of the target variable due to intervention of the source variable(s).

Analysis of causal influence anchored on the density evolution has been conducted by other researchers from different perspectives. Liang and Kleeman [Liang and Kleeman, 2005, Liang and Kleeman, 2007a, Liang and Kleeman, 2007b] provided a mathematical formalism for quantifying the information flow to a target variable from a source variable at the previous time step. Later, Yin and Duan extended it to the information flow coming from multiple components [Yin and Duan, 2018]. In addition, Bollt [Bollt, 2012] analyzes the interaction between two components through the resulting evolution of transfer entropy. While the existing researches focus on the influence from the dynamics at the previous step based on the system density evolution, the analysis in this chapter takes one step further such that we investigate the influence from one or multiple sources at any earlier time step based on the change of density evolution due to the intervention on source(s).

In the rest of the chapter, we first present the methodology for quantifying the change of a target variable due to the intervention on the lagged source component(s) by using Kullback-Leibler divergence – an information-theoretic metrics for measuring the difference between two densities [Kullback and Leibler, 1951]. Then, we analyze the component dependencies in the Lorenz chaotic model by assessing the interventional effect on each variable. Further, to compare the intervention results with a multivariate interaction analysis based on statistical dependence, we quantify the dependencies between target and lagged source(s) by using mutual information (MI) in Eq.(1.3) and transfer entropy (TE) in Eq.(1.5). Note that an exact causal history analysis in Chapter 3 is not conducted here. This is because freezing the self-feedback of the target in the corresponding interventional analysis would directly enforce the target to be constant over time, thereby losing the interventional effect from other variables and making the two analysis incomparable. Last, a short conclusion is drawn and future work is discussed.

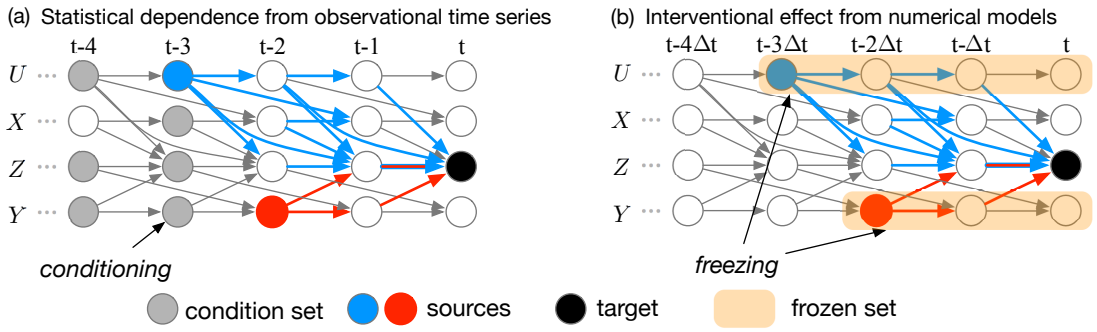

Figure 5.1: Illustration of influence from lagged source variables to a target variable in terms of (a) the statistical dependence driven from observed time series and (b) the interventional effect analyzed from numerical models discretized with time intervel Δt.

5.2 Method

Consider a multivariate continuous dynamical system $\vec{X}_t = \{X_t, Y_t, Z_t, ...\}_N$ consisting of N variables:

$$\frac{d\vec{X}_t}{dt} = \vec{F}(\vec{X}_t), \tag{5.1}$$

where $\vec{F} = \{F_X, F_Y, ...\}_N$ is the vector field. The temporal dynamics in Eq.(5.1) can be represented by using the DAG for time-series after discretization. Fig. 5.1(b) illustrates the DAG of a quadvariate system discretized with time interval Δt.

5.2.1 Intervention in the Dynamical Systems

The key idea of investigating how one or multiple lagged source variables $\vec{V} \subseteq \vec{X}$ at a previous time step $t - \tau$ ($\tau > 0$), $\vec{V}_{t-\tau}$, influence a target variable, Z_t, in Eq.(5.1) is to analyze the change of probability density function (*pdf*) of Z_t due to the intervention of the system on $\vec{V}_{t-\tau}$. Specifically, by intervention in the system, we mean fixing the sources $\vec{V}_{t-\tau}$ to be constants at given values.

To get Z_t's *pdf* and its changed *pdf* with the sources $\vec{V}_{t-\tau}$ intervened, it requires ensemble simulation of Eq.(5.1) as well as the interevention model. To achieve that, we discretize Eq.(5.1), leading to a mapping, $\vec{\Phi} = \{\Phi_X, \Phi_Y, ...\}_N : \mathbb{R}^N \to \mathbb{R}^N$ given by:

$$\vec{\Phi} : \begin{cases} X_t &= \Phi_X(\vec{X}_{t-\Delta t}) = \vec{X}_{t-\Delta t} + \Delta t \cdot F_X(\vec{X}_{t-\Delta t}) \\ Y_t &= \Phi_Y(\vec{X}_{t-\Delta t}) = \vec{X}_{t-\Delta t} + \Delta t \cdot F_Y(\vec{X}_{t-\Delta t}) \\ &\vdots \end{cases} \tag{5.2}$$

where Δt is the discretization temporal resolution. In addition, we need an intervened dynamical system with the sources $\vec{V}$ fixed. Such a system can be defined as a new mapping $\vec{\Phi}_{\overline{\vec{V}}} = \{\Phi_Z \in \vec{\Phi} \mid Z \notin \vec{V}\} : \mathbb{R}^N \to \mathbb{R}^{N-N_V}$, where N_V is the number of variables involved in $\vec{V}$. The new system $\vec{\Phi}_{\overline{\vec{V}}}$ takes $\vec{X}_{t-\Delta t}$ as inputs and computes all the variables excluding the sources at the next time step, $\vec{X}_t \backslash \vec{V}_t$.

5.2.2 Assessing the Effect of Intervention by Using Kullback-Leibler Divergence

Let's denote the *pdf* of a target Z_t generated from both the original system $\vec{\Phi}$ and the intervened system $\vec{\Phi}_{\overline{\vec{V}}}$ with sources $\vec{V}$ fixed at time $t-\tau$ ($\tau > 0$) as $\rho_Z(t)$ and $\rho_{Z|\vec{V}}(t|t-\tau)$, respectively. The interventional effect on Z_t from fixing $\vec{V}$ starting at time $t-\tau$ can now be evaluated as quantifying the difference between $\rho_Z(t)$ and $\rho_{Z|\vec{V}}(t|t-\tau)$ through Kullback-Leibler (KL) divergence [Kullback and Leibler, 1951], which is given by:

$$D_{KL}\Big(\rho_Z(t)||\rho_{Z|\vec{V}}(t|t-\tau)\Big) = \sum_{z_t} \rho_Z(t) \log \frac{\rho_Z(t)}{\rho_{Z|\vec{V}}(t|t-\tau)}. \tag{5.3}$$

$D_{KL}(p||q)$ is a nonnegative metrics, quantifying the distance between two *pdf*s p and q. D_{KL} equals to zero when the two *pdf*s are identical, and gets larger if the two *pdf*s differ significantly with each other. Given the ability for assessing the intervetional effect by evaluating the corresponding density change, we now detail the procedures for calculating the KL divergence in Eq.(5.3) based on ensemble simulation.

- Discretize the dynamical system from Eq.(5.1) to $\vec{\Phi}$ in Eq.(5.2).
- Obtain the intervened dynamical system $\vec{\Phi}_{\overline{\vec{V}}}$ from $\vec{\Phi}$ according to the sources $\vec{V}$
- Initialize the joint density of $\vec{X}_{t_0}$ at the start time t_0 with an assumed initial distribution $\rho_{\vec{X}}(t_0)$.
- Randomly draw N_s samples from $\rho_{\vec{X}}(t_0)$ to form an ensemble.
- Do ensemble predictions for the original system $\vec{\Phi}$ till time t.
- Do ensemble predictions for the intervened system $\vec{\Phi}_{\overline{\vec{V}}}$ from time $t-\tau$ to time t.
- Estimate the densities of the target Z_t in both systems $\vec{\Phi}$ and $\vec{\Phi}_{\overline{\vec{V}}}$, $\rho_Z(t)$ and $\rho_{Z|\vec{V}}(t|t-\tau)$, respectively.
- Compute the KL divergence between $\rho_Z(t)$ and $\rho_{Z|\vec{V}}(t|t-\tau)$ in Eq.(5.3).

5.3 Application – the Lorenz Chaotic Model

We now employ the methodology presented in Section 5.2 to evaluate the interventional effect on each component of the Lorenz model in Eq.(3.16) by fixing either one or multiple lagged source components. The simulation is conducted based on 4000 data points for each run with an ensemble of 5000 runs ($N_s = 5000$). For each variable, say $X_{t+\tau}$ for instance, we fix each other variable separately or jointly, that is, Y_t, Z_t, and $\{Y_t, Z_t\}$, at each run. The intervention in each of the above three case takes effect at time t ranging from 2000 to 2050, with time lag τ ranging from 1 to 100.

Furthermore, to compare the cause-effect relations induced by interventional effect and statistical association dependence, we also compute the temporal evolution of mutual information and transfer entropy between each target and lagged source(s) based on the ensemble simulation. Instead of using kNN methods for computing (conditional) mutual information, the information-theoretic measures in this section are computed by using the histogram method in generating the *pdf*. The histogram method is conducted based on 50 bins in each dimension with ranges from -40 to 40.

5.3.1 Influence of Interventional Effect on Density Evolution

The resulting temporal evolution of the density for each variable with and without interventions during t from 1900 to 2100 is plotted in Fig. 5.2. It can be observed that without interventional effect, the density evolutions of the three variables are stationary since the dynamics of the Lorenz model are absorbed in the strange attractor as shown in the diagnal plots of the first three rows in Fig. 5.2. However, once the intervention effect takes place, the density of each variable changes significantly and differs from each other, as illustrated in the off-diagnal plots of the first three rows in Fig. 5.2 when fixing other variables at time $t = 2000$. For X, its dynamics is more evenly distributed across -10 to 10 when Y is fixed, while fixing Z confines most of the trajectories of X close to zero. For Y, the interventional effect of Z is similar to its effect on X, but Y diverges to four specific trajectories at around ± 10 and ± 25 when X is fixed. For Z, intervening either X or Y spreads the dynamics of Z from positive values towards zero more or less. However, while the influence from Y directs the dynamics of Z more towards zero, the influence from X squeezes most trajectories around 25. In terms of the joint effect from intervening two variables, for both Y and Z, fixing the other two sources together results in a mixed trajectories of when intervening each source individually. Meanwhile, the changed dynamics of X by fixing Z and Y is identical to the effect from Y only. This is because Y is the direct influence on X as evident from Eq.(3.16).

The altered density evolution, induced by intervention in a part of system, encodes the information of how freezing one or multiple sources affect the evolution of a target. In the next subsection, we compute the

KL divergence Eq.(5.3) to quantify the density changes for each variable.

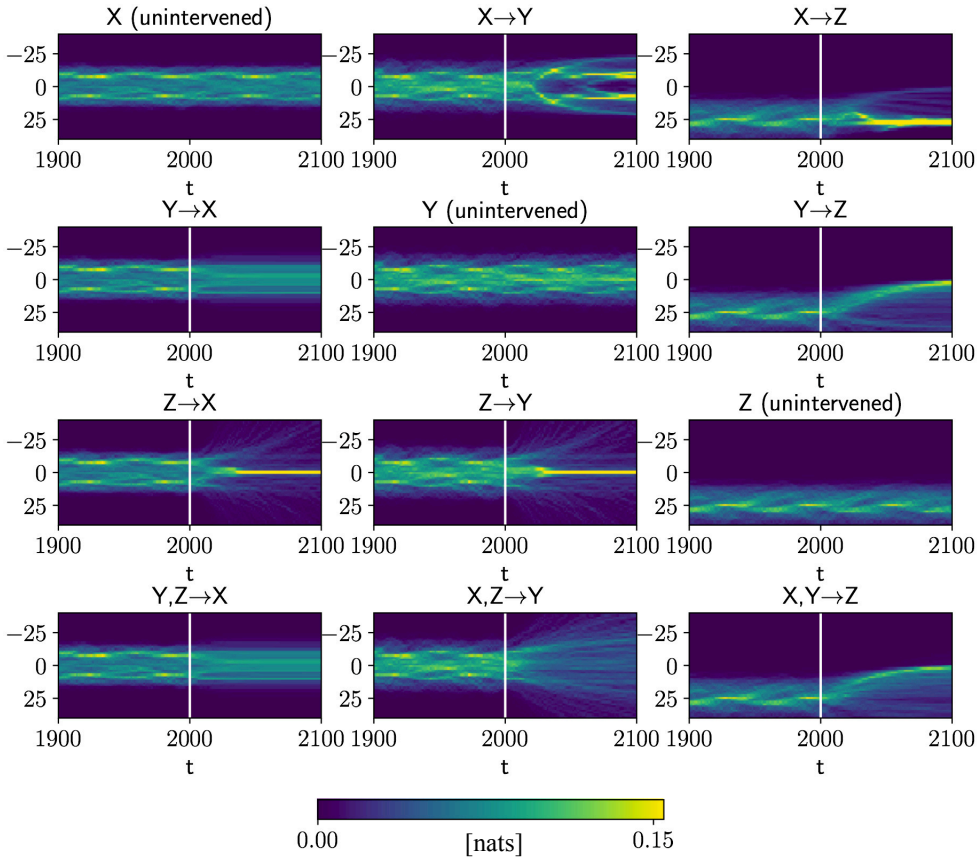

Figure 5.2: The density evolution of each variable in the Lorenz model with and without freezing the source(s) at time $t = 2000$. For instance, the plot of $Y \to X$ refers to the density evolution of X with variable Y fixed at time $t = 2000$, while the plot of $Y, Z \to X$ refers to the density evolution of X with variables Y and Z fixed at time $t = 2000$.

5.3.2 Comparing Causal Relation Due to Interventional and Association Effects

For each trajectory, we intervene each set of sources (for each target variable) starting at time t ranging from 2000 to 2050, and run the intervened system 100 time steps. KL divergence is then computed based on the two different densities, generated from both original Lorenz model and the intervened system. The corresponding MI and TE (in Eqs.(1.3) and (1.5), respectively) for each pair of source and target variables, are computed only based on the simulations without intervention. Specifically, The results of KL, MI, and TE when considering one and two lagged sources are plotted in Figs. 5.3 and 5.4, respectively.

Interventional effect from one lagged source. The results of KL divergence in the second column of Fig. 5.3 shows that the interventional effect on each component from each other variable greatly differs from

each other. For the target X, fixing Y does not change its dynamics significantly over time, whereas the corresponding changes in the density due to intervening Z increase swiftly when the time lag tau grows, as shown in Fig. 5.3(a). Based on the corresponding density evolution plots in the first column of Fig. 5.3(a), we see that while the resulting self-feedback interaction of X when treating Y as constant allows the dynamics of X to be stationary, the interaction between X and Y when fixing Z confines X around zero. In addition, the KL divergence plots for Y in Fig. 5.3(b) is slightly different from X. Though Y receives a similar influence from Z as X does, illustrated as a similar density change and the growth of KL divergence over $t + \tau$, the influence of X on Y is way more stronger than the other way around. It is due to the fact that while fixing Y results in the self-feedback interaction of X, fixing X still allows the interaction between Y and Z, thus complicating the dynamics of Y. Last, the divergence result for Z in Fig. 5.3(c) shows an enhanced changes of Z's density over time when intervening either X or Y. It can be explained by the fact that fixing either X or Y stills allows the interaction between Z and the other variable, leading to the deviation of the trajectory of Z.

Interventional effect from two lagged sources. The KL divergence results in the second column of Fig. 5.4 show that when fixing two variables, the temporal density of each target variable changes abruptly and then converges over time, with the most and least changes on Z and X, respectively. This is due to the similar dynamics of all the three variables when the other two are fixed. That is, $\frac{dV}{dt} = -aV + b$ where a and b are constant with $a > 0$ and $V \in \{X, Y, Z\}$), whose discretization further results in an autoregressive process without the noise term. The different degrees of density divergence are because of the different a values due to the chosen α and β parameters in the Lorenz model.

Comparing results of KL with MI and TE. The association effect quantified by MI and TE is greatly different from KL divergence, in terms of both indicating the important source driver and illustrating the dynamics of the system. First of all, compared with the analysis based on KL divergence, the corresponding results of MI and TE can refer to a totaly different conclusion on which source has a stronger influence on the target. This is especially true in the case of the individual influence of Y and Z on X, as shown in Fig. 5.3(a). While the KL divergence implies the stronger interventional effect from Z on X, MI and TE show a stronger statistical dependence effect between Y and X. A similar contradiction can be observed from the joint influence on each target from the other two variables in Fig. 5.4. As mentioned in the previous paragraph, Z receives the strongest interventional effect from the other two variables, and X receives the least. In contrast, the results of MI and TE illustrate that X is more strongly dependent on the rest two variables than Z. Furthermore, stripe patterns over $t+\tau$ can be observed in each plot of MI and TE in both Figs. 5.3 and 5.4, which is not shown in the KL divergence. These patterns illustrates the unique dynamics

in the strange attractor of the Lorenz model. That is, the model tries to fill the entire fractal domain by drawing many similar but slightly different butterfly trajectories, leading to quasiperiodic dependence among components over time.

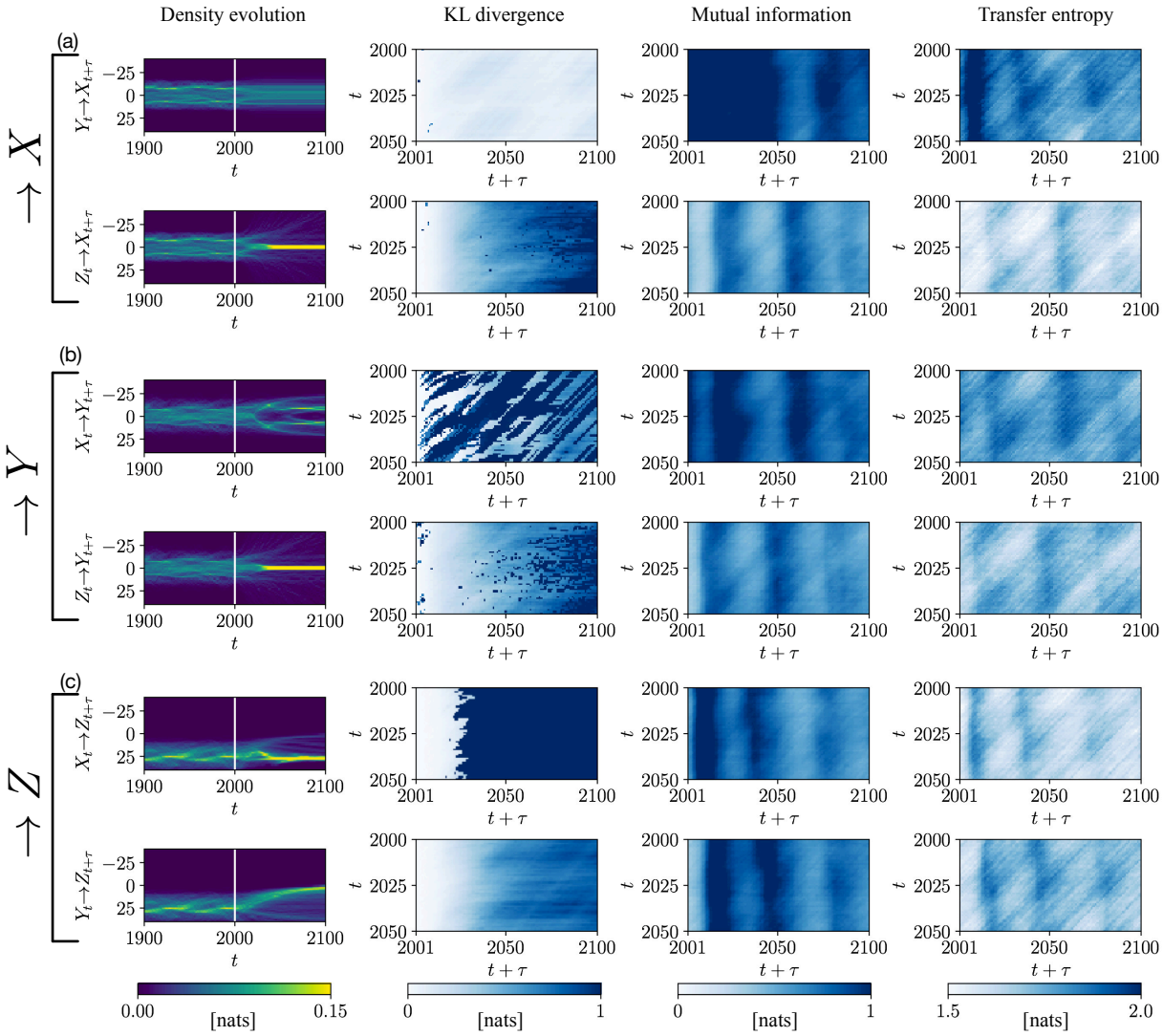

Figure 5.3: Results of Kullback-Leibler (KL) divergence for quantifying the density change of each target variable in the Lorenz model due to freezing one lagged source as well as the corresponding mutual information (MI) and transfer entropy (TE) between the lagged source and the target, with (a) X as the target; (b) Y as the target; and (c) Z as the target. For instance, in the first row of (a), from left to right, the four plots show the density evolution of X with Y fixed at time $t = 2000$, the KL divergence between the original density of X and the density of X at time $t + \tau$ with Y intervened at time t, the MI and TE between X at time $t + \tau$ and Y at time t, respectively.

The difference between the results of KL divergence and MI/TE in the Lorenz model analysis implies the complementary roles of employing numerical modelling and observed time series data to unravel the complex system dynamics. While MI and TE quantified from observations are able to illustrate the association

dependencies among the components, the interventional effects can be obtained by intervening and ensemble simulation of a known dynamics. The inteventional effect by investigating the structure of numerical models focuses on how the dynamics of a target variable changes by altering one or multiple sources. It would be extremely helpful in scenario control analysis, where the control or intervention in the system is required to evaluate the corresponding acclimation of a specific variable. On the other hand, when only observations are available, as the case in many natural systems, metrics such as MI and TE can provide insights on the dependencies among different components as well as indicate the corresponding cause-effect relation in a Granger sense.

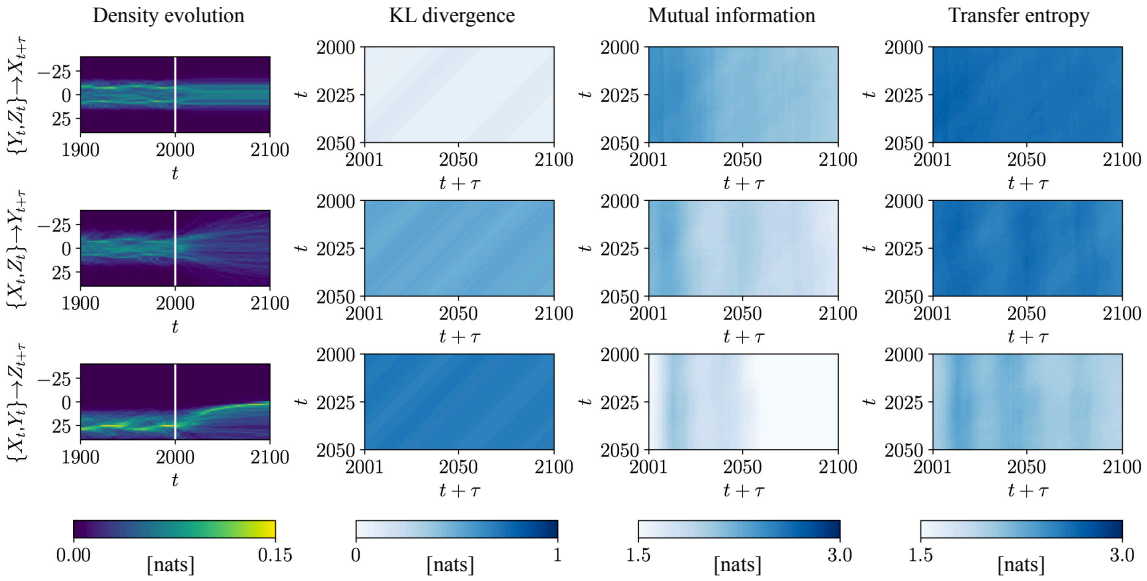

Figure 5.4: Results of Kullback-Leibler (KL) divergence for quantifying the density change of each target variable in the Lorenz model due to freezing two lagged sources as well as the corresponding mutual information (MI) and transfer entropy (TE) between the lagged source and the target, with (a) X as the target; (b) Y as the target; and (c) Z as the target. For instance, in the first row of (a), from left to right, the four plots show the density evolution of X with Y and Z fixed at time $t = 2000$, the KL divergence between the original density of X and the density of X at time $t + \tau$ with Y and Z intervened at time t, the MI and TE between X at time $t + \tau$ and Y, Z at time t, respectively.

5.4 Conclusion and Future Work

We analyzed the structure of a numerical model from an interventional-effect perspective. That is, in a modelled system, we ask how the density of a target variable responds to freezing one or multiple lagged source variables, quantified by KL divergence. This is conceptually different from the prior causal history analysis based on observational data, where system intervention and ensemble simulations are infeasible. Further, in the comparison between interventional effect and statistical dependency, the proposed causal

history analysis in Chapter 3 is not performed. This is because of the incomparability of the two types of causality due to that the target would remain constant when its self-dependency in causal history is frozen. Instead, MI and TE are computed for accounting for the corresponding statistical dependency on one or multiple lagged sources.

The analysis of the Lorenz model shows that the interventional effect, measured by the corresponding change in target's density, and the statistical-dependence effect as, measured by the MI/TE between the target and lagged source(s), provide two complementary views on the influence on a target variable from lagged source variable(s). While the interventional effect quantified by KL divergence illustrates how a target trajectory would change accordingly due to fixing source(s), the dependence effect quantified by MI and TE assesses the uncertainty reduction of the target from source(s). For instance, in the Lorenz model, variable X is more dependent on Y based on the MI/TE result, where the stripe pattern in Fig. 5.4 across the time lag τ also indicate the quasiperiodic dynamics of the model. Meanwhile, the KL divergence shows that X's dynamics is in fact strongly controlled by Z, evidenced by the corresponding drastic density change in Fig. 5.3(a).

The different perspectives on the interactions among variables from the interventional effect and the statistical dependence indicate the importance of numerical modelling in understanding the component interaction in natural systems from an interventional perspective, in addition to the purpose of simulation and prediction. For instance, it can be the case that the two perspectives provide contrasting or even contradictory results on the key source affecting a target, as the case of target variable X in the Lorenz model. Decision made solely based upon the analysis in observational data might therefore not be the optimal solution due to the lack of understanding on the interventional effect. Therefore, investigating such influence on components by intervention in systems represented by numerical models is very crucial and useful for the planning and decision making in control systems. In agricultural systems, such interventional effect analysis in ecohydrological models can provide insights as to what extent different field planning schemes would affect issues such as food production, water usage, carbon/nitrogen loss, and so forth, thereby improving agriculture management. In addition, based on a simulated control system, assessing how dam operations affects the dynamics of the ecosystem in the downstream can inform the local authorities for operational practices. Thus, planning and decision making that leverages the interactions among the components as such provides a lot of opportunities for future work in addressing different practical problems.

Chapter 6

Summary and Conclusions

The main theme of this work is to provide a better understanding on the whole system behavior of a complex system. We anchor it on the perspective of multivariate interaction by leveraging the importance of the joint effect from the interactions among all the components in the system, with an attempt to understand how **the whole is greater than sum of its parts**. The entire evolutionary dynamics of all components in the system is termed **causal history** in this study. Investigating the joint influence from the causal history on the present state of each individual variable in a system draws upon the understanding of the interactions within each pair of lagged variables as well as a specific set of variables in the system. A directed acyclic graphical model is employed to represent the dynamics of all the variables in the system represented as a time-series, and thus serves as a basis for illustrating different types of interactions through different pathways in the graph. Furthermore, to quantify and characterize the influence from one or multiple lagged source variables to a target variable, information theoretic approach is utilized due to its capability in capturing the nonlinear dependency across multiple components. The corresponding delineated influence is, therefore, termed **information flow** from source(s) to a target. We first investigated the whole system behavior in observed systems by developing information-theoretic metrics for characterizing the information flow to a target from two sources as well as from the entire causal history. The resulting unravelled cause-effect influence is consistent with the idea of Granger causality, that is, it evaluates the dependence between lagged variables of interest by conditioning on the remaining historical dynamics of the system. We then employed the idea of multivariate interaction to assess the structures of numerical models. Different from the analysis in observed systems, the cause-effect influence analyzed in modelled systems enables us to explore Pearl causality, that is, how intervening source(s) would induce a corresponding change on the target. This is due to the uniqueness of numerical models – the ability of being intervened and ensemble simulations. The multivariate interactions analyzed in observed and modelled systems thus provide two complementary views of the dynamics in a complex system. In this chapter, we summarize the main findings and discuss the potential future avenues of this study.

6.1 Characterizing Information Flow from Causal History

We developed an information-theoretic framework to characterize the information flow from the entire causal history to the present state of each target. Building on momentary information transfer (MIT) for quantifying the coupling strength between each pair of lagged variables, we characterized the information flow from two lagged sources through separable causal paths using momentary partial information decomposition (MPID) approach. MIT and MPID then serve as the basis for *causal history analysis* approach, for capturing the joint effect from different parts of the causal history. Specifically, we evaluated the information flow from immediate and distant histories partitioned by a time lag τ, and as a function thereof, in the causal history for investigating the influence from a recent and the complementary earlier dynamics of the system, respectively. Furthermore, due to the vital role of self-feedback in interactions in many natural systems, we also characterized the joint effects of the self- and cross-dependencies in both immediate and distant histories. These information-theoretic measures were implemented to analyze the dynamics of a trivariate logistic model and the Lorenz chaotic model. The key results show that:

- MPID is better at illustrating the structures of two causal paths conveying interactive information flows from two lagged sources to a target than PID.
- The convergence of the information given by distant causal history over the time lag τ illustrates the memory-dependence of a system, with zero- and nonzero-convergences representing short and long memories, respectively.

6.2 Understanding Whole System Behavior in Observed Systems

We implemented the proposed causal history analysis approach to investigate how the entire evolutionary dynamics shapes the present state of each variable in different systems. In addition to the logistic model and the Lorenz model, we further analyzed the dynamics of the Ornstein-Uhlenbeck process – a long-memory but non-chaotic model, and an observed stream chemistry dynamics – a fractal process when the dependencies of flow rate on stream solutes are excluded. The resulting information characterizations of the four systems, based on either observed or synthetic data, show that:

- A short-memory system, such as the trivariate logistic model, is only sustained by its recent dynamics including influences from both self- and cross-dependencies.
- A long-memory system, such as the Lorenz model, the OU process, and the observed stream chemistry

dynamics, is sustained by a self-dependence-dominated recent dynamics as well as a cross-dependence-dominated earlier dynamics.

- The $1/f$ fractal signature of each stream solute analyzed, with the influence of the flow rate corrected, is sustained by both its self-feedback interaction and the interactions with other components in the stream.

- Information characterization can distinguish different dependencies among components. For instance, it illustrates the different origins of the solutes in the stream chemistry dynamics analysis.

6.3 Assessing Variable Dependence in Modelled Systems

We investigated the cause-effect influence from lagged source(s) to each target in a system, from the point of view of how the density evolution of the target is altered due to the interventions on the source(s). Such interventional effect analysis provides a complementary view of a system's dynamics in addition to the Granger causality-based analysis on observed systems. We quantified the intervention-induced density change of each target due to one or multiple sources in the Lorenz model by using Kullback-Leibler (KL) divergence, and compared it with the statistical dependence between source(s) and target quantified by mutual information (MI) and transfer entropy (TE). The comparison between the computed KL and MI/TE, in the Lorenz model, showed that:

- The results of KL and MI/TE, quantifying to what extent a target is influenced by source(s), can be different. For instance, while variable Z in the Lorenz model has a stronger interventional effect on X, X is more statistically dependent on Y. It thus illustrates the complementary roles of intervetional effect and statistical dependence in delineating the cause-effect influences in a complex system.

- The statistical dependence, captured by MI/TE, shows the quasi-periodicity over time lag τ between source(s) and target. It is consistent with the quasi-repetitive butterfly trajectories within the strange attractor.

6.4 Future Work

This dissertation is the first work to understand whole system behaviors through the interactions happening in the entire evolutionary dynamics of the system based on time-series data. The proposed information-theoretic approach, along with the idea of multivariate interaction analysis, thus provides open avenues for

future researches to understand ecohydrological system dynamics and complex system analysis in general, including the following:

- Investigating a wide range of ecohydrological complex systems under different conditions, such as wetness and temperature influence. For instance, it is of interest to evaluate the difference between a dry and a wet plant system, or between systems in warm and cold environments, in terms of the information characterization from its historical dynamical trajectory.

- Evaluating the impact of anthropogenic activities on the dynamics of ecohydrological systems. The stream chemistry analysis is an example of assessing the role of flow rate on shaping the interactions among other variables in the system. The investigation of the influence from one specific variable on the causal relationships in the rest of the system provides insights on assessing the impact on the system's dynamics due to anthropogenic activities, which is considered as the influential component. For instance, the analysis could potentially serve as a basis to investigate the influence on the downstream surface water and groudwater interaction due to the upstream activities, such as dam operations.

- Analyzing the multivariate interactions through different causal history partitions. For example, one possibility can be evaluating the joint effect from different subsystems, by classifying all the components into a set of subsystems based on a classification criteria of interest.

- Studying the spatial interactions. It requires leveraging the existing causal history analysis approach to evaluate the dynamics of variables in different geographical locations.

- Identifying key source component(s) in contributing to a specific target from both interventional effect and statistical dependence perspectives using numerical models.

With the increasing availability of time-series observations and complexity of numerical models, the proposed multivariate interaction analysis framework would potentially serve as the foundation for a holistic understanding on complex system dynamics and thus enhance our comprehension of hydrology and other fields.

References

[Aguirre et al., 2014] Aguirre, J., Sevilla-Escoboza, R., Gutiérrez, R., Papo, D., and Buldú, J. M. (2014). Synchronization of interconnected networks: The role of connector nodes. *Phys. Rev. Lett.*, 112:248701.

[Aho et al., 1972] Aho, A., Garey, M., and Ullman, J. (1972). The transitive reduction of a directed graph. *SIAM Journal on Computing*, 1(2):131–137.

[Amblard and Michel, 2013] Amblard, P.-O. and Michel, O. J. J. (2013). The relation between granger causality and directed information theory: A review. *Entropy*, 15(1):113–143.

[Amenu et al., 2005] Amenu, G. G., Kumar, P., and Liang, X.-Z. (2005). Interannual variability of deep-layer hydrologic memory and mechanisms of its influence on surface energy fluxes. *Journal of Climate*, 18(23):5024–5045.

[Atay et al., 2004] Atay, F. M., Jost, J., and Wende, A. (2004). Delays, connection topology, and synchronization of coupled chaotic maps. *Phys. Rev. Lett.*, 92:144101.

[Balasis et al., 2013] Balasis, G., Donner, R. V., Potirakis, S. M., Runge, J., Papadimitriou, C., Daglis, I. A., Eftaxias, K., and Kurths, J. (2013). Statistical mechanics and information-theoretic perspectives on complexity in the earth system. *Entropy*, 15(11):4844–4888.

[Baldocchi et al., 2001] Baldocchi, D., Falge, E., Gu, L., Olson, R., Hollinger, D., Running, S., Anthoni, P., Bernhofer, C., Davis, K., Evans, R., Fuentes, J., Goldstein, A., Katul, G., Law, B., Lee, X., Malhi, Y., Meyers, T., Munger, W., Oechel, W., Paw, K. T., Pilegaard, K., Schmid, H. P., Valentini, R., Verma, S., Vesala, T., Wilson, K., and Wofsy, S. (2001). Fluxnet: A new tool to study the temporal and spatial variability of ecosystemscale carbon dioxide, water vapor, and energy flux densities. *Bulletin of the American Meteorological Society*, 82(11):2415–2434.

[Barrett, 2015] Barrett, A. B. (2015). Exploration of synergistic and redundant information sharing in static and dynamical gaussian systems. *Phys. Rev. E*, 91:052802.

[Bellman, 1957] Bellman, R. (1957). *Dynamic Programming*. Rand Corporation research study. Princeton University Press.

[Bertschinger et al., 2013] Bertschinger, N., Rauh, J., Olbrich, E., and Jost, J. (2013). Shared information—new insights and problems in decomposing information in complex systems. In Gilbert, T., Kirkilionis, M., and Nicolis, G., editors, *Proceedings of the European Conference on Complex Systems 2012*, pages 251–269, Cham. Springer International Publishing.

[Bertschinger et al., 2014] Bertschinger, N., Rauh, J., Olbrich, E., Jost, J., and Ay, N. (2014). Quantifying unique information. *Entropy*, 16(4):2161–2183.

[Bollt, 2012] Bollt, E. M. (2012). Synchronization as a process of sharing and transferring information. *International Journal of Bifurcation and Chaos*, 22(11):1250261.

[Bollt et al., 2018] Bollt, E. M., Sun, J., and Runge, J. (2018). Introduction to focus issue: Causation inference and information flow in dynamical systems: Theory and applications. *Chaos: An Interdisciplinary Journal of Nonlinear Science*, 28(7):075201.

[Bosnacki et al., 2010] Bosnacki, D., Lightenberg, W., Odenbrett, M., Wijs, A., and Hilbers, P. (2010). Parallel algorithms for transitive reduction of weighted graphs. *Math Maced*.

[Cafaro et al., 2015] Cafaro, C., Lord, W. M., Sun, J., and Bollt, E. M. (2015). Causation entropy from symbolic representations of dynamical systems. *Chaos: An Interdisciplinary Journal of Nonlinear Science*, 25(4):043106.

[Cover and Thomas, 2006] Cover, T. M. and Thomas, J. A. (2006). *Elements of Information Theory (Wiley Series in Telecommunications and Signal Processing)*. Wiley-Interscience.

[Eichler, 2012] Eichler, M. (2012). Graphical modelling of multivariate time series. *Probability Theory and Related Fields*, 153(1):233–268.

[Feng et al., 2004] Feng, X., Kirchner, J. W., and Neal, C. (2004). Measuring catchment-scale chemical retardation using spectral analysis of reactive and passive chemical tracer time series. *Journal of Hydrology*, 292(1):296 – 307.

[Finn and Lizier, 2018] Finn, C. and Lizier, J. T. (2018). Pointwise information decomposition using the specificity and ambiguity lattices. *arXiv preprint arXiv:1801.09010*.

[Frenzel and Pompe, 2007] Frenzel, S. and Pompe, B. (2007). Partial mutual information for coupling analysis of multivariate time series. *Phys. Rev. Lett.*, 99:204101.

[Goodwell et al., view] Goodwell, A. E., Jiang, P., Ruddell, B. L., and Kumar, P. (in review). Does information theory provide a new paradigm for earth science? identifying causality, interaction, and feedback. *Water Resources Research*.

[Goodwell and Kumar, 2017a] Goodwell, A. E. and Kumar, P. (2017a). Temporal information partitioning: Characterizing synergy, uniqueness, and redundancy in interacting environmental variables. *Water Resources Research*, 53(7):5920–5942.

[Goodwell and Kumar, 2017b] Goodwell, A. E. and Kumar, P. (2017b). Temporal information partitioning networks (tipnets): A process network approach to infer ecohydrologic shifts. *Water Resources Research*, 53(7):5899–5919.

[Goodwell et al., 2018] Goodwell, A. E., Kumar, P., Fellows, A. W., and Flerchinger, G. N. (2018). Dynamic process connectivity explains ecohydrologic responses to rainfall pulses and drought. *Proceedings of the National Academy of Sciences*.

[Granger, 1969] Granger, C. W. J. (1969). Investigating causal relations by econometric models and cross-spectral methods. *Econometrica*, 37(3):424–438.

[Griffith and Ho, 2015] Griffith, V. and Ho, T. (2015). Quantifying redundant information in predicting a target random variable. *Entropy*, 17(7):4644–4653.

[Griffith and Koch, 2014] Griffith, V. and Koch, C. (2014). *Quantifying Synergistic Mutual Information*, pages 159–190. Springer Berlin Heidelberg, Berlin, Heidelberg.

[Haken, 2006] Haken, H. (2006). *Information and Self-Organization*. Springer-Verlag Berlin Heidelberg.

[Harder et al., 2013] Harder, M., Salge, C., and Polani, D. (2013). Bivariate measure of redundant information. *Phys. Rev. E*, 87:012130.

[Ince, 2017] Ince, R. A. A. (2017). Measuring multivariate redundant information with pointwise common change in surprisal. *Entropy*, 19(7):318.

[Jiang and Kumar, 2018] Jiang, P. and Kumar, P. (2018). Interactions of information transfer along separable causal paths. *Phys. Rev. E*, 97:042310.

[Jiang and Kumar, 2019] Jiang, P. and Kumar, P. (2019). Information transfer from causal history in complex system dynamics. *Phys. Rev. E*, 99:012306.

[Jizba et al., 2012] Jizba, P., Kleinert, H., and Shefaat, M. (2012). Rnyis information transfer between financial time series. *Physica A: Statistical Mechanics and its Applications*, 391(10):2971 – 2989.

[Kirchner et al., 2000] Kirchner, J. W., Feng, X., and Neal, C. (2000). Fractal stream chemistry and its implications for contaminant transport in catchments. *Nature*, 403(6769):524–527.

[Kirchner and Neal, 2013] Kirchner, J. W. and Neal, C. (2013). Universal fractal scaling in stream chemistry and its implications for solute transport and water quality trend detection. *Proceedings of the National Academy of Sciences*, 110(30):12213–12218.

[Kramer, 1998] Kramer, G. (1998). *Directed information for channels with feedback*. PhD thesis, Swiss Federal Institute of Technology Zurich.

[Kraskov et al., 2004] Kraskov, A., Stögbauer, H., and Grassberger, P. (2004). Estimating mutual information. *Phys. Rev. E*, 69:066138.

[Kullback and Leibler, 1951] Kullback, S. and Leibler, R. A. (1951). On information and sufficiency. *Ann. Math. Statist.*, 22(1):79–86.

[Kumar and Ruddell, 2010] Kumar, P. and Ruddell, B. L. (2010). Information driven ecohydrologic self-organization. *Entropy*, 12(10):2085–2096.

[Lauritzen et al., 1990] Lauritzen, S. L., Dawid, A. P., Larsen, B. N., and Leimer, H. (1990). Independence properties of directed markov fields. *Networks*, 20(5):491–505.

[Liang and Kleeman, 2005] Liang, X. S. and Kleeman, R. (2005). Information transfer between dynamical system components. *Phys. Rev. Lett.*, 95:244101.

[Liang and Kleeman, 2007a] Liang, X. S. and Kleeman, R. (2007a). A rigorous formalism of information transfer between dynamical system components. i. discrete mapping. *Physica D: Nonlinear Phenomena*, 231(1):1 – 9.

[Liang and Kleeman, 2007b] Liang, X. S. and Kleeman, R. (2007b). A rigorous formalism of information transfer between dynamical system components. ii. continuous flow. *Physica D: Nonlinear Phenomena*, 227(2):173 – 182.

[Lizier et al., 2011] Lizier, J. T., Heinzle, J., Horstmann, A., Haynes, J.-D., and Prokopenko, M. (2011). Multivariate information-theoretic measures reveal directed information structure and task relevant changes in fmri connectivity. *Journal of Computational Neuroscience*, 30(1):85–107.

[Lorenz, 1963] Lorenz, E. N. (1963). Deterministic nonperiodic flow. *Journal of the Atmospheric Sciences*, 20(2):130–141.

[Majda and Gershgorin, 2011] Majda, A. J. and Gershgorin, B. (2011). Improving model fidelity and sensitivity for complex systems through empirical information theory. *Proceedings of the National Academy of Sciences*, 108(25):10044–10049.

[Martí et al., 2008] Martí, A. C., Ponce, M., and Masoller, C. (2008). Dynamics of delayed-coupled chaotic logistic maps: Influence of network topology, connectivity and delay times. *Pramana*, 70(6):1117–1125.

[Masoller and Atay, 2011] Masoller, C. and Atay, F. (2011). Complex transitions to synchronization in delay-coupled networks of logistic maps. *The European Physical Journal D*, 62(1):119.

[Neal et al., 2013] Neal, C., Reynolds, B., Kirchner, J. W., Rowland, P., Norris, D., Sleep, D., Lawlor, A., Woods, C., Thacker, S., Guyatt, H., Vincent, C., Lehto, K., Grant, S., Williams, J., Neal, M., Wickham, H., Harman, S., and Armstrong, L. (2013). High-frequency precipitation and stream water quality time series from plynlimon, wales: an openly accessible data resource spanning the periodic table. *Hydrological Processes*, 27(17):2531–2539.

[Neal et al., 1997] Neal, C., Wilkinson, J., Neal, M., Harrow, M., Wickham, H., Hill, L., and Morfitt, C. (1997). The hydrochemistry of the headwaters of the river severn, plynlimon. *Hydrology and Earth System Sciences*, 1(3):583–617.

[Nicolis and Prigogine, 1989] Nicolis, G. and Prigogine, I. (1989). *Exploring Complexity: An Introduction*. St. Martin's Press.

[Olbrich et al., 2015] Olbrich, E., Bertschinger, N., and Rauh, J. (2015). Information decomposition and synergy. *Entropy*, 17(5):3501–3517.

[Paik and Kumar, 2008] Paik, K. and Kumar, P. (2008). Emergence of self-similar tree network organization. *Complexity*, 13(4):30–37.

[Paniconi and Putti, 2015] Paniconi, C. and Putti, M. (2015). Physically based modeling in catchment hydrology at 50: Survey and outlook. *Water Resources Research*, 51(9):7090–7129.

[Paredes et al., 2013] Paredes, G., Alvarez-Llamoza, O., and Cosenza, M. G. (2013). Global interactions, information flow, and chaos synchronization. *Phys. Rev. E*, 88:042920.

[Pearl, 2000] Pearl, J. (2000). *Causality: Models, Reasoning, and Inference*. Cambridge University Press, New York, NY, USA.

[Pompe and Runge, 2011] Pompe, B. and Runge, J. (2011). Momentary information transfer as a coupling measure of time series. *Phys. Rev. E*, 83:051122.

[Rosas et al., 2018] Rosas, F., Mediano, P. A., Ugarte, M., and Jensen, H. J. (2018). An information-theoretic approach to self-organisation: Emergence of complex interdependencies in coupled dynamical systems. *Entropy*, 20(10).

[Rosenblum et al., 1997] Rosenblum, M. G., Pikovsky, A. S., and Kurths, J. (1997). From phase to lag synchronization in coupled chaotic oscillators. *Phys. Rev. Lett.*, 78:4193–4196.

[Ruddell and Kumar, 2009a] Ruddell, B. L. and Kumar, P. (2009a). Ecohydrologic process networks: 1. identification. *Water Resources Research*, 45(3).

[Ruddell and Kumar, 2009b] Ruddell, B. L. and Kumar, P. (2009b). Ecohydrologic process networks: 2. analysis and characterization. *Water Resources Research*, 45(3).

[Runge, 2015] Runge, J. (2015). Quantifying information transfer and mediation along causal pathways in complex systems. *Phys. Rev. E*, 92:062829.

[Runge et al., 2012a] Runge, J., Heitzig, J., Marwan, N., and Kurths, J. (2012a). Quantifying causal coupling strength: A lag-specific measure for multivariate time series related to transfer entropy. *Phys. Rev. E*, 86:061121.

[Runge et al., 2012b] Runge, J., Heitzig, J., Petoukhov, V., and Kurths, J. (2012b). Escaping the curse of dimensionality in estimating multivariate transfer entropy. *Phys. Rev. Lett.*, 108:258701.

[Runge et al., 2015] Runge, J., Petoukhov, V., Donges, J. F., Hlinka, J., Jajcay, N., Vejmelka, M., Hartman, D., Marwan, N., Paluš, M., and Kurths, J. (2015). Identifying causal gateways and mediators in complex spatio-temporal systems. *Nature communications*, 6:8502.

[Runge et al., 2014] Runge, J., Petoukhov, V., and Kurths, J. (2014). Quantifying the strength and delay of climatic interactions: The ambiguities of cross correlation and a novel measure based on graphical models. *Journal of Climate*, 27(2):720–739.

[Runge et al., 2017] Runge, J., Sejdinovic, D., and Flaxman, S. (2017). Detecting causal associations in large nonlinear time series datasets. *arXiv preprint arXiv:1702.07007*.

[Schneider and Kay, 1994] Schneider, E. and Kay, J. (1994). Life as a manifestation of the second law of thermodynamics. *Mathematical and Computer Modelling*, 19(6):25 – 48.

[Schreiber, 2000] Schreiber, T. (2000). Measuring information transfer. *Phys. Rev. Lett.*, 85:461–464.

[Shannon and Weaver, 1949] Shannon, C. E. and Weaver, W. (1949). *A Mathematical Theory of Communication*. University of Illinois Press, Urbana, IL.

[Silverman, 1986] Silverman, B. W. (1986). *Density estimation for statistics and data analysis*, volume 26. CRC press.

[Spirtes et al., 2000] Spirtes, P., Glymour, C., and Scheines, R. (2000). *Causation, Prediction, and Search.*, volume 81. MIT Press, Cambridge.

[Strogatz, 2000] Strogatz, S. H. (2000). *Nonlinear Dynamics And Chaos: With Applications To Physics, Biology, Chemistry, And Engineering (Studies in Nonlinearity)*. CRC Press.

[Sun and Bollt, 2014] Sun, J. and Bollt, E. M. (2014). Causation entropy identifies indirect influences, dominance of neighbors and anticipatory couplings. *Physica D: Nonlinear Phenomena*, 267:49 – 57.

[Tononi and Edelman, 1998] Tononi, G. and Edelman, G. M. (1998). Consciousness and complexity. *Science*, 282(5395):1846–1851.

[West, 2017] West, G. (2017). *Scale: the universal laws of growth, innovation, sustainability, and the pace of life in organisms, cities, economies, and companies*. Penguin.

[Williams and Beer, 2010] Williams, P. L. and Beer, R. D. (2010). Nonnegative decomposition of multivariate information. *CoRR*, abs/1004.2515.

[Yang et al., 2017] Yang, S., Paik, K., McGrath, G. S., Urich, C., Krueger, E., Kumar, P., and Rao, P. S. C. (2017). Functional topology of evolving urban drainage networks. *Water Resources Research*, 53(11):8966–8979.

[Yin and Duan, 2018] Yin, Y. and Duan, X. (2018). Information transfer among the components in multidimensional complex dynamical systems. *Entropy*, 20(10).

Appendix A

Some Properties of Shannon Entropy and Mutual Information

The conditional Shannon entropy holds the translationally invariant property [Runge et al., 2012b] such that

$$\begin{aligned} H(X + f(W)|V, W) &= \int p(w) H(X + f(w)|V, W = w) dw \\ &= \int p(w) H(X|V, W = w) dw \\ &= H(X|V, W), \end{aligned} \tag{A.1}$$

where X, V and W are random variables and f is an arbitrary function. Such translational invariance is also valid for the conditional mutual information and can be given as

$$\begin{aligned} I(X + f(W); Y|V, W) = &\quad H(X + f(W)|V, W) - H(X + f(W)|Y, V, W) \\ \overset{\text{Eq.(A.1)}}{=} &\quad H(X|V, W) - H(X|Y, V, W) \\ = &\quad I(X; Y|V, W), \end{aligned} \tag{A.2}$$

where Y is a random variable. Moreover, the translational invariance for the conditional mutual information can be generalized as

$$I(X + f(W); Y + g(V)|V, W) = I(X; Y|V, W), \tag{A.3}$$

where g is also an arbitrary function. The proof of Eq.(A.3) is similar to the proof for $I(X+f(W); Y|V, W) = I(X; Y|V, W)$ such that we emphasize the translational invariance of the conditions V this time. Another

way for generalizing the translational invariance for the conditional mutual information is

$$\begin{aligned} I(X+f(W), Z+h(W); Y|V,W) = &\quad H(X+f(W), Z+h(W)|V,W) - H(X+f(W), Z+h(W)|Y,V,W) \\ &\overset{\text{Eq.(A.1)}}{=} H(X,Z|V,W) - H(X,Z|Y,V,W) \\ &= \quad I(X,Z;Y|V,W), \end{aligned} \tag{A.4}$$

where Z and h are a random variable and an arbitrary function, respectively.

Moreover, if all the variables are Gaussian, the entropy of a d-dimensional process $\vec{X}$ conditional on another multivariate Gaussian process $\vec{Y}$ can be expressed as [Cover and Thomas, 2006]

$$H(\vec{X} \mid \vec{Y}) = \frac{1}{2} \ln \Big\{ (2\pi e)^d \frac{|\Gamma_{\vec{X},\vec{Y}}|}{|\Gamma_{\vec{Y}}|} \Big\}, \tag{A.5}$$

where $|\Gamma_{\vec{Y}}|$ and $|\Gamma_{\vec{X},\vec{Y}}|$ are the determinant of the covariance matrix of $\vec{Y}$ and $(\vec{X},\vec{Y})$, respectively.

Appendix B

Proof of the Coupling Strength Autonomy Property for MPID

To prove the coupling strength autonomy property for MPID shown in Section 2.4.1, we start from the derivation for MII-SCP and then give the solutions for the synergistic, unique and redundant information. We denote $\vec{W}$ as the condition adopted in MPID such that

$$\vec{W} = \vec{W}_1 \cup \vec{W}_2 \cup \vec{W}_3 \tag{B.1a}$$

where

$$\vec{W}_1 = P_{Z_t} \backslash (C_{X_{t-\tau_X} \to Z_t} \cup C_{Y_{t-\tau_Y} \to Z_t}), \tag{B.1b}$$

$$\vec{W}_2 = P_{C_{X_{t-\tau_X} \to Z_t}} \backslash C_{Y_{t-\tau_Y} \to Z_t}, \tag{B.1c}$$

$$\vec{W}_3 = P_{C_{Y_{t-\tau_Y} \to Z_t}} \backslash C_{X_{t-\tau_X} \to Z_t}. \tag{B.1d}$$

The interaction information in MPID can be written as

$$\begin{aligned} \Delta I^{MSCP}_{\{X_{t-\tau_X}, Y_{t-\tau_Y}\} \to Z_t} &= \mathcal{I}(X_{t-\tau_X}; Y_{t-\tau_Y}; Z_t \mid \vec{W}) \\ &= I(X_{t-\tau_X}; Y_{t-\tau_Y} \mid \{Z_t\} \cup \vec{W}) - I(X_{t-\tau_X}; Y_{t-\tau_Y} \mid \vec{W}), \end{aligned} \tag{B.2}$$

which means the expressions for the two conditional mutual information values $I(X_{t-\tau_X}; Y_{t-\tau_Y} \mid \{Z_t\} \cup \vec{W})$ and $I(X_{t-\tau_X}; Y_{t-\tau_Y} \mid \vec{W})$ are required.

(i) Assume the *additivity* condition holds. Then, $I(X_{t-\tau_X}; Y_{t-\tau_Y} \mid \vec{W})$ can be expressed as

$$\begin{aligned} I(X_{t-\tau_X}; Y_{t-\tau_Y} \mid \vec{W}) &\overset{\text{Eq.(2.13)}}{=} I(f_X(P^{\vec{B}}_{X_{t-\tau_X}}) + g_X(P_{X_{t-\tau_X}} \backslash P^{\vec{B}}_{X_{t-\tau_X}}) + \eta^X_{t-\tau_X}; \\ &\qquad f_Y(P^{\vec{B}}_{Y_{t-\tau_Y}}) + g_Y(P_{Y_{t-\tau_Y}} \backslash P^{\vec{B}}_{Y_{t-\tau_Y}}) + \eta^Y_{t-\tau_2} \mid \vec{W}) \\ &\overset{\text{Eq.(A.2)}}{=} I(f_X(P^{\vec{B}}_{X_{t-\tau_X}}) + \eta^X_{t-\tau_X}; f_Y(P^{\vec{B}}_{Y_{t-\tau_Y}}) + \eta^Y_{t-\tau_Y} \mid \vec{W}) \end{aligned} \tag{B.3}$$

The first equality holds due to the *additivity* condition defined in Eq.(2.13), while the second equality is

obtained based on the translational invariance in Eq.(A.2) because $P_{K_{t-\tau}} \backslash P^{\vec{B}}_{K_{t-\tau}} \in \vec{W}$ (where $K_{t-\tau} \in \vec{B}$).

Furthermore, due to the chain rule, $I(X_{t-\tau_X}; Y_{t-\tau_Y} \mid \{Z_t\} \cup \vec{W})$ in Eq.(B.2) can be expanded as

$$I(X_{t-\tau_X}; Y_{t-\tau_Y} \mid \{Z_t\} \cup \vec{W}) = I(X_{t-\tau_X}, Z_t; Y_{t-\tau_Y} \mid \vec{W}) - I(Y_{t-\tau_Y}; Z_t \mid \vec{W}). \tag{B.4}$$

$I(X_{t-\tau_X}, Z_t; Y_{t-\tau_Y} \mid \vec{W})$ in Eq.(B.4) can be further expressed as

$$\begin{aligned}
I(X_{t-\tau_X}, Z_t; Y_{t-\tau_Y} \mid \vec{W}) &\overset{\text{Eq.(2.13)}}{=} I(f_X(P^{\vec{B}}_{X_{t-\tau_X}}) + g_X(P_{X_{t-\tau_X}} \backslash P^{\vec{B}}_{X_{t-\tau_X}}) + \eta^X_{t-\tau_X}, f_Z(P^{\vec{B}}_{Z_t}) + g_Z(P_{Z_t} \backslash P^{\vec{B}}_{Z_t}) + \eta^Z_t; \\
&\qquad f_Y(P^{\vec{B}}_{Y_{t-\tau_Y}}) + g_Y(P_{Y_{t-\tau_Y}} \backslash P^{\vec{B}}_{Y_{t-\tau_Y}}) + \eta^Y_{t-\tau_Y}) \mid \vec{W}) \\
&\overset{\text{Eq.(A.2)}}{=} I(f_X(P^{\vec{B}}_{X_{t-\tau_X}}) + g_X(P_{X_{t-\tau_X}} \backslash P^{\vec{B}}_{X_{t-\tau_X}}) + \eta^X_{t-\tau_X}, f_Z(P^{\vec{B}}_{Z_t}) + g_Z(P_{Z_t} \backslash P^{\vec{B}}_{Z_t}) + \eta^Z_t; \\
&\qquad f_Y(P^{\vec{B}}_{Y_{t-\tau_Y}}) + \eta^Y_{t-\tau_Y} \mid \vec{W}) \\
&\overset{\text{Eq.(A.4)}}{=} I(f_X(P^{\vec{B}}_{X_{t-\tau_X}}) + \eta^X_{t-\tau_X}, f_Z(P^{\vec{B}}_{Z_t}) + \eta^Z_t; \\
&\qquad f_Y(P^{\vec{B}}_{Y_{t-\tau_Y}}) + \eta^Y_{t-\tau_Y} \mid \vec{W}).
\end{aligned} \tag{B.5}$$

The first equality is because of the *additivity* condition. For the second and third equalities, notice that g represents the function of the parents not in $\vec{B}$, $P_{K_{t-\tau}} \backslash P^{\vec{B}}_{K_{t-\tau}}$, which are a part of the condition set $\vec{W}$ (i.e., $P_{K_{t-\tau}} \backslash P^{\vec{B}}_{K_{t-\tau}} \in \vec{W}$). Therefore, the translational invariance in Eqs.(A.2) and (A.4) are applicable in the last two equalities in Eq.(B.5). Similarly, the second term on the right hand side of Eq.(B.4) can be changed into

$$\begin{aligned}
I(Y_{t-\tau_Y}; Z_t \mid \vec{W}) &\overset{\text{Eq.(2.13)}}{=} I(f_Y(P^{\vec{B}}_{Y_{t-\tau_Y}}) + g_Y(P_{Y_{t-\tau_Y}} \backslash P^{\vec{B}}_{Y_{t-\tau_Y}}) + \eta^Y_{t-\tau_Y}; \\
&\qquad f_Z(P^{\vec{B}}_{Z_t}) + g_Z(P_{Z_t} \backslash P^{\vec{B}}_{Z_t}) + \eta^Z_t \mid \vec{W}) \\
&\overset{\text{Eq.(A.3)}}{=} I(f_Y(P^{\vec{B}}_{Y_{t-\tau_Y}}) + \eta^Y_{t-\tau_Y}; f_Z(P^{\vec{B}}_{Z_t}) + \eta^Z_t \mid \vec{W}).
\end{aligned} \tag{B.6}$$

Combining Eqs.(B.3), (B.4), (B.5) and (B.6) into Eq.(B.2), we get

$$\begin{aligned}
\Delta I^{MSCP}_{\{X_{t-\tau_X}, Y_{t-\tau_Y}\} \to Z_t} =& I(f_X(P^{\vec{B}}_{X_{t-\tau_X}}) + \eta^X_{t-\tau_X}, f_Y(P^{\vec{B}}_{Y_{t-\tau_Y}}) + \eta^Y_{t-\tau_Y}; f_Z(P^{\vec{B}}_{Z_t}) + \eta^Z_t \mid \vec{W}) - \\
& I(f_X(P^{\vec{B}}_{X_{t-\tau_X}}) + \eta^X_{t-\tau_X}; f_Z(P^{\vec{B}}_{Z_t}) + \eta^Z_t \mid \vec{W}) - \\
& I(f_Y(P^{\vec{B}}_{Y_{t-\tau_Y}}) + \eta^Y_{t-\tau_Y}; f_Z(P^{\vec{B}}_{Z_t}) + \eta^Z_t \mid \vec{W}) \\
=& \mathcal{I}(f_X(P^{\vec{B}}_{X_{t-\tau_X}}) + \eta^X_{t-\tau_X}; f_Y(P^{\vec{B}}_{Y_{t-\tau_2}}) + \eta^Y_{t-\tau_Y}; f_Z(P^{\vec{B}}_{Z_t}) + \eta^Z_t \mid \vec{W}).
\end{aligned} \tag{B.7}$$

(ii) If *linearity* and *addivitity* hold, which means all the f functions are linear such that all the nodes on

the two causal paths and the target node are linearly dependent on each other, the interaction information in Eq.(B.7) can be reduced to

$$\begin{aligned}\Delta I^{MSCP}_{\{X_{t-\tau_X},Y_{t-\tau_Y}\}\to Z_t} =& I(\tilde{f}_X(\bullet)+\eta^X_{t-\tau_X},\tilde{f}_Y(\bullet)+\eta^Y_{t-\tau_Y};\tilde{f}_Z(\bullet)+\eta^Z_t \mid \vec{W})- \\ & I(\tilde{f}_X(\bullet)+\eta^X_{t-\tau_X};\tilde{f}_Z(\bullet)+\eta^Z_t \mid \vec{W}) - I(\tilde{f}_Y(\bullet)+\eta^Y_{t-\tau_Y};\tilde{f}_Z(\bullet)+\eta^Z_t \mid \vec{W}) \quad (\textit{linearity}) \\ =& \mathcal{I}(\tilde{f}_X(\bullet)+\eta^X_{t-\tau_X};\tilde{f}_Y(\bullet)+\eta^Y_{t-\tau_Y};\tilde{f}_Z(\bullet)+\eta^Z_t \mid \vec{W}), \end{aligned} \tag{B.8a}$$

where both $\tilde{f}_X(\bullet)$, $\tilde{f}_Y(\bullet)$ and $\tilde{f}_Z(\bullet)$ are the linear functions of all the noise terms η_t in the union of the two causal paths and the target node (i.e., $\vec{B}$). The first equality results from the fact that each parent in the linear function f can be iteratively decomposed into the summation of both the noise terms η and the function g of the external nodes (i.e, the parents of the two causal paths and the target node), and therefore the translational invariance in Eqs.(A.2)-(A.4) can be used for canceling out the g functions. Furthermore, because all the noise terms η are i.i.d., the condition $\vec{W}$ is independent of η and Eq.(B.8a) can be simplified as

$$\Delta I^{MSCP}_{\{X_{t-\tau_X},Y_{t-\tau_Y}\}\to Z_t} = \mathcal{I}(\tilde{f}_X(\bullet)+\eta^X_{t-\tau_X};\tilde{f}_Y(\bullet)+\eta^Y_{t-\tau_Y};\tilde{f}_Z(\bullet)+\eta^Z_t), \tag{B.9}$$

yielding Eq.(2.15a). Similarly, the translationally invariant property can be used to simplify the momentary interaction partitioning in Eqs.(2.11a)-(2.11b) as

$$R_c = R_{min,c} + I_{s,c}(R_{MMI,c} - R_{min,c}) \tag{B.10a}$$

$$S_c = \Delta I^{MSCP} + R_c \tag{B.10b}$$

$$U_{X,c} = I(\tilde{f}_X(\bullet)+\eta^X_{t-\tau_X};\tilde{f}_Z(\bullet)+\eta^Z_t) - R_c \tag{B.10c}$$

$$U_{Y,c} = I(\tilde{f}_Y(\bullet)+\eta^Y_{t-\tau_Y};\tilde{f}_Z(\bullet)+\eta^Z_t) - R_c, \tag{B.10d}$$

where

$$
\begin{aligned}
R_{MMI,c} &= \min[I(\tilde{f}_X(\bullet) + \eta^X_{t-\tau_X}; \tilde{f}_Z(\bullet) + \eta^Z_t), \\
&\qquad I(\tilde{f}_Y(\bullet) + \eta^Y_{t-\tau_Y}; \tilde{f}_Z(\bullet) + \eta^Z_t)] \\
I_{s,c} &= \frac{I(\tilde{f}_X(\bullet) + \eta^X_{t-\tau_X}; \tilde{f}_Y(\bullet) + \eta^Y_{t-\tau_2})}{\min[H(\tilde{f}_X(\bullet) + \eta^X_{t-\tau_X}), H(\tilde{f}_Y(\bullet) + \eta^Y_{t-\tau_Y})]} \\
R_{min,c} &= \begin{cases} 0, & \text{if } \Delta I^{MSCP} \geq 0 \\ -\Delta I^{MSCP}, & \text{otherwise.} \end{cases}
\end{aligned}
$$

It is obviously that under the *linearity* and *additivity* conditions, MPID is independent of the condition $\vec{W}$, resulting in the coupling strength autonomy property.

(iii) If *separability* and *additivity* hold, $P^{\vec{B}}_{X_{t-\tau_X}}$ and $P^{\vec{B}}_{Y_{t-\tau_Y}}$ are empty because X (or Z) is not in the causal path $C_{Y_{t-\tau_Y}\to Z_t}$ (or $C_{X_{t-\tau_X}\to Z_t}$). Therefore, $f_X(P^{\vec{B}}_{X_{t-\tau_X}})$ and $f_Y(P^{\vec{B}}_{Y_{t-\tau_Y}})$ are zero, which allows Eq.(B.7) to be revised as

$$
\begin{aligned}
\Delta I^{MSCP}_{\{X_{t-\tau_X}, Y_{t-\tau_Y}\}\to Z_t} =& \mathcal{I}(\eta^X_{t-\tau_X}; \eta^Y_{t-\tau_Y}; f_Z(P^{\vec{B}}_{Z_t}) + \eta^Z_t \mid \vec{W}) \\
=& I(\eta^X_{t-\tau_X}; \eta^Y_{t-\tau_Y} \mid \{f_Z(P^{\vec{B}}_{Z_t}) + \eta^Z_t\} \cup \vec{W}) - I(\eta^X_{t-\tau_X}; \eta^Y_{t-\tau_Y} \mid \vec{W}) \\
=& I(\eta^X_{t-\tau_X}; \eta^Y_{t-\tau_Y} \mid \{f_Z(P^{\vec{B}}_{Z_t}) + \eta^Z_t\} \cup \vec{W}),
\end{aligned} \tag{B.11}
$$

yielding Eq.(2.17a). The final equality holds because η^X_t and η^Y_t are i.i.d. and the nodes in the $\vec{W}$ are not the common children of $\eta^X_{t-\tau_X}$ and $\eta^Y_{t-\tau_Y}$, leading to $I(\eta^X_{t-\tau_X}; \eta^Y_{t-\tau_Y} \mid \vec{W}) = 0$. Also, notice that due to the *separability* condition, $I(X_{t-\tau_X}; Y_{t-\tau_Y} \mid \vec{W}) = I(\eta^X_{t-\tau_X}; \eta^Y_{t-\tau_Y} \mid \vec{W}) = 0$ (here, g_X and g_Y cancel out because of the translational invariance). Hence, $I_{s,c}$ in Eq.(2.11b) is reduced to zero (since all the noises η are i.i.d.), resulting in the minimum value of the redundancy such that $R_c = R_{min,c}$ according to Eq.(2.11b). Therefore, the synergistic and redundant information can be expressed as

$$
R_c = R_{min,c} \tag{B.12}
$$

$$
S_c = \Delta I^{MSCP} + R_c. \tag{B.13}
$$

The two unique information can also be obtained based on the *separability* condition such that

$$U_{X,c} = I(\eta^X_{t-\tau_X}; f_Z(P^{\vec{B}}_{Z_t}) + \eta^Z_t \mid \vec{W}) - R_c \tag{B.14}$$

$$U_{Y,c} = I(\eta^Y_{t-\tau_Y}; f_Z(P^{\vec{B}}_{Z_t}) + \eta^Z_t \mid \vec{W}) - R_c. \tag{B.15}$$

(iv) If all the three conditions hold, we can easily obtain MPID by combining the results of both the situations (ii) and (iii) such that

$$\Delta I^{MSCP}_{\{X_{t-\tau_X}, Y_{t-\tau_Y}\} \to Z_t} = I(\eta^X_{t-\tau_X}; \eta^Y_{t-\tau_Y} \mid \tilde{f}_Z(\bullet) + \eta^Z_t) \tag{B.16a}$$

$$R_c = R_{min,c} \tag{B.16b}$$

$$S_c = \Delta I^{MSCP} + R_c \tag{B.16c}$$

$$U_{X,c} = I(\eta^X_{t-\tau_X}; \tilde{f}_Z(\bullet) + \eta^Z_t) - R_c \tag{B.16d}$$

$$U_{Y,c} = I(\eta^Y_{t-\tau_Y}; \tilde{f}_Z(\bullet) + \eta^Z_t) - R_c. \tag{B.16e}$$

Appendix C

Analytical Solutions of the Linear Common Driver Model

In the following, we show the derivation of the analytical solutions of $\Delta I^{MSCP}_{\{X_{t-1},Y_{t-1}\}\to Z_t}$ and $\mathcal{I}(X_{t-1};Y_{t-1};Z_t)$ in Eqs.(2.19c) and (2.20) for the linear common driver model in Eq.(2.18).

Variances and Covariances

We derive some variances and covariances of the linear model Eq.(2.18) for the further usage in the derivation of the analytical solutions of $\Delta I^{MSCP}_{\{X_{t-1},Y_{t-1}\}\to Z_t}$ and $\mathcal{I}(X_{t-1};Y_{t-1};Z_t)$.

The variances of the four sub-processes (i.e., V, X, Y, Z) can be expressed as

$$\begin{aligned}
\Gamma_V &= \sigma_V^2 \\
\Gamma_X &= c_{VX}^2\Gamma_V + \sigma_X^2 \\
\Gamma_Y &= c_{VY}^2\Gamma_V + \sigma_Y^2 \\
\Gamma_Z &= c_{XZ}^2\Gamma_X + c_{YZ}^2\Gamma_Y + \sigma_Z^2.
\end{aligned}$$

Also, some of the used covariances between two variables (e.g., X and Y) with a lag τ, denoted as $\Gamma_{XY}(\tau) = E[X_{t+\tau}Y_t]$ (where E represents the expectation function), are given by

$$\begin{aligned}
\Gamma_{XY}(0) &= c_{VX}c_{VY}\Gamma_V \\
\Gamma_{ZX}(1) &= c_{XZ}\Gamma_X + c_{YZ}\Gamma_{XY}(0) \\
\Gamma_{ZY}(1) &= c_{YZ}\Gamma_Y + c_{XZ}\Gamma_{XY}(0) \\
\Gamma_{XV}(1) &= c_{VX}\Gamma_V \\
\Gamma_{YV}(1) &= c_{VY}\Gamma_V \\
\Gamma_{ZV}(2) &= c_{XZ}\Gamma_{XV}(1) + c_{YZ}\Gamma_{YV}(1).
\end{aligned}$$

The Momentary Interaction Information for Separable Causal Paths $\Delta I^{MSCP}_{\{X_{t-1},Y_{t-1}\}\to Z_t}$

As shown in Fig. 2.3b, the condition set $\vec{W}$ for $\Delta I^{MSCP}_{\{X_{t-1},Y_{t-1}\}\to Z_t}$ is $\{V_{t-2}\}$. Therefore, $\Delta I^{MSCP}_{\{X_{t-1},Y_{t-1}\}\to Z_t}$ can be written as

$$\begin{aligned}\Delta I^{MSCP}_{\{X_{t-1},Y_{t-1}\}\to Z_t} =& \mathcal{I}(X_{t-1};Y_{t-1};Z_t \mid V_{t-2}) \\ =& I(X_{t-1};Y_{t-1} \mid Z_t, V_{t-2}) - I(X_{t-\tau_1};Y_{t-\tau_2} \mid V_{t-2}) \\ =& H(X_{t-1} \mid Z_t, V_{t-2}) - H(X_{t-1} \mid Y_{t-1}, Z_t, V_{t-2}) \\ & - H(X_{t-1} \mid V_{t-2}) + H(X_{t-1} \mid Y_{t-1}, V_{t-2}). \end{aligned} \tag{C.1}$$

Because all the processes in the linear model are Gaussian, based on Eq.(A.5), each component in $\Delta I^{MSCP}_{\{X_{t-1},Y_{t-1}\}\to Z_t}$ is given by

$$\begin{aligned} H(X_{t-1} \mid Z_t, V_{t-2}) &= \frac{1}{2}\ln\Big\{2\pi e \frac{|\Gamma_{X_{t-1},Z_t,V_{t-2}}|}{|\Gamma_{Z_t,V_{t-2}}|}\Big\} \\ H(X_{t-1} \mid Y_{t-1}, Z_t, V_{t-2}) &= \frac{1}{2}\ln\Big\{2\pi e \frac{|\Gamma_{X_{t-1},Y_{t-1},Z_t,V_{t-2}}|}{|\Gamma_{Y_{t-1},Z_t,V_{t-2}}|}\Big\} \\ H(X_{t-1} \mid V_{t-2}) &= \frac{1}{2}\ln\Big\{2\pi e \frac{|\Gamma_{X_{t-1},V_{t-2}}|}{|\Gamma_{V_{t-2}}|}\Big\} \\ H(X_{t-1} \mid Y_{t-1}, V_{t-2}) &= \frac{1}{2}\ln\Big\{2\pi e \frac{|\Gamma_{X_{t-1},Y_{t-1},V_{t-2}}|}{|\Gamma_{Y_{t-1},V_{t-2}}|}\Big\}. \end{aligned} \tag{C.2}$$

To derive the analytical solutions of the above conditional entropies, we need to solve the determinants involved in the above equations. Consider the example of $H(X_{t-1} \mid V_{t-2})$. The determinant of the covariance matrix $|\Gamma_{X_{t-1},V_{t-2}}|$ can be expressed as

$$\begin{aligned} |\Gamma_{X_{t-1},V_{t-2}}| &= \begin{vmatrix} \Gamma_X & \Gamma_{XV}(1) \\ \Gamma_{XV}(1) & \Gamma_V \end{vmatrix} \\ &= \Gamma_X\Gamma_V - \Gamma_{XV}(1)^2 \\ &= \sigma_X^2\Gamma_V. \end{aligned} \tag{C.3}$$

Also, because $|\Gamma_{V_{t-2}}| = \Gamma_V$, the analytical solution of $H(X_{t-1} \mid V_{t-2})$ is given by

$$H(X_{t-1} \mid V_{t-2}) = \frac{1}{2}\ln\{2\pi e\sigma_X^2\}. \tag{C.4}$$

Therefore, by solving all the determinants above and putting all the analytical solutions of the four con-

ditional entropy back to Eq.(C.1), we obtain the analyticial solution of $\Delta I^{MSCP}_{\{X_{t-1},Y_{t-1}\}\to Z_t}$ as shown in Eq.(2.19c).

It is noted that because all the three conditions (i.e., *separability*, *linearity* and *additivity*) hold for the linear common driver model, the solution in Eq.(2.19c) can also be achieved by solving $\Delta I^{MSCP}_{\{X_{t-\tau_1},Y_{t-\tau_2}\}\to Z_t} = \mathcal{I}(\eta^X_{t-\tau_1}; \eta^Y_{t-\tau_2}; \tilde{f_Z}(\bullet) + \eta^Z_t)$ directly, which is not shown here.

Interaction Information $\mathcal{I}(X_{t-1}; Y_{t-1}; Z_t)$

$\mathcal{I}(X_{t-1}; Y_{t-1}; Z_t)$ can be expanded as

$$\begin{aligned}\mathcal{I}(X_{t-1}; Y_{t-1}; Z_t) =& I(X_{t-1}; Y_{t-1} \mid Z_t) - I(X_{t-\tau_1}; Y_{t-\tau_2}) \\ =& H(X_{t-1} \mid Z_t) - H(X_{t-1} \mid Y_{t-1}, Z_t) - H(X_{t-1}) + H(X_{t-1} \mid Y_{t-1})\end{aligned} \tag{C.5}$$

Similarly, the Gaussian process-based $\mathcal{I}(X_{t-1}; Y_{t-1}; Z_t)$ can be further revised according to Eq.(A.5) as,

$$\begin{aligned}\mathcal{I}(X_{t-1}; Y_{t-1}; Z_t) =& \frac{1}{2}\ln\left\{2\pi e\frac{|\Gamma_{X_{t-1},Z_t}|}{|\Gamma_{Z_t}|}\right\} - \frac{1}{2}\ln\left\{2\pi e\frac{|\Gamma_{X_{t-1},Y_{t-1},Z_t}|}{|\Gamma_{Y_{t-1},Z_t}|}\right\} - \\ & \frac{1}{2}\ln\left\{2\pi e|\Gamma_{X_{t-1}}|\right\} + \frac{1}{2}\ln\left\{2\pi e\frac{|\Gamma_{X_{t-1},Y_{t-1}}|}{|\Gamma_{Y_{t-1}}|}\right\} \\ =& \frac{1}{2}\ln\left\{\frac{|\Gamma_{X_{t-1},Z_t}||\Gamma_{Y_{t-1},Z_t}||\Gamma_{X_{t-1},Y_{t-1}}|}{|\Gamma_{Z_t}||\Gamma_{X_{t-1},Y_{t-1},Z_t}||\Gamma_{X_{t-1}}||\Gamma_{Y_{t-1}}|}\right\}.\end{aligned} \tag{C.6}$$

By solving all the determinants in Eq.(C.6), we can obtain the solution in Eq.(2.20).

Appendix D

Derivations for Information from Immediate Causal History

This section provides the derivations of Eqs.(3.6). We separate the immediate causal history $C_{\vec{V}\Rightarrow Z_t}$ into two sets: (1) those belonging to the parents of Z_t, $P_{Z_t}^{C_{\vec{V}\Rightarrow Z_t}} = P_{Z_t} \cap C_{\vec{V}\Rightarrow Z_t}$, and (2) the remaining nodes, $C_{\vec{V}\Rightarrow Z_t} \backslash P_{Z_t}^{C_{\vec{V}\Rightarrow Z_t}}$. Then, using the chain rule, $\mathcal{J}$ defined in Eq.(3.5) can be written as:

$$\begin{aligned}
\mathcal{J} =& I(Z_t; P_{Z_t}^{C_{\vec{V}\Rightarrow Z_t}}, C_{\vec{V}\Rightarrow Z_t} \backslash P_{Z_t}^{C_{\vec{V}\Rightarrow Z_t}} \mid \vec{W}_\tau) && \text{(D.1)}\\
=& I(Z_t; P_{Z_t}^{C_{\vec{V}\Rightarrow Z_t}} \mid \vec{W}_\tau) && \text{(D.2)}\\
&+ \underbrace{I(Z_t; C_{\vec{V}\Rightarrow Z_t} \backslash P_{Z_t}^{C_{\vec{V}\Rightarrow Z_t}} \mid \vec{W}_\tau, P_{Z_t}^{C_{\vec{V}\Rightarrow Z_t}})}_{=0} && \text{(D.3)}\\
=& I(Z_t; P_{Z_t}^{C_{\vec{V}\Rightarrow Z_t}} \mid \vec{W}_\tau), && \text{(D.4)}
\end{aligned}$$

yielding Eq.(3.6). The chain rule of the conditional mutual information (CMI) facilitates the transition from Eq.(D.1) to Eq.(D.2). Moreover, in the 2^{nd} term of Eq.(D.2), $I(Z_t; C_{\vec{V}\Rightarrow Z_t} \backslash P_{Z_t}^{C_{\vec{V}\Rightarrow Z_t}} \mid \vec{W}_\tau, P_{Z_t}^{C_{\vec{V}\Rightarrow Z_t}})$, the parents of Z_t are contained in the condition set, which is the union of $P_{Z_t}^{C_{\vec{V}\Rightarrow Z_t}}$ and $\vec{W}_\tau$, including the parents of Z_t in $C_{\vec{V}\Rightarrow Z_t}$ and the remaining parents not in the subgraph, respectively. Therefore, due to the Markov property, given P_{Z_t} (included in the union of $\vec{W}_\tau$ and $P_{Z_t}^{C_{\vec{V}\Rightarrow Z_t}}$), Z_t is independent of its non-descendants, which contains both $C_{\vec{V}\Rightarrow Z_t} \backslash P_{Z_t}^{C_{\vec{V}\Rightarrow Z_t}}$ and the remaining nodes in the condition set $\{\vec{W}_\tau, P_{Z_t}^{C_{\vec{V}\Rightarrow Z_t}}\}$, thus leading to $I(Z_t; C_{\vec{V}\Rightarrow Z_t} \backslash P_{Z_t}^{C_{\vec{V}\Rightarrow Z_t}} \mid \vec{W}_\tau, P_{Z_t}^{C_{\vec{V}\Rightarrow Z_t}}) = 0$.

Appendix E

Construction of the Time Series Graph for Water Chemistry Data

The catchment chemistry data in the Upper Hafren in Wales, sampled and analyzed every 7-h from March 2007 to Jan 2009, are available as the supporting information of [Kirchner and Neal, 2013]. In this study we use, the logarithmic flow rate (ln Q) and six water quality variables (i.e., Na^+, Cl^-, Al^{3+}, Ca^{2+}, $SO4^{2-}$ and pH), as well as the data with flow-dependent variations corrected [Kirchner and Neal, 2013], are used. We construct two time series graphs for the raw data and the flow rate-corrected one, separately, with the total number 2375 data points including gaps for each graph. The existence of the gaps in the data would reduce the lengths of samples in computing conditional mutual information (CMI) or mutual information (MI), thus potentially worsening the estimation. To minimize this effect, we use the whole dataset to get the sample data points for estimating MI or CMI and then remove the data points containing gaps in the samples [Goodwell and Kumar, 2017a].

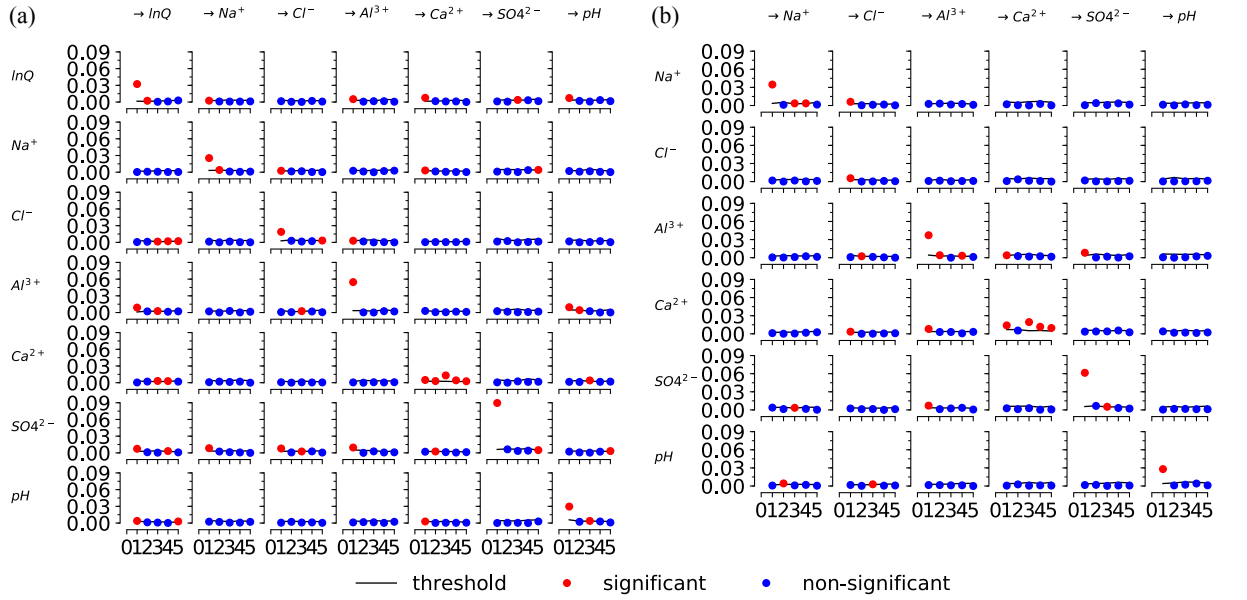

Figure E.1: Illustration of the estimated lag functions (y-axis: the coupling strength [nats] computed based on momentary information transfer (MIT) [Runge et al., 2012a]; x-axis: the time lag τ) of the catchment chemistry data by using Tigramite algorithm for: (a) the logarithm of flow rate and six chemistry variable; and (b) the six chemistry variables with the variation of the logarithm of flow rate excluded.

The time series graph is constructed by using Tigramite algorithm [Runge et al., 2012b, Runge, 2015, Runge et al., 2015, Runge et al., 2017], which is a modified PC algorithm [Spirtes et al., 2000] and anchored on the conditional independence test to remove any spurious relationship between two nodes. We employ the k-nearest-neighbor (kNN) CMI-based conditional independence test, with the number of nearest-neighbor $k = 100$ (high k facilitates a low variance of the estimated CMI [Frenzel and Pompe, 2007]). Each test is conducted based on 100 samples with a significance level $\alpha = 95\%$. The graphs are constructed with a maximum time lag $\tau_{max} = 5$. The resulting dependencies for the two networks are shown in Fig. E.1, sketching the lag function in terms of the momentary information transfer [Runge et al., 2012a] between each pair of lagged components. Based on the two time series graphs, $\mathcal{D}$ and $\mathcal{T}$ for each variable are computed based on Eqs.(3.4) and (3.3), respectively, by using kNN approach with $k = 5$. The dimensions of $\mathcal{T}$, $\mathcal{D}$, and $\mathcal{J}$ are shown in Fig. E.3. As the computation of $\mathcal{D}$ requires higher dimensions, the numbers of data points used for computing $\mathcal{D}$ are shown in Fig. E.2, where in each case more than 1000 are used. Further, to check the significance of $\mathcal{D}$, shuffle test is conducted for $\mathcal{D}$ with a significance level of 95% based on 100 shuffles. The result of shuffle tests in Fig. E.4 shows most $\mathcal{D}$ are statistically significant.

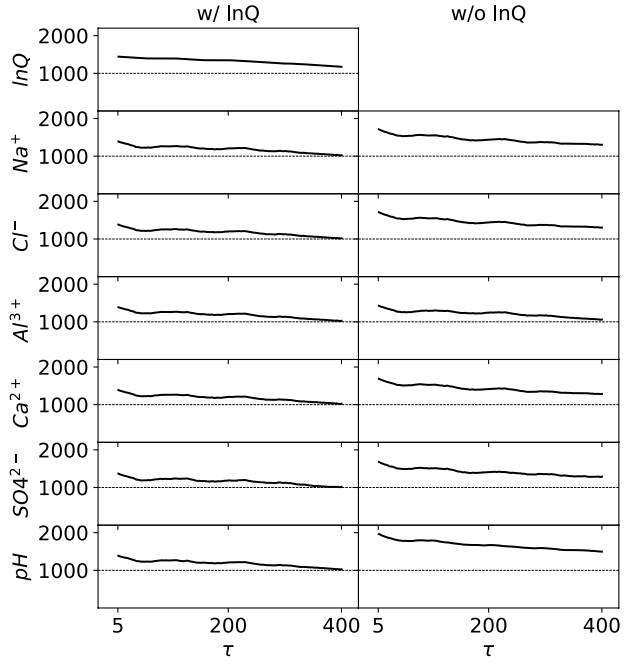

Figure E.2: Number of data points for computing $\mathcal{D}$ in Eq.(3.4) in terms of the time lag τ for each variable in the two time series graphs constructed in Fig. E.1.

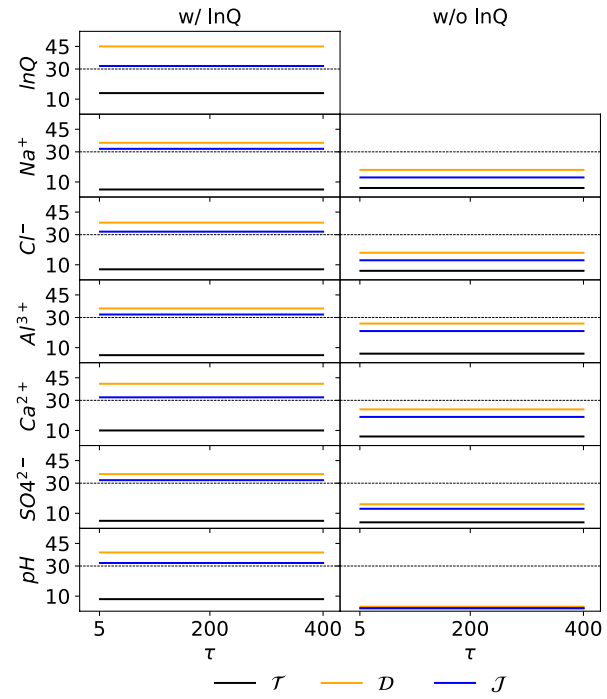

Figure E.3: The cardinality of the estimated $\mathcal{T}$, $\mathcal{D}$ and $\mathcal{J}$ in Eq.(3.3), Eq.(3.4) and Eq.(3.6), respectively, in terms of the time lag τ for each variable in the two time series graphs constructed in Fig. E.1.

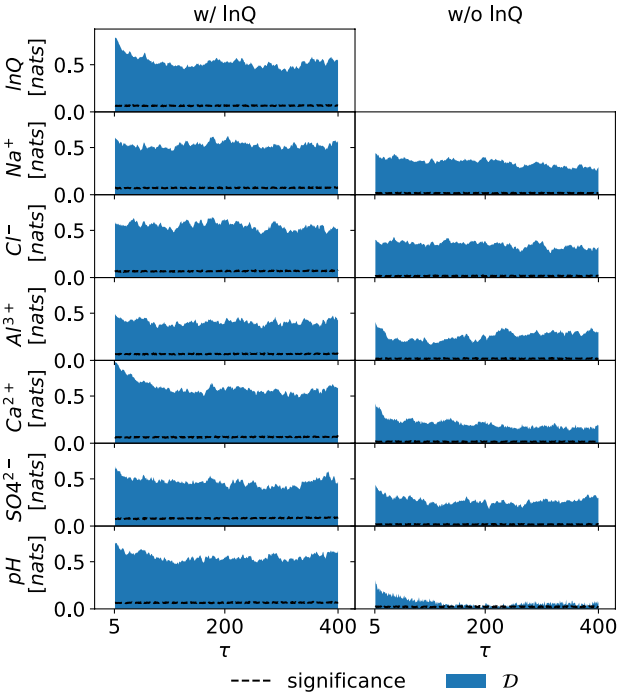

Figure E.4: The estimated $\mathcal{D}$ in Eq.(3.4) from the two networks constructed in Fig. E.1 as well as the corresponding threshold for shuffle test with significance level $\alpha = 0.05$.

Appendix F

Verification of Momentary Information Weighted Transitive Reduction

This appendix aims to verify the feasibility of MIWTR in reducing the cardinality of the condition set $\vec{W}$ in Eq.(3.4). We compute and compare the information flow from the immediate and distant causal histories $\mathcal{J}$ and $\mathcal{D}$ as well as the corresponding (momentary) partial information decomposition in Eqs.(4.1)-(4.2), with and without MIWTR in a quadvariate logistic model. The model is given by:

$$X_{i,t} = \frac{1-\epsilon}{4}\sum_{j=1}^{4} 4X_{j,t-1}(1-X_{j,t-1}) + \epsilon\eta_t^{X_i}, i \in \{1,2,3,4\} \tag{F.1}$$

where $\eta_t^{X_i} \in [0,1]$ is a uniform noise term and its coupling strength ϵ is set as 0.2.

The procedures of computing the information flows are as follows. We first use the Tigramite package to construct the directed acyclic time-series graph based on the synthetic data generated from Eq.(F.1). Given the graph describing the causal history, MIWTR is employed to simplify the condition set $\vec{W}$ according to the procedures in Section 4.3. $\mathcal{J}$ and $\mathcal{D}$ and their PIDs are then computed, with time lag τ ranging from 5 to 50,using k-nearest-neighbor method with $k = 5$. The parameter setting of the Tigramite is the same as the Appendix B of [Jiang and Kumar, 2019]. Further, to analyze how the data length affects the performance of MIWTR, we compute the information flow with time-series lengths 200, 400, 600, 1000, 5000, 10000.

The cardinalities of $\mathcal{D}$ and $\mathcal{J}$ with and without MIWTR are plotted in Fig. F.1(a). It can be observed that the dimensions decrease with increasing length of synthetic data. This is because more training datasets allow a more reliable estimation of the directed acyclic time-series graph. The estimated graph becomes stable when data length is larger than 1000, indicated by the convergence of the decreasing cardinalities. Furthermore, for a given data length, we also observe significant drops of dimensions for both $\mathcal{D}$ and $\mathcal{J}$ due to the reduction of $\vec{W}$ by using MIWTR. The reduced dimension of $\vec{W}$ is around 10 for data length greater than 1000.

The plots of $\mathcal{D}$ and $\mathcal{J}$ with and without MIWTR are shown in Fig. F.1(b). We can observe that both the results using MIWTR (solid lines) and without MIWTR (dashed lines) converge and are pretty close to each other, especially for data length greater than 1000. It implies that in this quadvariate logistic model,

the implementation of MIWTR in reducing the dimensions can ensure a reliable estimation of $\mathcal{D}$ and $\mathcal{J}$ given enough time-series data (> 1000).

The (momentary) PIDs for $\mathcal{D}$ and $\mathcal{J}$ with MIWTR are plotted in Figs. F.2(a) and F.3(a), respectively. Both $\mathcal{D}$ and $\mathcal{J}$ contains dominant redundant information, which are $R_{\mathcal{D}}$ and $R_{\mathcal{J}}$. It illustrates the symmetric structure of the model in Eq. F.1. Also, the differences between the information partitioning with and without MIWTR, in Figs. F.2(b) and F.3(b), shows that the differences are close to zero when more than 1000 data points are used. This is consistent with the conclusion that the cardinality reduction based on MIWTR does not affect the estimation of information-theoretic measures significantly when the time-series data is sufficient.

In the analysis of stream chemistry data and weather station data in Section 4.4, the cardinalities of $\mathcal{D}$ and $\mathcal{J}$ of all the variables are reduced to be less than or around 20 by using MIWTR as shown in Fig. F.4. Based on the quadvariate logistic model example, the associated estimations of information flows in Figs. 4.4 are reasonable, because the corresponding time-series lengths of the data (around 1000-4000) are sufficient to achieve reliable estimation.

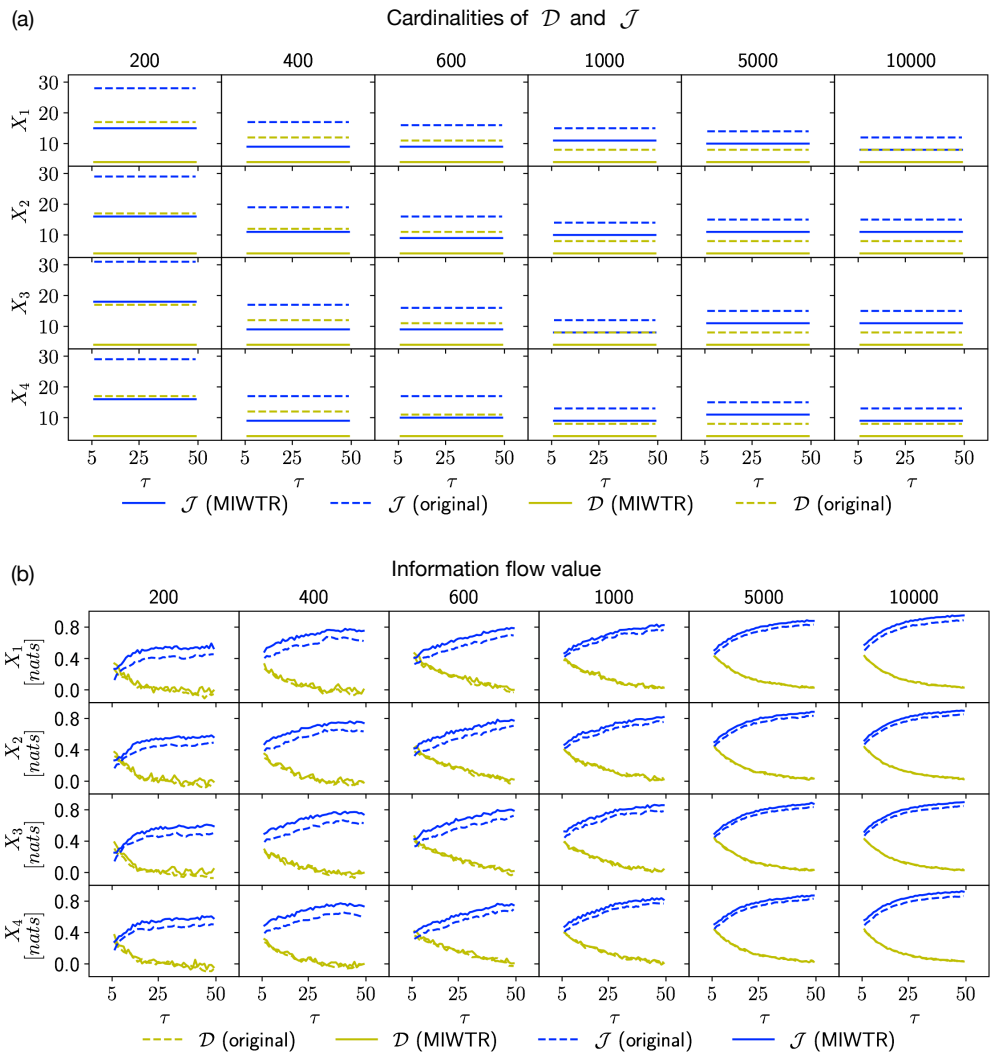

Figure F.1: Plots of the cardinalities and the values of $\mathcal{D}$ and $\mathcal{J}$ of each variable in Eq.(F.1) over the tima lag τ. based on data length of 200, 400, 600, 1000, 5000 and 10000. (a) The cardinalities of the estimated $\mathcal{D}$ and $\mathcal{J}$ (the dashed lines) in Eqs.(3.4) and (3.6), respectively, as well as the corresponding cardinalities based on momentary information weighted transitive reduction (MIWTR, the solid lines) of each variable with the time-series graphs constructed by using Tigramite. (b) The corresponding values of $\mathcal{D}$ and $\mathcal{J}$ with and without MIWTR.

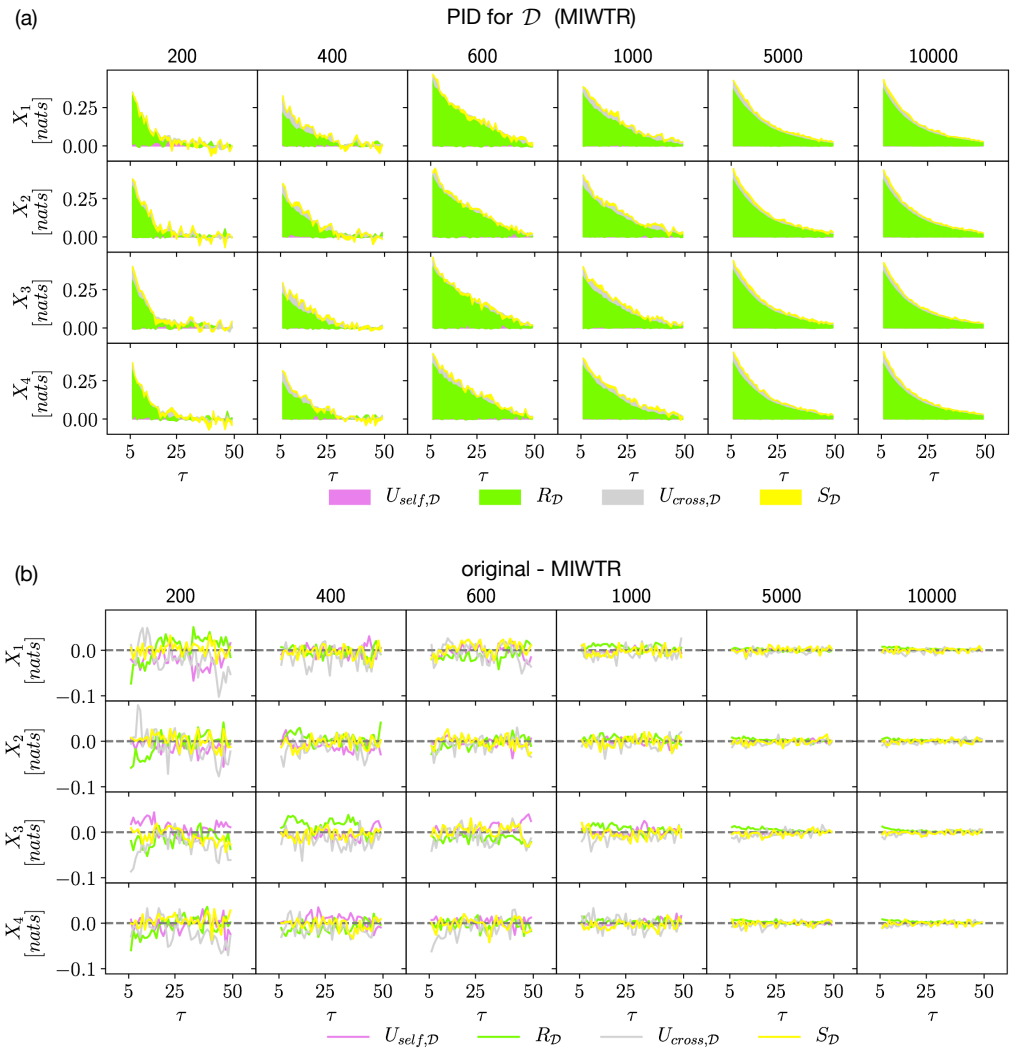

Figure F.2: Plots of the partial information decomposition (PID) of $\mathcal{D}$ of each variable in Eq.(F.1) over the tima lag τ. based on data length of 200, 400, 600, 1000, 5000 and 10000. (a) The PID of $\mathcal{D}$ based on MIWTR. (b) The difference between $\mathcal{D}$ without and with MIWTR.

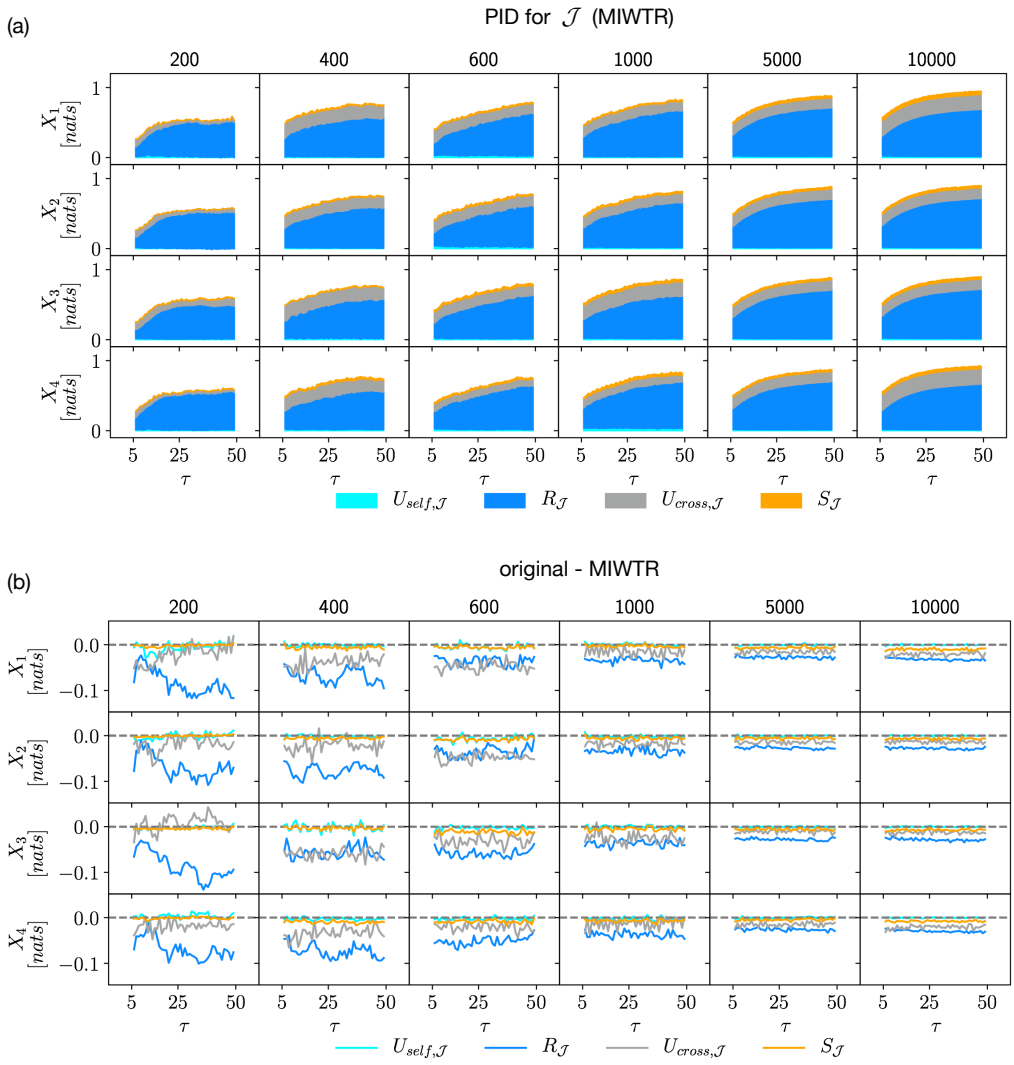

Figure F.3: Plots of the momentary partial information decomposition (PID) of $\mathcal{J}$ of each variable in Eq.(F.1) over the tima lag τ. based on data length of 200, 400, 600, 1000, 5000 and 10000. (a) The PID of $\mathcal{J}$ based on MIWTR. (b) The difference between $\mathcal{J}$ without and with MIWTR.

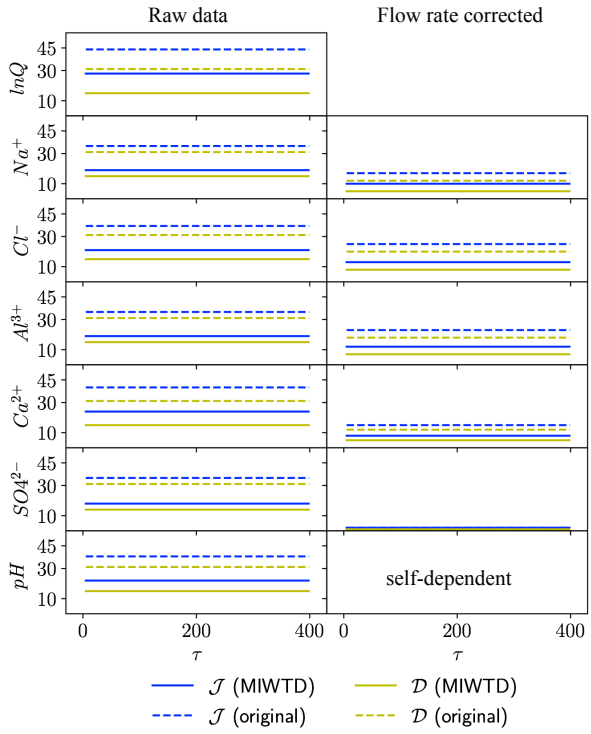

Figure F.4: The cardinalities of the estimated $\mathcal{D}$ and $\mathcal{J}$ (the dashed lines) in Eqs.(3.4) and (3.6), respectively, as well as the corresponding cardinalities based on momentary information weighted transitive reduction (MIWTR, the solid lines) of each variable in the stream chemistry system based on the two time-series graphs for the stream solute data constructed in Fig. 3.6.